



CENTER FOR INFRASTRUCTURE ENGINEERING STUDIES

Shear Performance of RC Beams Strengthened In Situ with Composites

by

Raghu H. Annaiah

John J. Myers

Antonio Nanni

Department of Civil Engineering

University of Missouri - Rolla

March 2001

CIES

99-11

Disclaimer

The contents of this report reflect the views of the author(s), who are responsible for the facts and the accuracy of information presented herein. This document is disseminated under the sponsorship of the Center for Infrastructure Engineering Studies (CIES), University of Missouri -Rolla, in the interest of information exchange. CIES assumes no liability for the contents or use thereof.

The mission of CIES is to provide leadership in research and education for solving society's problems affecting the nation's infrastructure systems. CIES is the primary conduit for communication among those on the UMR campus interested in infrastructure studies and provides coordination for collaborative efforts. CIES activities include interdisciplinary research and development with projects tailored to address needs of federal agencies, state agencies, and private industry as well as technology transfer and continuing/distance education to the engineering community and industry.

Center for Infrastructure Engineering Studies (CIES)
University of Missouri-Rolla
223 Engineering Research Lab
1870 Miner Circle
Rolla, MO 65409-070
Tel: (573) 341-6223; fax -6215
E-mail: cies@umr.edu
www.cies.umr

**Shear Performance of RC Beams
Strengthened In Situ with Composites**

by

Raghu H. Annaiah

John J. Myers

Antonio Nanni

Department of Civil Engineering

University of Missouri - Rolla

Report No. CIES 99-11

**Center for Infrastructure Engineering Studies
University of Missouri - Rolla**

ABSTRACT

Shear failures of reinforced concrete (RC) structural elements are catastrophic and occur with no advance warning. Conventional shear strengthening methods like external post tensioning, member enlargement along with internal transverse steel, and bonded steel plates are time consuming and complex. Shear strengthening with the help of advanced composite materials, known as fiber reinforced polymer (FRP), offers significant advantage over the conventional methods in terms of cost and time.

The overall goal of this study was to investigate the shear performance and modes of failure of RC Tshaped joists strengthened with externally bonded FRP sheets. In order to achieve this goal, an experiment consisting of testing of twenty, full-scale RC joists was carried out at the Malcolm Bliss Hospital, St.Louis, MO. The selected building was completed in 1964 and provided an ideal test bed for carrying out experiments on an existing structure. To date research in strengthening has been restricted to laboratory experimentation. As part of the research program, the study examined the effectiveness of FRP reinforcement in enhancing the shear capacity of RC joists. Furthermore, an innovative end anchor system, which allowed a better exploitation of the strengthening system, was also tested.

The experimental results indicated that externally bonded FRP can be used to enhance the shear capacity of a member. An attempt has been made to validate the existing design guidelines for shear strengthening using the data obtained in this research.

TABLE OF CONTENTS

ABSTRACT.....	ii
LIST OF ILLUSTRATIONS.....	vi
LIST OF TABLES.....	xi
SECTION 1: INTRODUCTION.....	1
1.1. BACKGROUND.....	1
1.2. SCOPE AND OBJECTIVE.....	2
1.3. SUMMARY.....	2
SECTION 2: LITERATURE OVERVIEW.....	4
2.1 GENERAL.....	4
2.2 DEFINITION OF FRP.....	4
2.3 APPLICATION OF FRP IN STRUCTURAL STRENGTHENING.....	5
2.4. SHEAR STRENGTHENING OF RC BEAMS USING FRP.....	6
2.5 SHEAR STRENGTHENING OPTIONS.....	9
2.5.1 GENERAL.....	9
2.5.2 BONDED SURFACE CONFIGURATIONS.....	9
2.5.3 END ANCHOR.....	10
2.5.4 SHEAR REINFORCEMENT SPACING.....	11
2.5.5. FIBER ORIENTATION.....	12
SECTION 3: EXPERIMENTAL PROGRAM.....	13
3.1 GENERAL.....	13
3.2 MATERIALS.....	13
3.2.1 CONCRETE.....	13
3.2.2 STEEL REINFORCEMENTS.....	14
3.2.3 COMPOSITE STRENGTHENING SYSTEM.....	15
3.3 INSTALLATION PROCESS.....	16
3.4 DESCRIPTION OF RC MEMBERS & STRENGTHENING SCHEMES.....	20
3.4.1 SHORT-SPAN STRENGTHENING SCHEME.....	20
3.4.2 LONG-SPAN STRENGTHENING SCHEME.....	26

SECTION 4: DESIGN APPROACH.....	31
4.1 GENERAL.....	31
4.2 SHEAR DESIGN OF RC STRENGTHENED BEAMS IN ACI CODE FORMAT.....	32
4.2.1 ACI CODE PROVISION FOR SHEAR.....	32
4.3 SHEAR CAPACITY OF A CFRP STRENGTHENING SECTION.....	33
4.3.1 CONTRIBUTION OF CFRP REINFORCEMENT (V_p) TO THE SHEAR CAPACITY.....	33
4.4 DESIGN PREDICTIONS.....	37
SECTION 5: ANALYTICAL MODEL.....	39
5.1 GENERAL.....	39
5.2 LOAD DEFLECTION BEHAVIOR.....	40
5.3 ANALYTICAL BEAM MODEL.....	43
5.4 DOUBLE INTEGRATION METHOD.....	44
5.5 BRANSON EQUATION.....	46
5.6 VALIDATION OF THE ANALYTICAL APPROACH.....	48
SECTION 6: TEST SETUP.....	56
6.1 INSTRUMENTATION.....	56
6.2 TEST SETUP.....	59
SECTION 7: TEST RESULTS.....	62
7.1 SHORT-SPAN MEMBERS.....	62
7.1.1 DISCUSSION OF FAILURE MODES.....	63
7.1.2 COMPARISON OF RESULTS.....	68
7.2 LONG-SPAN MEMBERS.....	75
7.2.1 DISCUSSION OF FAILURE MODES.....	75
7.2.2 COMPARISON OF RESULTS.....	81
SECTION 8: SUMMARY.....	83
8.1 SUMMARY.....	83
8.2 CONCLUSIONS.....	83
8.3 RECOMMENDATIONS FOR FUTURE WORK.....	84

APPENDICES

A. TEST RESULTS.....	86
B. ANALYTICAL CURVES.....	108
C. DESIGN EXAMPLES.....	119
BIBLIOGRAPHY.....	125

LIST OF ILLUSTRATIONS

2.1: Comparison of CFRP, AFRP, & GFRP sheets and reinforcing steel in terms of stress-strain relationship.....	5
2.2: Various FRP wrapping schemes.....	10
2.3: End anchor options.....	11
2.4: Shear reinforcement distribution's.....	11
2.5: Fiber orientation.....	12
3.1: Components of the strengthening system.....	16
3.2: Chipping of concrete.....	16
3.3: Application of primer.....	17
3.4: Application of putty.....	17
3.5: Rolling of FRP sheets after he application of saturant.....	18
3.6: Grooves for end anchor.....	19
3.7: Application of epoxy paste to hold the end anchors.....	19
3.8: Layout plan of the test specimen.....	22
3.9: Specimen JS1 (unstrengthened).....	23
3.10: Specimen JS2 (Single wrap).....	23
3.11: Shear wrap and Positive strip.....	24
3.12: Specimen JS3 (Single wrap with end anchors).....	24
3.13: Single wrap with end anchors.....	25
3.14: Specimen JS4 (Double wrap without end anchors).....	25
3.15: Specimen JS5/JS6 (carbon/Aramid-Double wrap with end anchors).....	26
3.16: Layout plan of the test specimen.....	28
3.17: Specimen JL1 (Unstrengthened member).....	29
3.18: Specimen JL2 (Single wrap without end anchors).....	29
3.19: Specimen JL3 (Single wrap with Negative strengthening).....	30
3.20: Specimen JL4 (Single wrap with negative strengthening and end anchor).....	30
4.1: Definition of area of FRP in shear reinforcement.....	34
5.1: Typical loading and support configuration of experimental beams.....	39
5.2: Cross section @ x-x.....	39

5.3: Idealized Load-Deflection curves for FRP strengthened RC beam.....	42
5.4: Effect of tension cracking on reinforcing steel stress, concrete tension stress and flexure.....	42
5.5: Typical moment-curvature curve for conventionally reinforced concrete beams and RC strengthened with FRP.....	43
5.6: Typical loading and support configuration for design.....	43
5.7: Model beam with differential settlement.....	44
5.8: Equivalent model of cracked beam with deflected shape.....	46
5.9: Geometry of the cross section used for validation.....	48
5.10: Uncracked transformed section.....	49
5.11: Flow chart describing the analytical model approach.....	52
5.12: Deflection curves for JS3A.....	54
5.13: Experimental validation of shear capacity at ultimate load.....	55
6.1: LVDT setup.....	58
6.2: Inclinator.....	58
6.3: Location of strain gages.....	58
6.4: Extensometer.....	59
6.5: Schematic representation of push down test setup.....	60
6.6: Load setup.....	60
6.7: Instrumentation for short-span.....	61
6.8: Instrumentation for long-span.....	61
7.1: Representation of shear cracks in unstrengthened member.....	63
7.2: Shear cracks in unstrengthened member at failure.....	63
7.3: Sheets peeled off to reveal the shear cracks in an unanchored member.....	64
7.4: Peeling in unanchored member.....	65
7.5: Sheets peeled off to reveal the shear cracks in a strengthened member.....	65
7.6: Failure of the end anchored member due to anchor pull out.....	66
7.7: Load vs. Strain diagram of JS3A, JS5A & JS6A specimens.....	67
7.8: Load vs. Deflection curves of JS2A & JS4A members.....	69
7.9: Load vs. Deflection curves of JS3A & JS5A members.....	70
7.10: Load vs. Strain diagram of JS3 & JS5 specimens.....	71

7.11: Deflection curve of JS3A & JS5A members.....	71
7.12: Load vs. Rotation of JS3A & JS5A members.....	72
7.13: Load vs. Strain diagram of JS3A & JS2A specimens.....	73
7.14: Load vs. Strain diagram of JS4A & JS5A specimens.....	74
7.15: Load vs. Strain diagram of JS5A & JS6A specimens.....	75
7.16: Pictorial representation of shear cracks in unstrengthened member.....	77
7.17: Shear failure of unstrengthened members.....	77
7.18: Peeling failure in an unanchored member.....	78
7.19: Negative flexure failure.....	79
7.20: Negative flexure failure.....	80
7.21: Schematic representation of negative flexure cracks.....	80
7.22: Comparison of Load vs Deflection behavior of specimens JL1 & JL2.....	81
7.23: Comparison of Load vs Deflection behavior of all specimens.....	82
A1: Deflected shape of JS1A.....	87
A2: Deflected shape of JS1B.....	87
A3: Deflected shape of JS3A.....	88
A4: Deflected shape of JS3B.....	88
A5: Deflected shape of JS4A.....	89
A6: Deflected shape of JS4B.....	89
A7: Deflected shape of JS5A.....	90
A8: Deflected shape of JS5B.....	90
A9: Deflected shape of JS6A.....	91
A10: Deflected shape of JS6B.....	91
A11: Deflected shape of JL1A.....	92
A12: Deflected shape of JL1B.....	92
A13: Deflected shape of JL2A.....	93
A14: Deflected shape of JL2B.....	93
A15: Deflected shape of JL3A.....	94
A16: Deflected shape of JL3B.....	94
A17: Location of inclinometers for short and long-span members.....	95
A18: Inclinometer readings for JS1A.....	95

A19: Inclinometer readings for JS1B.....	96
A20: Inclinometer readings for JS3B.....	96
A21: Inclinometer readings for JS4A.....	97
A22: Inclinometer readings for JS4B.....	97
A23: Inclinometer readings for JS5A.....	98
A24: Inclinometer readings for JS5B.....	98
A25: Inclinometer readings for JS6A.....	99
A26: Inclinometer readings for JS6B.....	99
A27: Inclinometer readings for JL1A.....	100
A28: Inclinometer readings for JL1B.....	100
A29: Inclinometer readings for JL2A.....	101
A30: Inclinometer readings for JL2B.....	101
A31: Inclinometer readings for JL3A.....	102
A32: Inclinometer readings for JL3B.....	102
A33: Inclinometer readings for JL4A.....	103
A34: Inclinometer readings for JL4B.....	103
A35: Strain gage readings for JS3A.....	104
A36: Strain gage readings for JS3B.....	104
A37: Strain gage reading for JS5B.....	105
A38: Strain gage reading for JL3A.....	105
A39: Strain gage reading for JL3B.....	106
A40: Strain gage reading for JL4A.....	106
A41: Strain gage reading for JL4B.....	107
B1: Model bending moment curves for JS1.....	109
B2: Model bending moment curves for JS3.....	109
B3: Model bending moment curves for JS4.....	110
B4: Model bending moment curves for JS5.....	110
B5: Model bending moment curves for JS6.....	111
B6: Deflection Curves for Unstrengthened Beam.....	111
B7: Deflection Curves JS3.....	112
B8: Deflection Curves JS4.....	112

B9: Deflection Curves JS5.....	113
B10: Deflection Curves JS6.....	113
B11: Shear Force Curves JS1.....	114
B12: Shear Force Curves JS2.....	114
B13: Shear Force Curves JS3.....	115
B14: Shear Force Curves JS4.....	115
B15: Shear Force Curves JS6.....	116
B16: Shear Force Curves JL1.....	116
B17: Shear Force Curves JL2.....	117
B18: Shear Force Curves JL3.....	117
B19: Shear Force Curves JL4.....	118
C-1: T-beam cross-section.....	120
C-2: Shear diagram showing demand versus existing capacity.....	121
C-3: Final Shear Force Diagram.....	124

LIST OF TABLES

Table 2.1: Shear Strengthe Of RC Beams (Funakawa).....	7
Table 3.1: Resin properties in Tension.....	15
Table 3.2: Different strengtheing systems in the series JS.....	20
Table 3.3: Different strengthening schemes for the series JL.....	27
Table 4.1: Values obtained using design Equations.....	38
Table 5.1: Moment of inertia calculations.....	50
Table 5.2: Deflection values for JS3A using different approach.....	54
Table 6.1: Summary of instrumentation used during the test.....	57
Table 7.1: Experimental results of short-span joists.....	62
Table 7.2: Experimental results of long-span joists.....	76

NOTATIONS

a	Distance of the load from the nearest support, in
A_{fs}	Area of CFRP shear reinforcement = $2 t_f w_f$, in ²
A'_f	Area of CFRP in negative moment region, in ²
A_f	Area of CFRP in positive moment region, in ²
A_s	Area of steel in compression region, in ²
A'_s	Area of steel in tension region, in ²
B	Distance of the load from the far end support, in
b_w	Width of the web of beam cross section (ACI format), in
D	Depth from the top of the section to the tension steel reinforcement centroid, in
d_f	Effective depth of the CFRP shear reinforcement (usually equal to d for rectangular sections and $d-t_s$ for T-sections), in
E_f	Elastic modulus of FRP, ksi
f'_c	Nominal concrete compressive strength of concrete (ACI format), ksi
f_{fe}	Effective tensile stress in the FRP sheet in the direction of the principal fibers (stress level in the FRP at ultimate), ksi
f_{fu}	Ultimate tensile strength of the FRP sheet in the direction of the principal fibers, ksi
f_y	Yield strength of steel reinforcement, ksi
H	Total height of the T section, in
I	Moment of inertia of the member, in ⁴
I_{cr}	Cracked moment of inertia of the member, in ⁴
I_e	Effective moment of inertia of the entire beam, in ⁴
I_{em}	Moment of inertia at the mid-span, in ⁴
$I_{em1,2}$	Effective moment of inertia's at the ends, in ⁴
I_g	Gross moment of inertia of the member, in ⁴
JL	Long-span joist series
JS	Short-span joist series
L	Total span length, in
L_e	Effective bond length, in

M_a	Moment at support 'A', kip-in
M_b	Moment at support 'B', kip-in
M_{cr}	Cracking bending moment, kip-in
M_u	Factored bending moment at section, kip-in
$M_{u,exp}$	Experimental bending moment value, kip-in
$M_{u,th}$	Theoretical bending moment for any given load, kip-in
n_f	Modular ratio for fiber
n_c	Modular ratio for concrete
P	Applied load, lbs.
P_{max}	Ultimate load carried by CFRP sheet, lbs.
R	Reduction coefficient (ratio of effective average stress or strain in the FRP sheet to its ultimate strength or elongation)
S	Spacing of steel stirrups, in
s_f	Spacing of FRP strips, in
t_f	Thickness of the FRP sheet on one side of the beam, in
t_s	Slab thickness, in
V_c	Nominal shear strength provided by concrete, kips
V_f	Nominal shear strength provided by FRP shear reinforcement (ACI format), kips
V_n	Nominal shear strength (ACI format), kips
V_s	Nominal shear strength provided by steel shear reinforcement (ACI format), kips
V_u	Factored shear force at section (ACI format), kips
$V_{u,th}$	Theoretical shear strength for any given load, kips
$V_{u,exp}$	Experimental shear strength, kips
w_f	Width of FRP strip, in
w_{fe}	Effective width of FRP sheet, in
x	Any distance along the span of the member, in
y	Deflection at any point along the span, in
α	Angle between inclined stirrups and longitudinal axis of member
β	Angle between the principal fiber orientation and the longitudinal axis of the beam
Δ_d	Differential settlement at support 'A', in

Δ_{\max}	Maximum deflection , in
ϵ_{fe}	Effective strain of FRP, in/in
ϵ_{fu}	Ultimate tensile elongation of the fiber material in the FRP composite, in/in
ϕ	Strength reduction factor (ACI format)
ρ_f	FRP fraction area = $(2t_f / b_w) (w_f / s_f)$
ρ_w	Ratio of longitudinal reinforcement (ACI format)

1. INTRODUCTION

1.1 BACKGROUND

Shear collapse of reinforced concrete (RC) members is catastrophic and occurs suddenly with no advance warning. On several occasions existing RC members have been found to be deficient in shear. Deficiencies in shear can be due to insufficient shear reinforcement, use of outdated standards or codes, a reduction in the steel area due to corrosion, construction defects and increase in the service load due to change of the occupancy of the building.

Strengthening of reinforced concrete structures using externally bonded carbon FRP sheets is an effective method of improving the structural performance under both service load and ultimate load conditions. It is also a rather simple and economical approach to meet the increased load capacity of the structure. Use of composites offers several advantages like ease of bonding to curved or irregular surfaces and the fact that the fibers can be oriented in the desired direction. Lightweight, high stiffness, high strength and good durability of FRP make it an excellent choice for infrastructure strengthening. The conventional shear strengthening methods such as external/internal post tensioning, member enlargement along with internal transverse steel, and bonded steel plates are expensive, requiring extensive equipment, time and considerable displacement of resources. Various RC structural elements like joists, slabs and columns can be strengthened using externally bonded FRP sheets. The FRP sheets can be applied to the sides of the web of the joists, or wrapped around the columns to provide additional shear strength. In recent years several studies have been conducted to study the flexural strengthening of RC members, however, few have concentrated on shear strengthening (Khalifa, 1998).

1.2 SCOPE AND OBJECTIVES

The overall scope of this experimental study was to investigate the shear performance and modes of failure of the RC joists strengthened with externally bonded FRP sheets. Specific objectives included:

- a) To examine the effectiveness of FRP reinforcement in increasing the shear capacity of RC T-shaped members
- b) To compare the results of different systems of strengthening
- c) To validate design procedures

In order to fulfill these objectives, an experimental program was undertaken at the Malcolm Bliss Hospital in St. Louis, Missouri. The experimental program included testing of existing floor joists that were part of an integral floor system. These joists were isolated by saw cutting the floor slab along the longitudinal span. A total of twenty joists were thus isolated and tested to failure. These test specimens were broadly grouped into two series based upon their span lengths.

1.3 SUMMARY OF CONTENTS

Chapter 2 of this thesis contains a brief review of FRP materials and their applications to the structural engineering field. Research programs conducted to investigate the shear performance as well as to evaluate the shear capacity of strengthened concrete members are surveyed. Details of various shear-strengthening schemes are explained.

Chapter 3 describes the materials and the installation process for the members strengthened in the field.

Chapter 4 discusses the design Equations used for calculating the shear capacity of the RC beams strengthened with externally bonded FRP. A summary of the design values for all the members is tabulated in this chapter.

Chapter 5 describes an analytical approach undertaken to determine the internal forces developed during the experimental program. A model has been developed for the analysis of the experimental data.

Chapter 6 discusses the test setup, instrumentation and the testing method used during the experimental program.

Chapter 7 contains the experimental test results. The observed crack pattern and the failure modes are detailed in this chapter. In addition, a comparison of the test results attributed to each mode of failure is also presented in this chapter.

Chapter 8 provides the concluding remarks and recommendations for future work. Three appendices attached to this thesis contain, Appendix A consists of figures documenting the load-deflection response of the joists investigated within the context of this study. In addition, the strain gage and inclinometer readings acquired from the data acquisition during testing is also reported.

Appendix B presents the shear forces from the design, the analytical model and the experimental results for all the members at failure load.

Appendix C presents a design example in which the shear capacity is calculated for a member strengthened with FRP sheets.

2. LITERATURE REVIEW

2.1 GENERAL

In the last decade, the use of FRP composites to reinforce concrete members has emerged as one of the most promising technologies in material/structural engineering. There is a wide range of applications for FRP reinforcement that covers new construction as well as rehabilitation of existing structures. This section provides information on FRP materials and their applications in structural engineering and focuses on shear strengthening of RC beams with externally bonded FRP composites. The research programs conducted to investigate the shear performance and to evaluate the shear capacity of the strengthened beams are reviewed.

2.2 DEFINITION OF FRP

FRP composites consist of high strength fibers (carbon, glass and aramid) embedded in a polymer resin. All these fibers are available commercially as continuous filaments. The fibers are the main load-carrying element and have a wide range of strengths and stiffnesses with a linear stress-strain relationship up to failure.

The fibers are impregnated with a polymer resin, which in turn surrounds and binds the fibers together. The resin acts as a protective coat on the fibers against possible damage. The resin also helps in maintaining the alignment of the fibers thus ensuring a uniform distribution of the load through them. Polymers are available in two categories: thermosetting polymers (e.g. epoxy and polyester) and thermoplastic polymers (e.g. nylon).

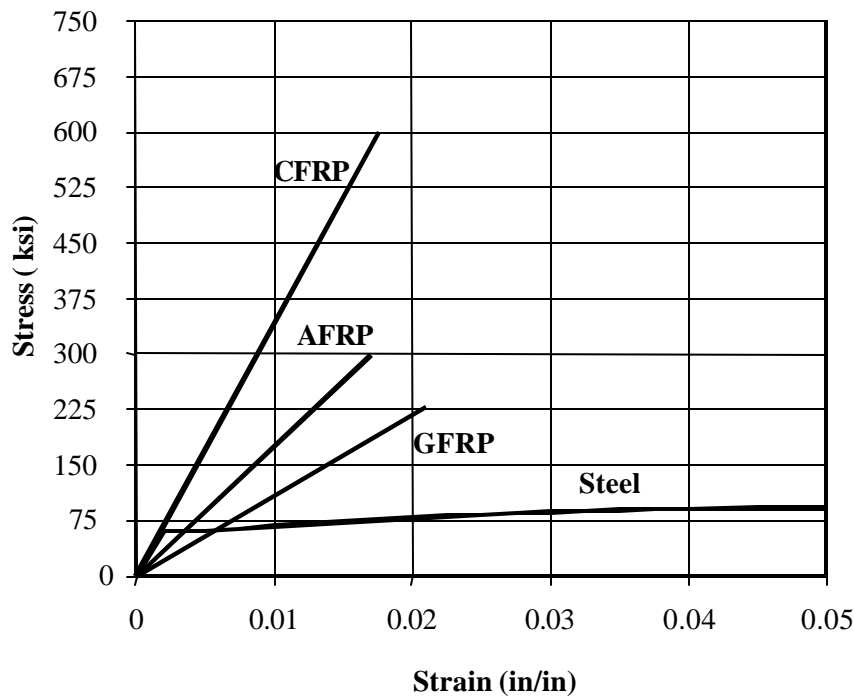


Figure 2.1: Comparison among CFRP, AFRP, and GFRP sheets and reinforcing steel in terms of stress-strain relationship

FRP composites have become more popular and widely accepted by designers, contractors, and owners due to combinations of their unique characteristics. FRP composites have significantly higher strength-to-weight ratio than metals and other construction materials. In addition, these materials are non-corrosive, non-magnetic, and generally resistant to chemicals. A comparison among carbon FRP, aramid FRP (AFRP), and glass FRP (GFRP) sheets (based on fiber area only), and reinforcing steel in terms of stress strain relationship is illustrated in Figure 2.1.

2.3 APPLICATION OF FRP IN STRUCTURAL STRENGTHENING

The initial developments of FRP-strengthening techniques were initiated in 1987, in Switzerland, under the leadership of Meier (1987). It was there that the first on-site repair by externally bonded FRP took place in 1991. Since then, strengthening by externally bonded FRP composites has been studied worldwide. The sudden increase in the use of FRP composites was attained after the 1995 Hyogoken Nanbu Earthquake in

Japan. By 1997, more than 1,500 concrete structures worldwide had been reinforced with externally bonded FRP composites.

Strengthening with externally bonded FRP reinforcement has been shown to be applicable to many types of RC structures. Currently, this method has been implemented to strengthen such structural elements as columns, beams, slabs, walls, chimneys, tunnels, and silos. The uses of external FRP reinforcement may be generally classified as flexural strengthening, improving the confinement and ductility of compression members, and shear strengthening. Although several studies have been conducted to investigate the flexural strengthening of RC members with externally bonded FRP reinforcement, studies on shear strengthening have been limited.

2.4 SHEAR STRENGTHENING OF RC BEAMS USING FRP

This section presents some of the published research studies regarding the shear strengthening of RC members with externally bonded FRP reinforcement.

Some researchers have studied RC beams strengthened with externally bonded fiber sheet in the past decade. Detailed experimental and analytical studies have been undertaken in the past. Some of these studies have been described in the following paragraphs.

Arduini, et al. (1997) carried out experiments on double span beams subjected to two concentrated loads. These beams were strengthened with CFRP sheets. The parameters under consideration were the RC cross-section and the number and position of the sheets. They concluded that premature debonding and shear failure of the concrete cover near the position of flexure cracks reduced the stiffness of the beams. They also concluded that in case of deep beams large cracks appear and spread in a typical punching mechanism at the central support 'A't high loads. But for flat beams the addition of CFRP can increase the initial stiffness only.

Funakawa, et al. (1997) carried out an experimental study of continuous beams strengthened with fiber sheets. They studied four specimens, wrapped with FRP sheets. The variables were the type of sheets and number of sheets. They concluded that the number of sheets greatly influenced the shear strength of the RC beams. Table 2.1

summarizes the results observed in their experiment work. They concluded that with the increase in the number of plies the shear strength of the member also increased proportionally. Also at higher percentage of FRP reinforcement the experimental values tended to be overestimated. This in turn affected the failure mode. At low percentages the failure was due to fiber rupture, but as the percentage of FRP reinforcement increases the failure is without fiber rupture.

Table 2.1: Shear Strength of RC Beams (Funakawa)

Specimen	Number of FRP Sheets	% Gain in Shear Strength
S1	0	0.0
S2	1	5.6
S3	2	11.1
S4	3	16.7

Taerwe, et al. (1997) studied the behavior of RC beams strengthened in shear by external application of CFRP sheets. Seven full-scale, RC beams were tested under four point bending. Vertical strains were measured using electrical strain gages. Also beam deflections, flexural strain at midspan and crack pattern were also measured. Two beams were taken as control specimens. The predominant failure mode observed was failure due to peeling. The presence of CFRP strips increases the shear strength of the beams. They concluded that the contribution of stirrups to shear resistance decreases due to the presence of CFRP sheets. The peeling of sheets was attributed due to insufficient anchorage length.

Umezu, et al. (1997), carried out an extensive experimental program in order to determine the effects of aramid and carbon FRP sheets on the shear capacity of simply supported RC beams. They used total wrap as strengthening schemes for all their test beams. Most of the test specimen exhibited failure due to peeling of CFRP sheets. They observed that beams strengthened with aramid or carbon show a tendency for simultaneous shear failure & sheet failure at low loads. The application of FRP sheets was found to enhance shear capacity and deformation characteristics. In their analysis, they stated that the contribution of AFRP to shear capacity could be evaluated by the

truss theory, based on an average stress of AFRP equal to the tensile strength of the sheet multiplied by a reduction coefficient determined from the test results.

Sato, et al. (1997) studied the resisting behavior of reinforced concrete beams with CFRP sheets. They studied the failure mode and also the stiffness of the beam strengthened with CFRP sheets. Beam strengthened with end anchors showed greater stiffness compared to the beam without end anchors. They observed that the delamination of sheets affected not only the stiffness of the beam but also the ultimate shear strength of the specimens. The beams strengthened with mechanical anchorage were more effective as the bond strength of CFRP sheet with the bond anchorage is greater than that without the mechanical anchorage.

Araki, et al. (1997) conducted experiments of the beams strengthened with “continuous fiber sheets” on existing RC beams. Thirteen beams were strengthened with different schemes and tested under unsymmetric moment condition. They concluded that that the shear capacity increased in proportion to the amount of sheets. They also concluded that as the amount of CFRP sheets increased the displacement attained under maximum load also increased.

Saadathmanesh and Ehsani (1991) studied RC beams strengthened with glass fiber reinforced plastic (GFRP) plates to their tension faces. Some important conclusions were drawn from his research; for instance, the gain in the ultimate strength was more significant in beams with lower steel reinforcement ratio. Also, the presence of the plates reduced the crack size in the beams; however, the ductility was reduced.

From the review of the literature, it is evident that all these experimental studies focussed on the capabilities of externally bonded FRP composites to enhance the shear capacity of RC beams and investigation of the possible failure modes. Further more all these experimental works were carried out in the lab. These specimens were tested as simply supported members, subjected to single/multiple point loads. A relatively good agreement between the model and the experimental results can be attributed to the fact that the same set of that is used for calibration and comparison.

The design Equations that have been arrived at are a result of exhaustive experimental work carried out by numerous researchers in the laboratories over the past decade. All these test specimens were tested as simply supported members in

laboratories. The usefulness/validity of these design Equations will depend on how closely the experiments and design/predicted values agree with each other. Any further refinement of the existing design Equations must be based on data collected from the field. A better interpretation of the structural behavior will enable us to attain a realistic design approach. Based on the present level of experimental knowledge and the above review, it can be concluded that more field experimental and analytical work is needed to investigate the performance and factors affecting the shear capacity of strengthened beams, and to propose a better and more rational design approach.

2.5 SHEAR STRENGTHENING OPTIONS

2.5.1 GENERAL

In shear strengthening situations of RC beam, externally bonded FRP reinforcement is used to wrap the beam cross section with the fibers in the transverse direction in order to reinforce diagonal tension cracks in much the same way as steel stirrups. From this general approach, several configurations of FRP shear reinforcement have been devised and investigated. The goal of this section is to describe several alternatives that are available to the designer.

2.5.2 BONDED SURFACE CONFIGURATIONS

In shear strengthening situations of RC beams, three options of FRP bonded surface configurations, as shown in (Figure 2.2), have been investigated (Nanni, 1993). The first option is to apply the FRP reinforcement on both sides of the beam. The effectiveness of this configuration is limited due to possible debonding failure of the FRP reinforcement. The second option is to wrap the sides and bottom of the beam, U-wrap. The U-wrap is practical and is relatively effective in increasing the shear capacity of the beams (Sato, 1997). However, when the shear cracks develop at approximately 45 degree, the FRP reinforcement (U-wrap) may have minimal bonded length near the compression flange of a T-section, usually leading to a premature failure due to debonding. This situation is even more critical in negative moment regions as cracks

develop from the topside of the member. It has been found that fully wrap or U-wrap with end anchor is the alternative solution for U-wrap if debonding is to be avoided. (Sato, 1997). However, total wrap is not practical from a constructability standpoint. The presence of monolithic slabs often prevents wrapping the sheet around the top of the section. One option might be to drill holes through the slab and wrap strips of FRP around the section. However this method is rather complicated. On the other hand, it has been shown that the anchorage of the ends of U-wrap is practical and effective (Sato, 1997)

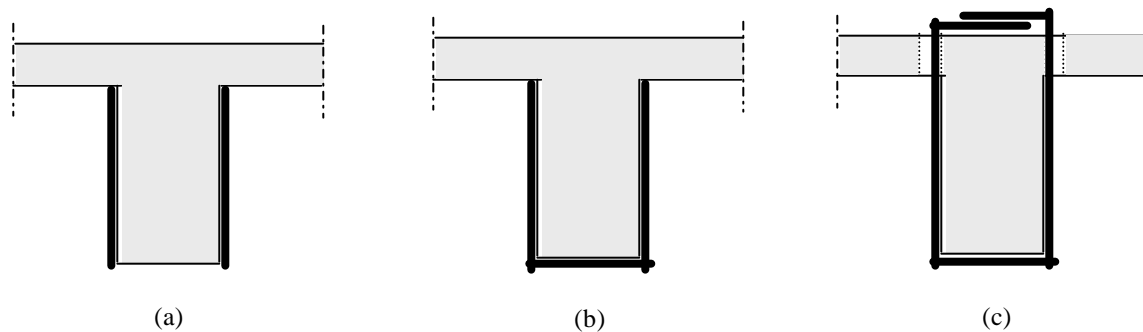


Figure 2.2: Various schemes for wrapping transverse FRP reinforcement (a) FRP bonded to the two beam sides (b) FRP “U” wrap (c) FRP wrapped entirely around the beam

2.5.3 END ANCHOR

It has been shown that the anchorage of the ends of the sheets with steel plates and bolts is effective and can increase the shear capacity of RC members (Figure. 2.3). In the case of U-wraps, it was observed that anchoring increased the shear capacity by about 20% above that of specimens with no end anchorage. By using this technique and testing specimens under a cyclic load, Sato et al. (1997) showed that the seismic retrofitting of RC beams using FRP sheets becomes practical and efficient. Mechanical anchors made of steel, although effective in the laboratory are not very practical for field application due to drawbacks such as stress concentration and, in the case of bolting, discontinuity of the FRP at drilling locations. In the case of carbon FRP, the likelihood of galvanic corrosion due to steel-carbon fiber contact is also a concern.

In order to eliminate the problems associated with traditional anchors, an innovative anchoring system was proposed using FRP materials only. A system called U-anchor was used as an end anchoring method.

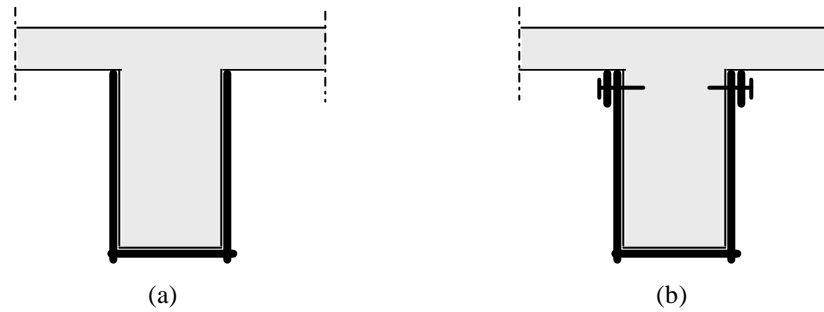


Figure 2.3: End anchor options (a) U-wrap without end anchor (b) U-wrap with end anchor

2.5.4 SHEAR REINFORCEMENT SPACING

The transverse FRP reinforcement may be in the form of a continuous wrap or as spaced strips as illustrated in Figure 2.4. The use of strips may be effective in optimizing the amount of material used.

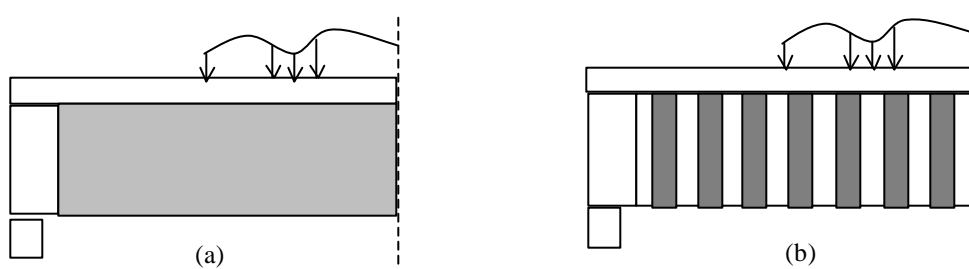


Figure 2.4: Shear reinforcement distributions (a) Continuous (b) Strips

2.5.5 FIBER ORIENTATION

Because FRP is an anisotropic material with high strength in the direction of the fibers, the fibers may be oriented in such a way to best reinforce diagonal tension cracks. This is achieved by the use of inclined strips (Figure 2.5). However, vertical plies are easier to install just as in the case of vertical and inclined stirrups.

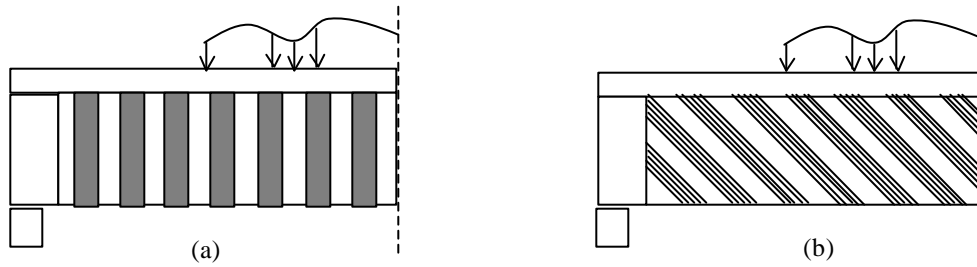


Figure 2.5: Fiber orientation (a) 90° wrap (b) 45° wrap

3. EXPERIMENTAL PROGRAM

3.1 GENERAL

The experimental approach in this study consisted of testing twenty, full-scale, RC T-joists. The T-joists were grouped into two series designated as JS (short-span joist) and JL (long-span joist) based on their span lengths. Series JS members had a clear span of 104-in (2641-mm). Series JL members had a clear span of 300-in (7620-mm). The short-span members were designed and constructed without any shear reinforcements. However the long-span members were constructed with a flare extending to a distance of 36-in (914-mm) at the inner support. This flare was provided to add additional shear capacity to the member at the inner support.

The floor consisted of a one-way continuous slab system. The transverse clear distance between the web of the neighboring joists was 20-in (510-mm). The test members consisted of T-sections with a flange width of 26-in (660-mm). These members were sawcut at the centerline between the joists to isolate individual member during testing. The web had a width of 6-in (152-mm). Saw cutting was required, as it would be impossible to fail the joist, which was built as an integral part of a floor system. The members were tested to failure by applying unsymmetric moments. The load was applied closer to one of the supports so as to develop high shear at one end.

3.2 MATERIALS

3.2.1 CONCRETE

As this research was carried out on an existing structure, the compressive strength of the concrete was determined by testing sample cores acquired from different locations of the building. These cores were 3.2-in in diameter and 6-in in length (80x150-mm). The average concrete strength was found to be 3000-psi (20.68-MPa). The strength of the concrete for design purposes was estimated by taking into

consideration the factors effecting the core strength namely, aspect ratio, and coring effects

Aspect ratio:

Based on the aspect ratio the strength was estimated using Chung's (ASTM, 1989) Equation. He stated that the core strength varies, based on the l/d ratio of the specimens. Chung proposed an Equation for l/d correction factors from 2.0 to 0.4. The l/d ratio for these specimens was close to 2.0, thus the correction factor was found to be negligible.

Coring effects:

The drilling operations can damage some of the bond between the cut aggregate-paste interface or dislodge coarse aggregates, possibly reducing the cores compressive strength.

As per ACI 318-99 (5.6.5.4), concrete in an area represented by core tests shall be considered structurally adequate if the average of three cores is equal to at least 85 percent of f_c ?, and no single core is less than 75 percent of f_c ?. Based on this the estimated concrete strength is calculated to be $3000/0.85 = 3529$ -psi (24.33 MPa).

For all design purposes the concrete strength was taken to be 3500-psi (24.13-MPa).

3.2.2 STEEL REINFORCEMENTS

The longitudinal reinforcement consisted of high strength steel rebars. Reinforcement of the members of series JS consisted of 2-#4 (12.7-mm dia.) and 2-#6 (19-mm dia.) diameter bars. The reinforcements used in the series JL were 2-#10 (32-mm dia.) diameter bars. The reinforcement data was obtained from the construction documents. As per the building specifications A-15 grade steel reinforcements was used. For all design purposes the yield strength of steel was taken to as 50-ksi (344-MPa) and modulus of elasticity was taken to be 29000-ksi (200,000-MPa).

3.2.3 COMPOSITE STRENGTHENING SYSTEM

The composite strengthening system consists of the following elements: putty, primer, saturant and composite fiber sheets.

Resins: The fibers were bonded to the concrete surface with the help of three epoxy-based resins. The resins were the primer, putty and the saturant. The mechanical properties of these materials, as reported by the manufacturers (Master builders, 1998) are summarized in Table 3.1.

Table 3.1: Resin Properties in Tension

Material	Stress at yield (ksi)	Stress at rupture (ksi)	Strain at yield (in/in)	Strain at rupture (in/in)	Elastic modulus (ksi)	Poisson's ratio
Primer	2.1	2.45	0.040	0.040	103.7	0.48
Putty	1.9	2.1	0.020	0.070	259.6	0.48
Saturant	7.8	7.9	0.025	0.035	440.2	0.40

Conversion factor: 1-in = 25.4-mm, 1-ksi = 6.895 MPa

Carbon and Aramid Fiber Sheets: The carbon sheets used in this program were in the form of dry unidirectional flexible sheets. The sheets had a paper backing and were supplied in a roll of 20-in (500-mm) width. The carbon fibers were manufactured (Master builders, 1998) by pyrolyzing polyacrylonitrile (PAN) based precursor fibers at temperatures of approximately 2732^oF (1500^oC). The result of polymerization process was a highly aligned carbon fiber chain. The carbon fiber filaments were assembled into untwisted tows that were then used to create a continuous unidirectional sheet.

The tensile strength, modulus of elasticity and thickness of CFRP sheet as reported by the manufacturers are 550-ksi (3790-MPa), 33067-ksi (228,000-MPa) and 0.0065-in (0.165 mm (fiber only)), respectively.

GFRP rods: #4 GFRP rods were used for anchoring the sheets. The modulus of elasticity and ultimate tensile strength as reported by the manufacturers (Marshall Industries) are 6-ksi (42-MPa) and 116-ksi (800-MPa), respectively.

3.3 INSTALLATION PROCESS

FRP sheets were attached to the concrete surface by manual lay-up. The components of strengthening system are illustrated in Figure 3.1.

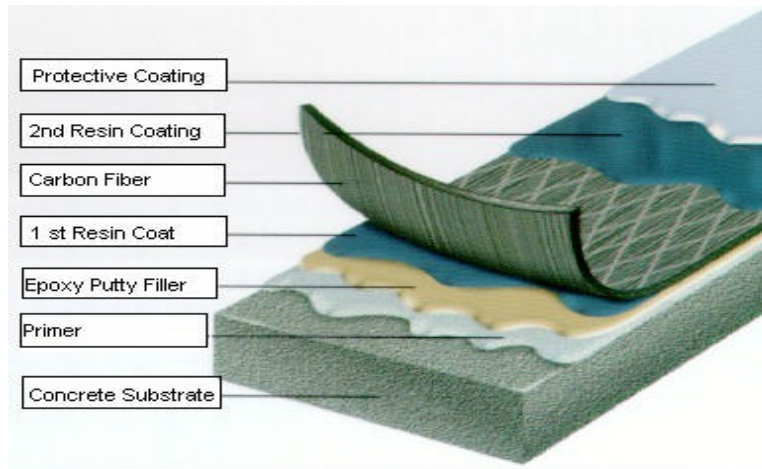


Figure 3.1: Components of the strengthening system

The procedure employed to apply the FRP sheets can be summarized as follows:

- Prior to the strengthening of each joist, the surface was prepared by chipping (Figure 3.2) and grinding of uneven locations. The joist was sand blasted with crystalline silica, having an effective size at filtration of 0.00984-in (0.25-mm), with an air pressure of 75/100-psi (517/689.5 MPa). The sand blasting removes the loose particles, and increases the roughness of the surface. Increased roughness improves the bond characteristics of the FRP sheets with the concrete surface.



Figure 3.2: Chipping

- The prepared concrete surface was then coated with a layer of epoxy-based primer (Figure 3.3) using a short nap-roller and allowed to cure for 4-hrs. The function of the primer is to penetrate the concrete pores to provide an improved adhesive bond for the saturating resin.



Figure 3.3: Application of primer

- After the primer has become tack-free, a thin layer of putty, a thick epoxy-based paste (Figure 3.4) was applied using a trowel. The putty was allowed to cure for 4 hrs. The function of the putty is to level the surface and to patch the small holes. This step is not required when a smooth/even surface is already present.



Figure 3.4: Application of putty

- After the putty has become tack-free, the first coat of saturant resin was applied using a medium nap roller. The function of the saturant resin is to impregnate the dry fibers, to maintain the fibers in their intended orientations, to distribute stress to the fibers, and to protect the fibers from abrasion and environmental effects
- The FRP sheets were measured and cut to the desired dimensions. Each sheet was then placed on the concrete surface and gently pressed into the saturant. Care must be taken to see that the FRP is not damaged during this entire process. Prior to removing the backing paper, a trowel was used to remove any air bubbles. After the backing paper was removed, a ribbed roller was rolled in the fiber direction to facilitate impregnation by separating the fibers (Figure 3.5).
- Finally the FRP is coated with another layer of the saturant, and allowed to cure. The recommended minimum curing period is 24-hr prior to allowing a strengthened component or system back into service.



Figure 3.5: Rolling of FRP sheet after the application of saturant

The end anchors were applied as stated below:

- Grooves are made at the intersection of the web and the flange. The grooves are of square cross-section (Figure 3.6) with the dimensions of one and a half times the diameter of the rod. Number four deformed GFRP rods were used as end anchors.

- Before installing the rods, the fiber sheets were bonded to the groove during the wet lay-up process. Then each groove was filled halfway with a high viscous epoxy paste (Figure 3.7).



Figure 3.6: Grooves for end anchor

- The FRP rods are thrust into the groove. The remaining of the groove was filled with the paste.



Figure 3.7: Application of epoxy paste to hold the end anchors

3.4 DESCRIPTION OF RC MEMBERS AND STRENGTHENING SCHEMES:

The strengthening can be broadly classified into two schemes depending on the span lengths of the members. The short-span strengthening scheme and the long-span strengthening scheme.

3.4.1 SHORT-SPAN STRENGTHENING SCHEME

The short-span series consisted of twelve members, representing six systems. Each system consisted of two members. The strengthening was provided to increase the shear capacity. The positive and negative strengthening was provided to prevent the flexural mode of failure. Various strengthening schemes used for strengthening the short-span series are summarized in Table 3.2.

The following paragraphs briefly explain the various strengthening systems for the short-span members.

Table 3.2: Different Strengthening Systems for Series JS

Member ¹	External strengthening				
	FRP type	Schemes			
		Shear		Positive flexure (4-in wide ply)	Negative flexure (20-in wide ply)
		No. of plies	Anchor		
JS1		0	No	--	--
JS2	Carbon	1	No	1	1
JS3	Carbon	1	Yes	1	1
JS4	Carbon	2	No	3	2
JS5	Carbon	2	Yes	3	2
JS6	Aramid	2	Yes	3	2

¹Each member consisted of two specimens.

Conversion factor: 1-in = 25.4-mm

Figure 3.8 illustrates the location of the short-span members in the building. The test members were located on the third and fourth floor of a five-story building.

Specimens JS1 consisted of two unstrengthened members that were selected as control specimens (Figure 3.9).

The specimens of JS2 (Figure 3.10) were strengthened with one-ply continuous shear wrap of high tensile strength CFRP sheets with the fiber direction oriented perpendicular to the longitudinal axis of the specimen. The positive flexure region was strengthened with a 4 in (102-mm) wide sheet at the soffit of the web (Figure 3.11). Strengthening for negative flexure region was provided with 20-in (510-mm) wide CFRP sheets centered on the flange.

The specimens of JS3 (Figure 3.12) were strengthened for shear with one-ply continuous shear wrap, which were anchored (Figure 3.13) using glass rods. The positive and negative strengthening was provided as described for specimen JS3.

The specimens of JS4 (Figure 3.14) were strengthened with two continuous shear wrap of high tensile strength CFRP sheets. The positive strengthening consisted of three 4-in (102-mm) wide CFRP sheets and the negative strengthening consisted of two 20-in (2-510-mm) wide CFRP sheets. The sheets were applied in alternate layers for the positive and the shear reinforcement.

The specimens of JS5 (Figure 3.15) were strengthened two continuous shear wrap CFRP sheets. These sheets were anchored with the help of glass rods. The positive strengthening consisted of three 4 in (3-102-mm) wide CFRP sheets and the negative strengthening consisted of two 20-in (2-510-mm) wide CFRP sheets. The sheets were applied alternatively for the positive and the shear reinforcement.

The specimens of JS6 were strengthened with aramid sheets, the strengthening scheme was similar to that of specimen JS5.

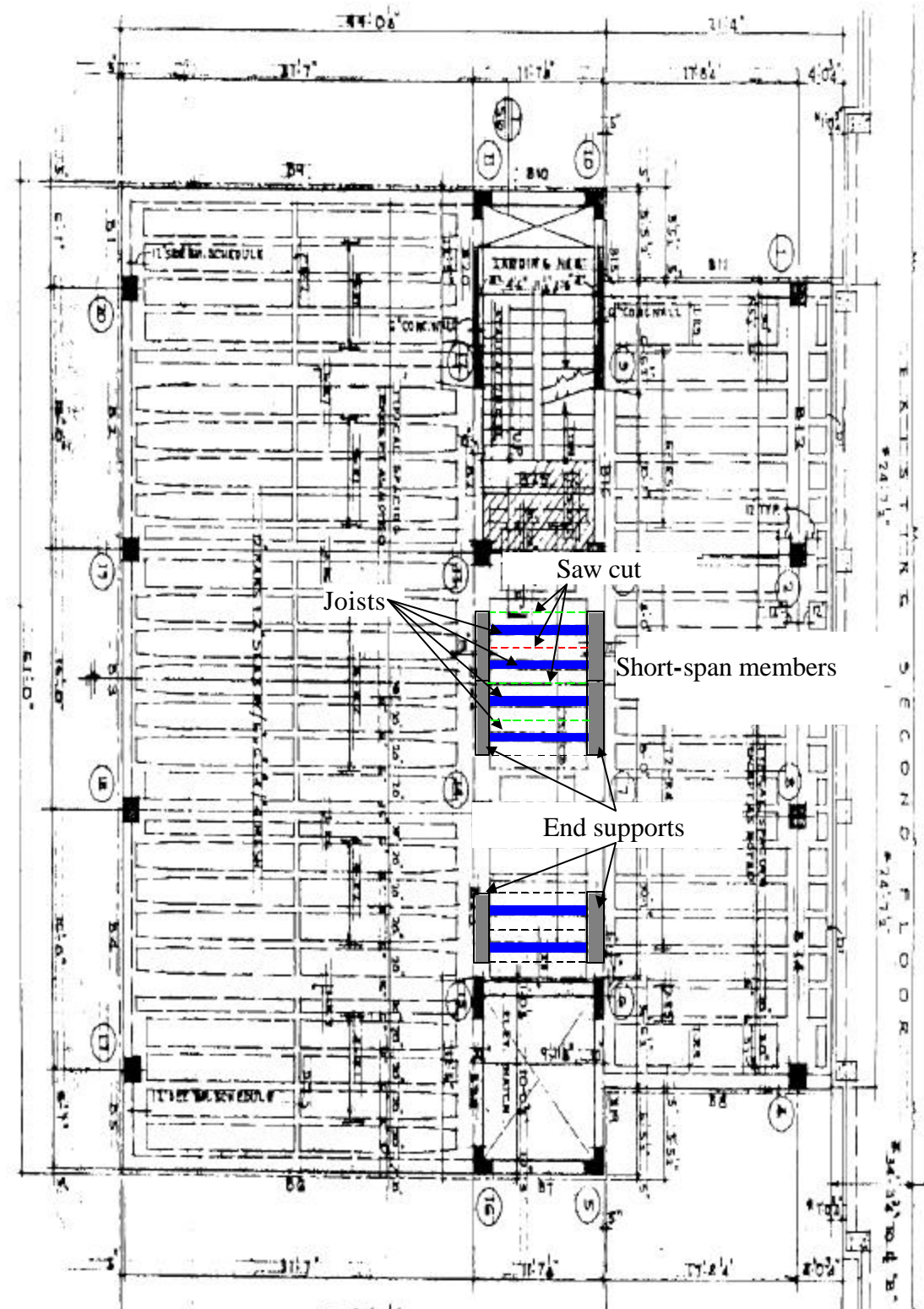


Figure 3.8: Layout plan of the test specimen

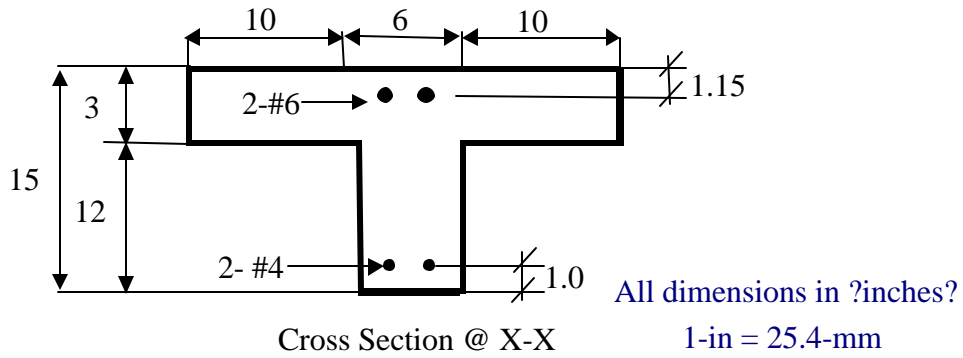
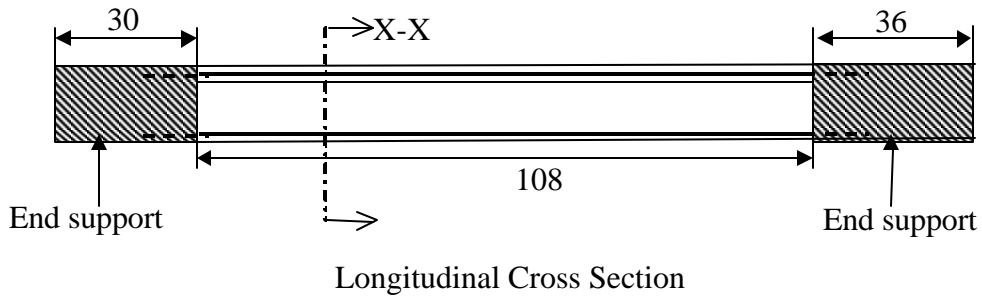


Figure 3.9: Specimen JS1 (Unstrengthened)

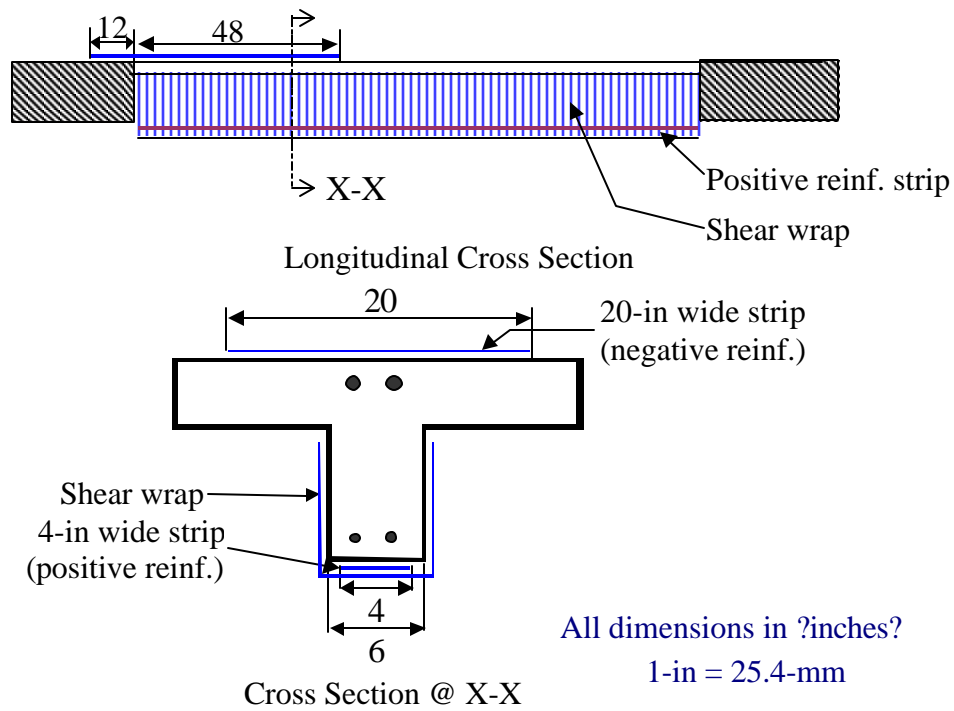


Figure 3.10: Specimen JS2 (Single shear wrap)

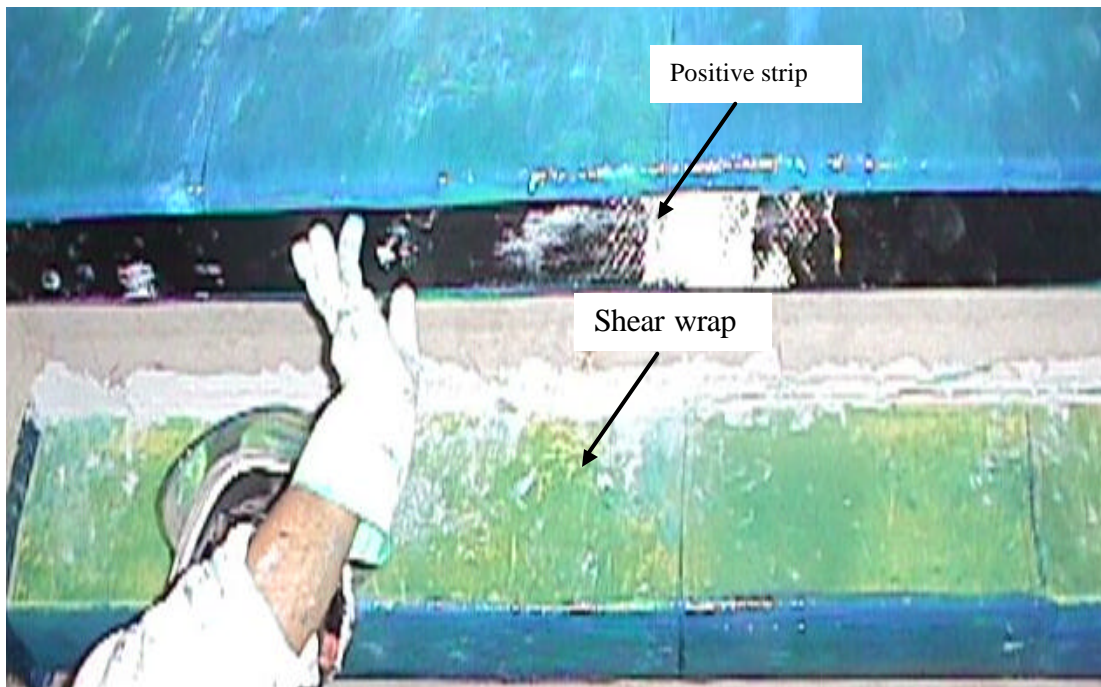


Figure 3.11: Shear wrap and positive strip

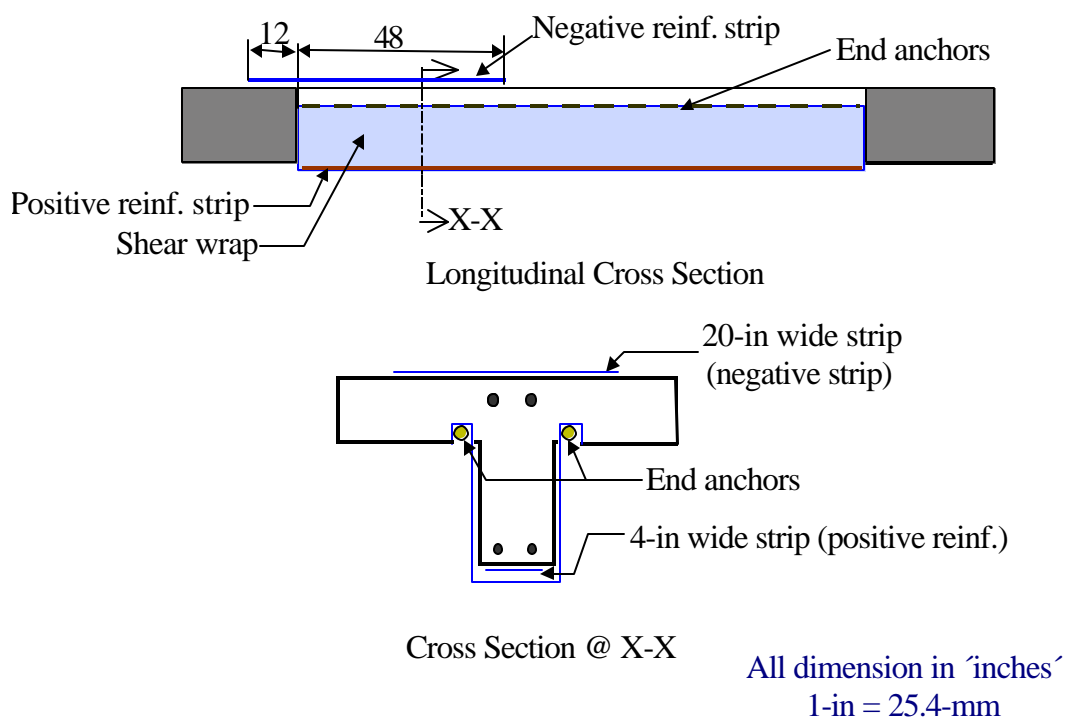


Figure 3.12: Specimen JS3 (Single shear wrap with end anchor)

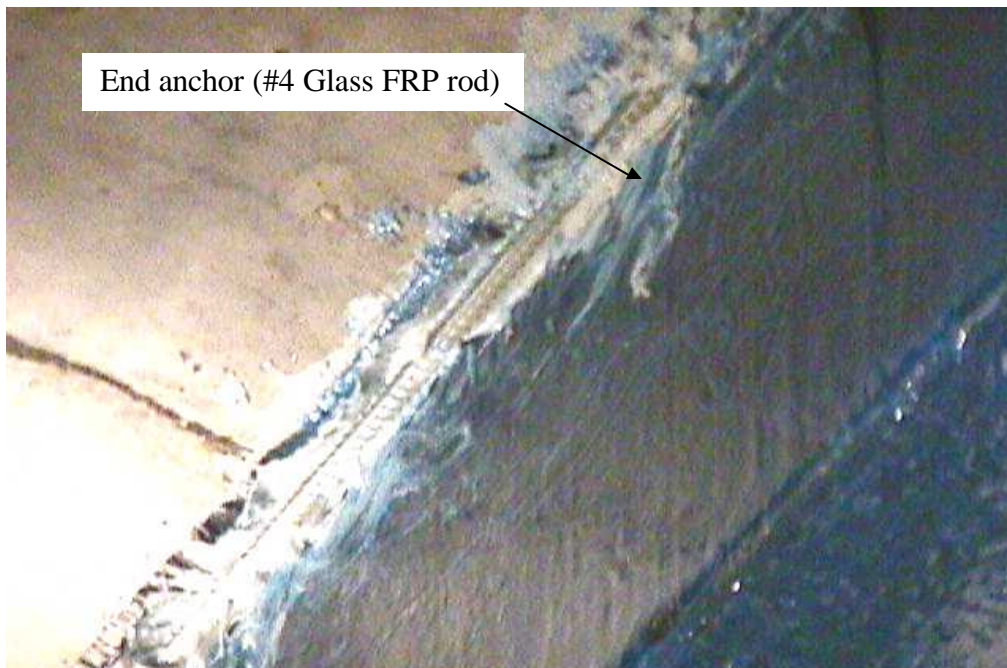


Figure 3.13: Single shear wrap with end anchor

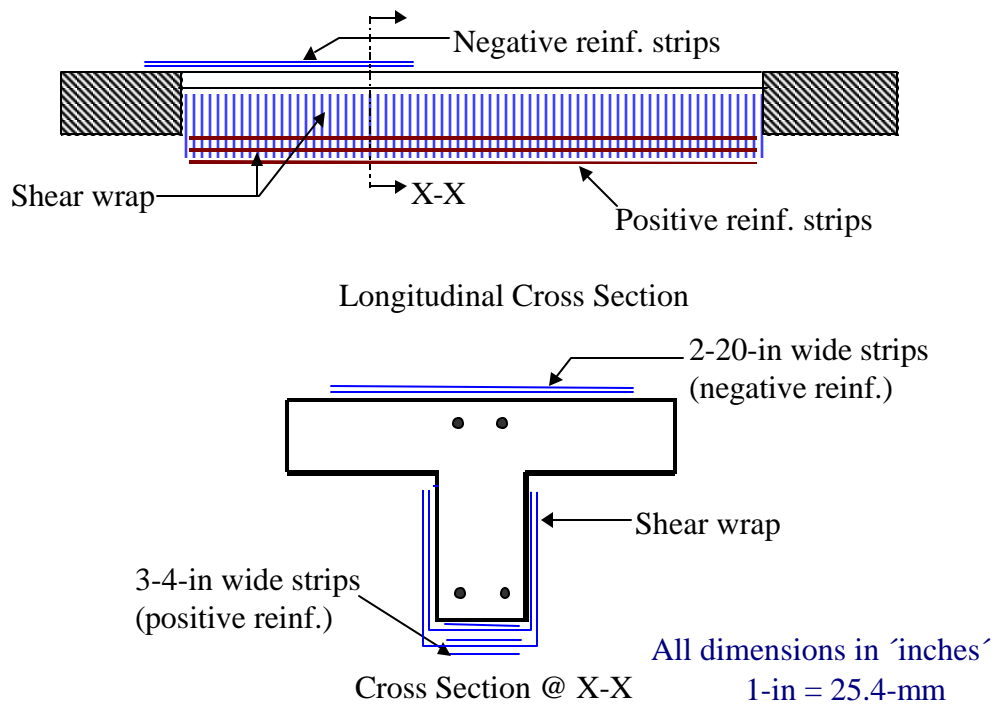


Figure 3.14: Specimen JS4 (Double shear wrap without end anchors)

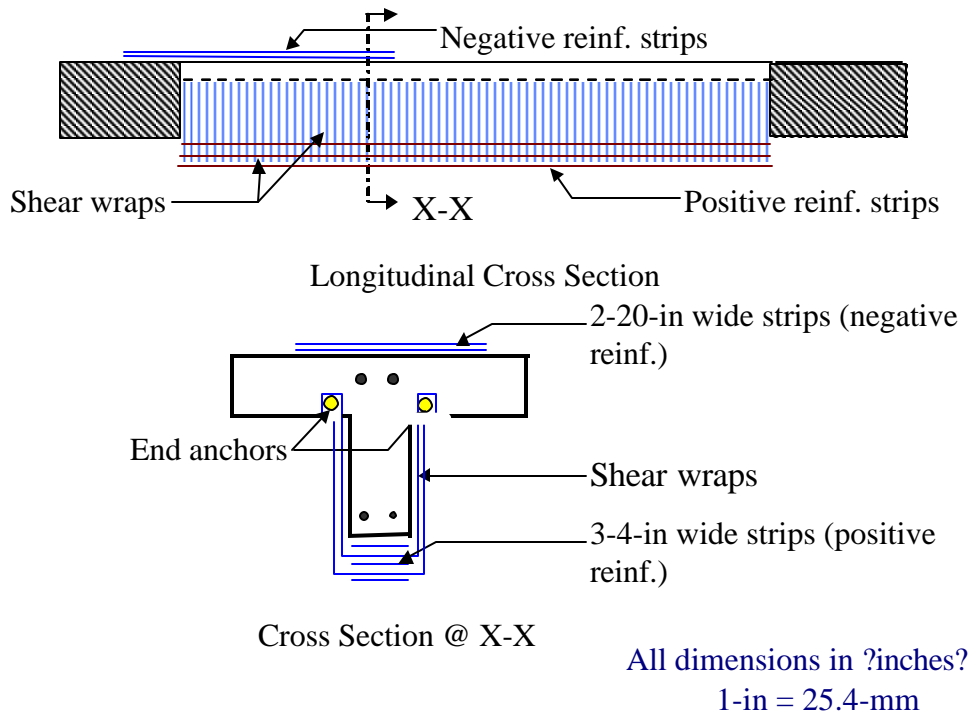


Figure 3.15: Specimen JS5/JS6 (Carbon/Aramid- double shear wrap with end anchors)

3.4.2 LONG-SPAN STRENGTHENING SCHEME

The long-span series (JL) consisted of eight members constituting four systems. Two specimens from the series JL were left unstrengthened as control members. The remaining six specimens were strengthened with externally bonded CFRP sheets. Various strengthening schemes used for strengthening the long-span series are summarized in Table 3.3.

Figure 3.16 illustrates the location of the long-span members in the building. The test members were located on the third and fourth floor of a five-story building.

Specimens of JL1 consisted of two unstrengthened members, which were used as control specimens (Figure 3.17). The remaining members were strengthened with different strengthening systems.

Specimens of JL2 (Figure 3.18) were strengthened with one-ply continuous shear wrap of high tensile strength CFRP sheets with the fibers oriented in the direction

perpendicular to the longitudinal axis of the specimen up to a distance of 96-in (2440-mm) from the near-end support¹.

Specimens of JL3 (Figure 3.19) were strengthened with one-ply continuous shear wrap of high tensile strength CFRP sheets with fibers oriented in the direction perpendicular to the longitudinal axis of the specimen up to a distance of 96-in (2440-mm) from the end support. The negative flexural strengthening of the member closer to the loading end was done using CFRP sheets.

The specimens of the JL4 (Figure 3.20) were strengthened with a continuous shear wrap up to a distance of 96-in (2440-mm) from the near-end support. The sheets were anchored using #4 deformed glass rods.

Table 3.3: Different Strengthening Systems for Series JL

Member ²	External Strengthening			
	CFRP type	Schemes		
		Shear		Negative flexure No. of plies (20-in wide ply)
		No. of plies	Anchors	
JL1	---	0	No	0
JL2	Carbon	1	No	0
JL3	Carbon	1	No	1
JL4	Carbon	1	Yes	2

² Each member consisted of two specimens.

Conversion factor: 1-in = 25.4-mm

¹ Support in close proximity to the point of applied loading.

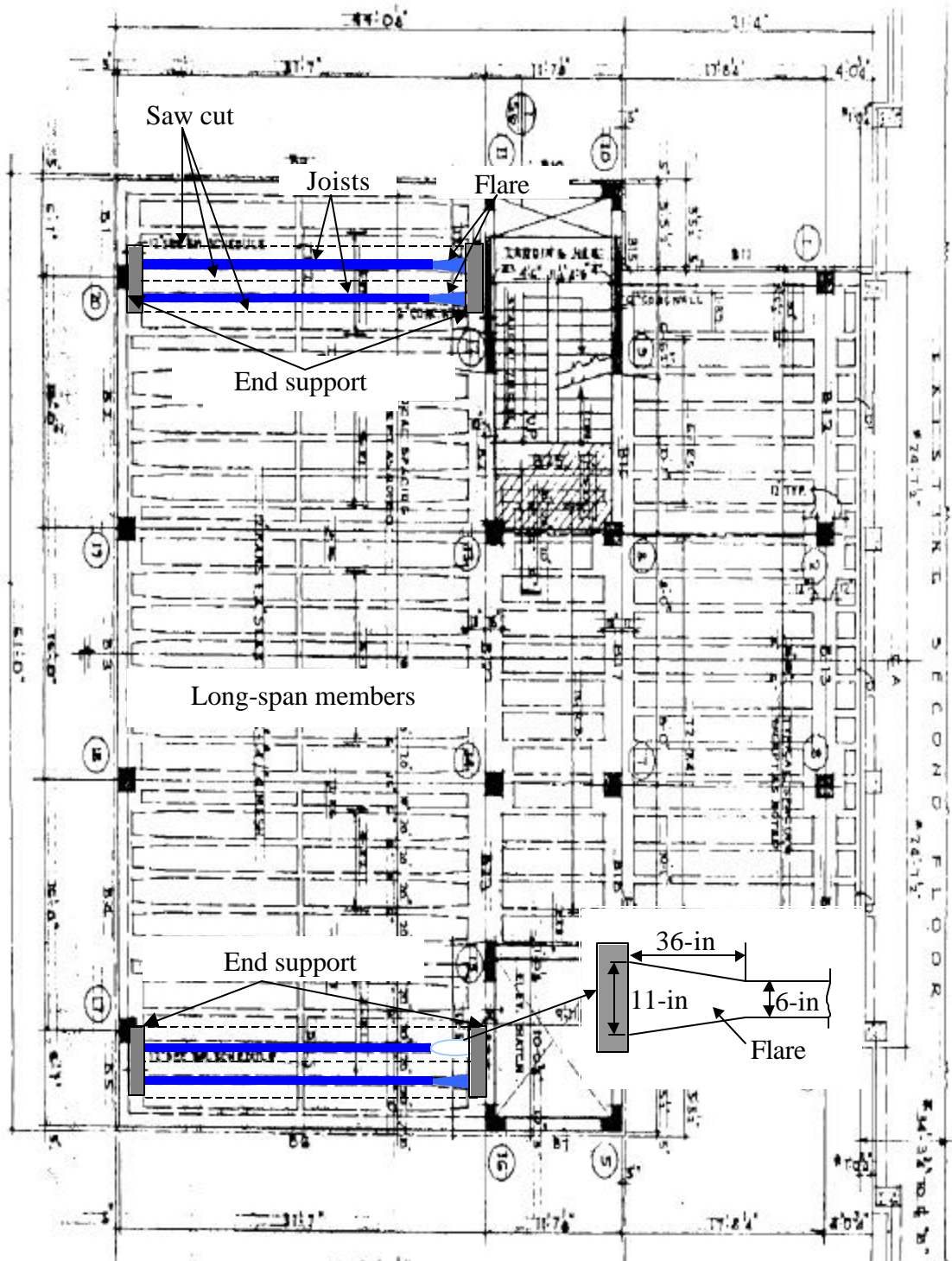


Figure 3.16: Layout plan of the test specimen

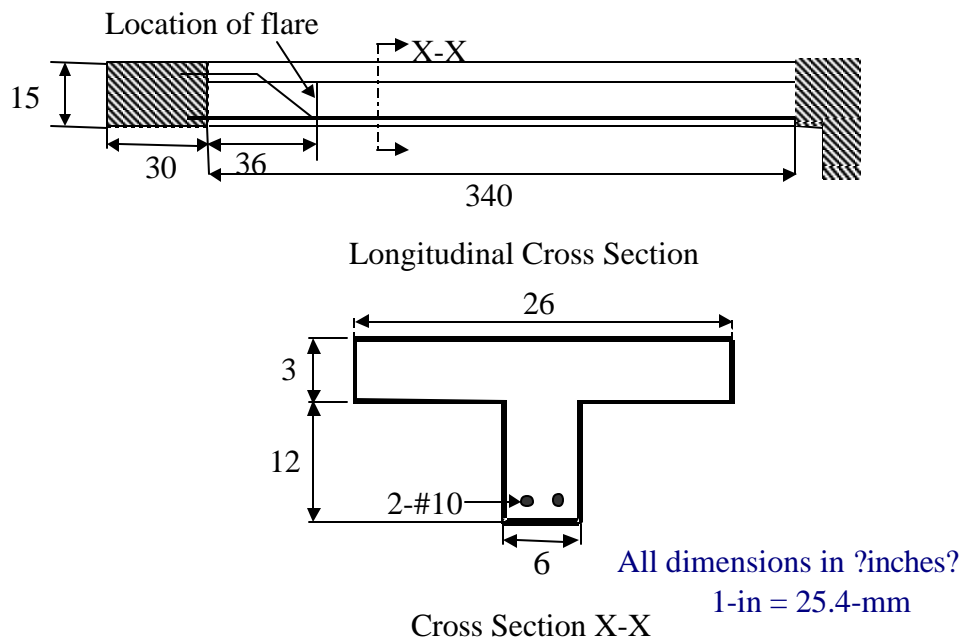


Figure 3.17: Specimen JL1 (Unstrengthened member)

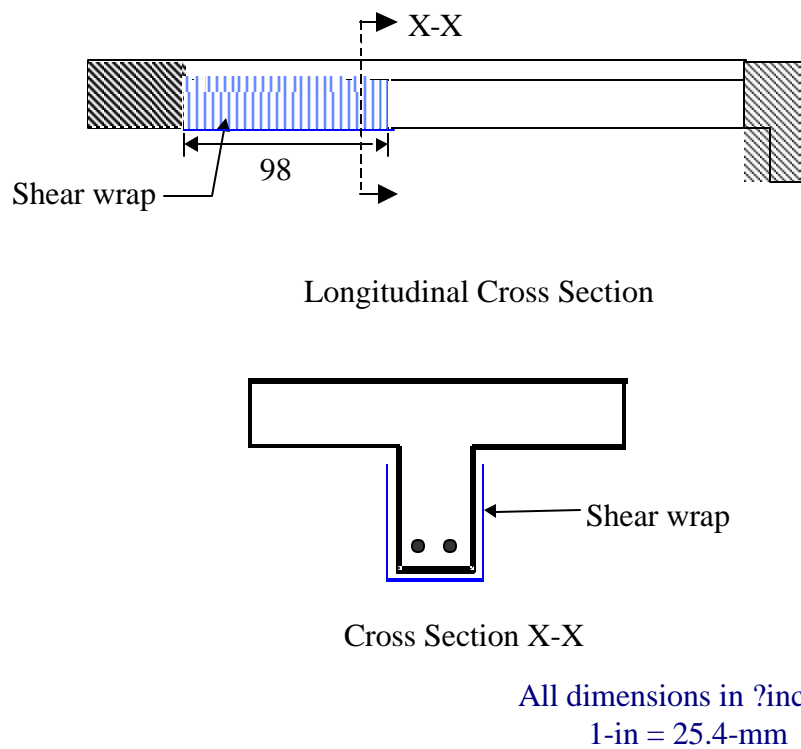


Figure 3.18: Specimen JL2 (Single shear wrap)

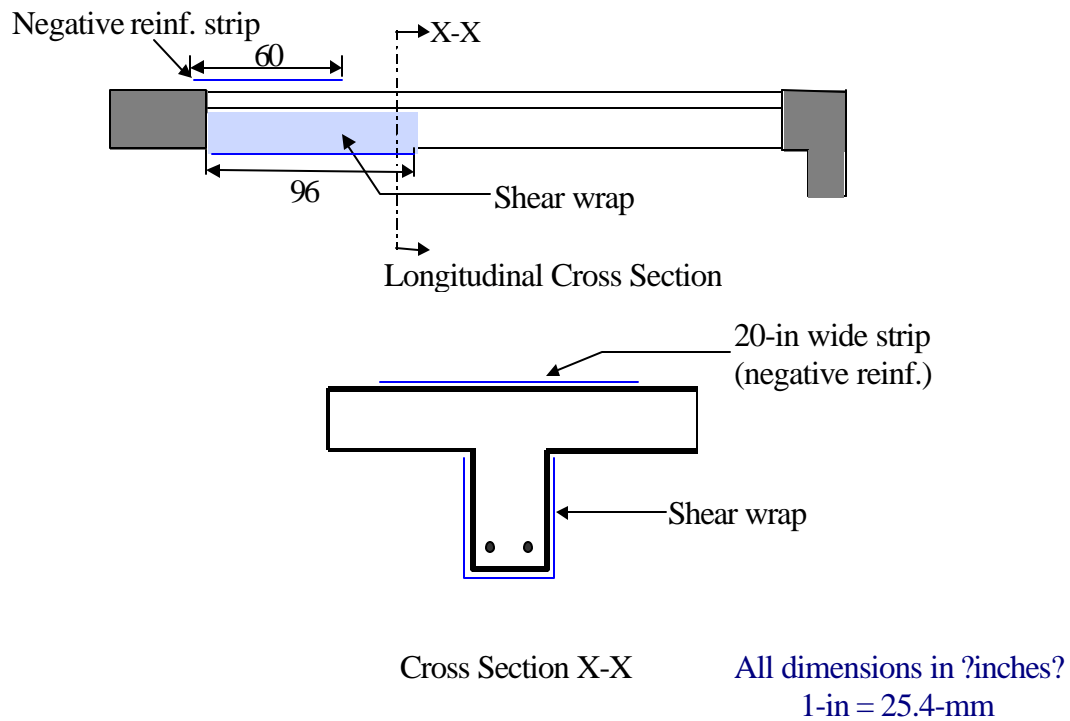


Figure 3.19: Specimen JL3 (Single shear wrap with negative strengthening)

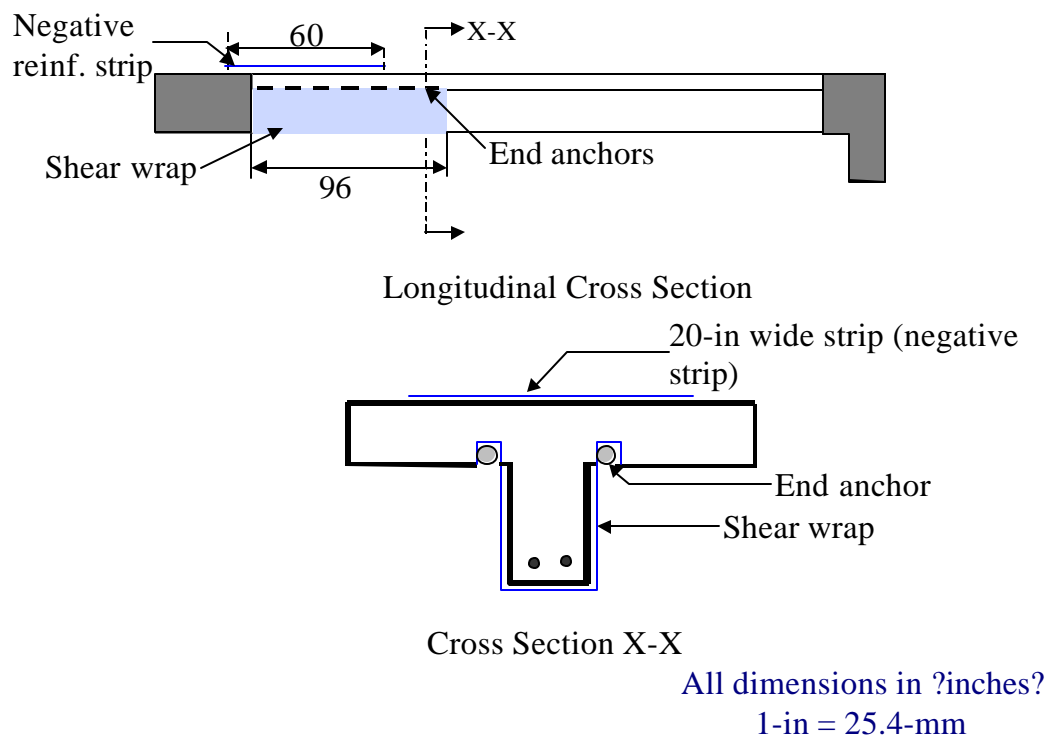


Figure 3.20: Specimen JL4 (Single shear wrap with end anchors)

4. DESIGN APPROACH

4.1 GENERAL

In this experimental program the design approach suggested by Khalifa (1999) has been used for calculating the shear capacity of a CFRP strengthened section. This proposed design approach is based on the results of various experimental programs and the data collected from other research studies. The contribution of externally bonded FRP to the shear capacity is influenced by the following factors:

- Type of FRP, and its unidirectional rigidity
- Amount and distribution of FRP reinforcement
- Fiber orientation
- Wrapping schemes (total wrap, U-wrap, or fiber attached on the two web sides of the beam)
- Presence of FRP end anchor
- Concrete strength
- Concrete surface preparation and surface roughness
- Steel shear reinforcement index
- Loads and support conditions (i.e., shear strengthening in negative or positive moment regions)
- Shear span-to-depth ratio

This design approach has taken into consideration some of the above mentioned factors. In the following paragraphs the ACI design code for shear and Khalifa's design Equations for calculating the capacity of a CFRP strengthened section is discussed elaborately.

4.2 SHEAR DESIGN OF RC STRENGTHENED BEAMS IN ACI CODE FORMAT

4.2.1 ACI CODE PROVISION FOR SHEAR

In the ACI 318-95, the basic design Equation for the shear capacity of a concrete member is expressed as,

$$V_u \leq \phi V_n \quad (4-1)$$

(ACI Eq. 11-1)

where V_u is the total shear force applied at a given section due to the factored loads; ϕ is the strength reduction factor, taken equal to 0.85, and V_n is the nominal shear strength equal to:

$$V_n = V_c + V_s \quad (4-2)$$

(ACI Eq. 11-2)

where V_c is the nominal shear strength provided by concrete (which for a cracked section is attributable to aggregate interlock, dowel action of longitudinal reinforcement, and the diagonal tensile strength of the uncracked portion of concrete), and V_s is the nominal shear strength provided by steel shear reinforcement.

The nominal shear strength provided by concrete, V_c , is assumed to be the same for beams with or without shear reinforcement and is taken as the shear causing significant inclined cracking.

$$V_c = \left(1.9\sqrt{f'_c} + 2500 \rho_w \frac{V_u d}{M_u} \right) b_w d \quad (4-3)$$

(ACI Eq. 11-5)

where ρ_w is the ratio of longitudinal tensile steel; M_u is the factored moment occurring simultaneously with V_u at section considered. The quantity $V_u d/M_u$ shall not be taken greater than 1. The second term expressed in Equation (4-3) is generally small. Therefore, ACI 318-95 allows the use of the following simplified Equation.

$$V_c = 2\sqrt{f'_c} b_w d \quad (4-4)$$

(ACI Eq. 11-3)

4.3 SHEAR CAPACITY OF A CFRP STRENGTHENED SECTION

In traditional shear design approaches (including the ACI Code), the nominal shear strength of a RC section, is the sum of the shear contribution of concrete and steel shear reinforcement. For beams strengthened with externally bonded FRP reinforcement, the shear strength may be computed by the addition of a third term to account for the FRP contribution. This is expressed as follows,

$$V_n = V_c + V_s + V_f \quad (4-5)$$

where V_f is the shear contribution of externally bonded FRP. The design shear strength is obtained by multiplying the nominal shear strength by a strength reduction factor, ϕ . It has been suggested that the strength reduction factor $\phi = 0.85$ given in ACI 318-95 be maintained for the concrete and steel terms.

4.3.1 CONTRIBUTION OF CFRP REINFORCEMENT (V_f) TO THE SHEAR CAPACITY

General: To compute the nominal shear strength as expressed in Equation (4-5), it is necessary to quantify the contribution of CFRP reinforcement to the shear capacity (V_f). At the ultimate limit state for the member in shear, it is not possible to attain the full strength of the FRP. Failure is governed by either fracture of the FRP sheet at average stress levels well below FRP ultimate capacity due to stress concentrations, debonding of the FRP sheet from the concrete surface, or a significant decrease in the post-cracking concrete shear strength from a loss of aggregate interlock. The design procedure takes all of these possible failure modes into consideration.

Basic Design Equation: The expression to compute CFRP sheet contribution is given in Equation (4-6). The shear contribution is computed by assuming a shear crack angle of 45 degrees, computing the area of reinforcement that crosses this potential crack, and multiplying the area by the strength of the material.

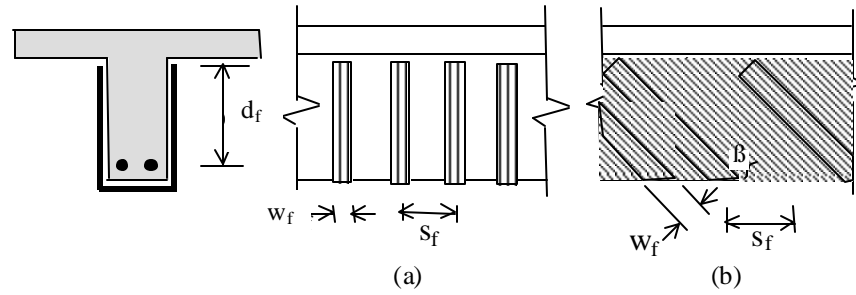


Figure 4-1. Definition of area of FRP in shear reinforcement

(a) Vertical FRP strips (b) Inclined strips

$$V_f = \frac{A_f f_{fe} (\sin\beta + \cos\beta) d_f}{s_f} \quad (4-6)$$

In Equation (4-6), A_f is the area of one strip of transverse FRP reinforcement covering two sides of the beam. This area may be expressed as follows,

$$A_f = 2 n t_f w_f \quad (4-7)$$

where t_f is the FRP reinforcement thickness, n is the number of plies and w_f is the width of the strip.

The effective depth of FRP strip, d_f , is the vertical projection of the shear crack (assumed to be 45°) minus the distance from the top of the crack to the end of the sheet. Because shear cracks typically initiate as vertical cracks until they reach the depth of longitudinal steel reinforcement, the effective depth, d_f , should be measured from the centroid of the steel at the bottom section. Typically, the strips extend only to the soffit of the slab. Therefore, the effective depth of FRP strip, d_f , may be computed by subtracting the slab depth from the depth of the steel, d .

The other variable in Equation (4-6) is the effective average stress in the FRP sheet at ultimate, f_{fe} . The effective average FRP stress, taken smaller than its ultimate strength, is computed by applying a reduction coefficient, R , to the design FRP tensile strength, f_{tu} , as expressed in Equation (4-8).

$$f_{fe} = R f_{fu} \quad (4-8)$$

The reduction coefficient is determined based on the possible failure modes. The failure can be expressed in terms of fracture of the CFRP sheet, or debonding of CFRP sheet from concrete substrate. In either case, an upper limit of reduction coefficient is established to control the shear crack width and the loss of aggregate interlock. The nominal shear capacity of the CFRP reinforcement relating to these failure modes is function of the reduction coefficient. The controlling failure mode is determined by taking the lowest reduction coefficient.

CFRP is linearly elastic until failure, the effective average strain, ϵ_{fe} , at ultimate limit state, may be computed by Equation (4-9),

$$\epsilon_{fe} = R \epsilon_{fu} \quad (4-9)$$

where ϵ_{fu} is the ultimate tensile strain of CFRP. Equation (4-6) may be rewritten as follows,

$$V_f = \rho_f E_f \epsilon_{fe} b_w (\sin \beta + \cos \beta) d_f \quad (4-10)$$

Here, the effective average stress, f_{fe} , is replaced with the effective average strain times the modulus of elasticity, ρ_f is the volumetric FRP reinforcement ratio (ratio of the volume of fibers to the volume of encased concrete), $\beta = 90^\circ$ (fiber orientation),

where $\rho_f = \frac{A_f}{b_w \cdot s_f} = \frac{2 \cdot t_f}{b_w} \left(\frac{w_f}{s_f} \right)$; in the case of a continuous wrap ($w_f / s_f = 1$)

Reduction Coefficient based on CFRP Sheet Fracture Failure:

To determine the reduction coefficient, R, based on the CFRP sheet fracture failure is given by the Equation (Khalifa 1999),

$$R = 26.62 (\rho_f E_f)^2 - 8.44 (\rho_f E_f) + 0.78 \quad (4-11)$$

The above equation is valid for $\rho_f E_f < 0.101 \text{-Msi}$. (1-Msi = 1000-ksi)

Reduction Coefficient based on CFRP Debonding Failure: If the CFRP sheet is U-wrapped without end anchor or bonded only to the sides of the beam, the performance is controlled by the interfacial bond between the FRP and concrete. In these situations, a failure mode based on the bond mechanism must be investigated. Once shear forces develop inclined cracks in the concrete, high tensile stresses develop in the portions of CFRP sheet that bridge these cracks. The tensile stresses in vertically oriented CFRP sheets are a result of the vertical separation of rigid bodies of concrete on either side of the crack. These tensile stresses must be transferred to the concrete on each side of the crack by interfacial bond stresses. If this interfacial bond is compromised before fracture of the CFRP sheet, a debonding failure occurs. In order to address the debonding failure mode, another approach based on the bond characteristics of CFRP sheets with concrete is used.

For the case of shear strengthening, once a shear crack develops, only that portion of FRP extending past the crack by the effective length will be capable of carrying shear. Thus an effective width (w_{fe}) of FRP is taken into consideration. The effective width depends on the shear crack angle (assumed to be 45^0). The value of w_{fe} is calculated as:

$$w_{fe} = d_f - L_e \quad \text{if the sheet is in the form of a U-wrap without end anchors}$$

$$w_{fe} = d_f - 2 L_e \quad \text{if the sheet is bonded only to the sides of the beam}$$

This expression may be used in Equations (4-8) and (4-10), except that only those strips within the width, w_{fe} , are effective. This adjustment may be made by multiplying R by the ratio of w_{fe}/d_f . Thus, the final expression for R is given in Equation (4-12), (Khalifa 1999).

$$R = \frac{(f_c)^{2/3} w_{fe}}{e_{fu} d_f} [199.9 - 6.156(t_f E_f)] \times 10^{-6} \quad (4-12)$$

The above equations are valid for $t_f E_f$ values $0.514 \geq t_f E_f \geq 0.14 \text{ in} - \text{Msi}$.

Upper Limit of the Reduction Coefficient: In order to control the shear crack width and loss of aggregate interlock, an upper limit of the reduction coefficient was established.

$$R = \frac{0.006}{e_{fu}} \quad (4-13)$$

This limit is such that the average strain in CFRP materials at ultimate can not be greater than 0.006 in/in (without the strength reduction factor). The suggested value of the upper limit is mainly based on evaluation of the available test results and it gives conservative results. However, an analytical study to link the allowable shear crack width with the effective average strain in both external shear reinforcement (CFRP sheet) and the internal one (steel stirrups) is needed, and a further adjustment to that upper limit may be suggested.

4.4 DESIGN PREDICTIONS

The preceding section presents the foundation work for the design approach used in the experimental calculation. The design procedure was used for predicting the failure mode (peeling/debonding, fiber rupture & loss of aggregate interlock) of the specimens based on the engineering properties of the material and the geometry of the cross section.

Khalifa's design Equations were used to calculate the shear capacities of the specimens strengthened with different strengthening schemes. The shear contribution of the CFRP, as expressed in Equation (4.8), may then be found from the following expressions,

$$V_f = \frac{A_f f_{fe} (\sin \mathbf{b} + \cos \mathbf{b}) d_f}{s_f} \leq \left(\frac{8\sqrt{f'_c} b_w d}{V_s} - V_s \right) \text{ with } s_f \leq w_f + \frac{d}{4} \quad (4-14)$$

The shear capacity of the beam may finally be computed as:

$$fV_n = f(V_c + V_s + \mathbf{y}V_f) \quad (4-15)$$

The additional reduction factor, \mathbf{y} , should be selected based on the known characteristics of the application but should not exceed 0.85 for three and two-sided wrapping schemes.

Table 4.1 summarizes the expected design capacity and the predicted failure mode of the specimens. Prediction of failure was based on the lowest value of the reduction factors (R1, R2 & R3). The values of R1 correspond to failure due to FRP rupture. The values of R2 correspond to failure due to FRP debonding, and R3 correspond to failure due to loss of aggregate interlock. V_f corresponds to the shear contribution of FRP in a

strengthened member. $V_{f, \text{Lim}}$ corresponds to the limiting contribution of FRP due to external reinforcements, to prevent failure due to web crushing, and is given by Equation (4.16).

$$V_{f, \text{Lim}} = 8\sqrt{f'_c} b_w d \quad (4-16)$$

V_n corresponds to the nominal shear capacity of the strengthened member expressed by Equation (4.17)

$$V_n = V_c + \gamma V_f \quad (4-17)$$

$$\text{here, } V_c = 2\sqrt{f'_c} b_w d$$

A detailed design example is presented in Appendix C to illustrate how the values of V_n and R_i are computed.

Table 4.1: Values obtained using the Design Equations

Member	Strengthening schemes				V_c (kip)	$R1^1$	$R2^2$	$R3^3$	V_f (kip)	$V_{f, \text{lim}}$ (kip)	V_n (kip)
	Shear		Flexure								
	# of plies	Anchor	Neg.	Pos.							
JS1	--	--	--	--	10	--	--	--	--	--	10.0
JS2	1	No	1	1	10	0.314	0.224	0.36	17.6	39.4	25.0
JS3	1	Yes	1	1	10	0.314	0.600	0.36	24.5	39.4	35.7
JS4	2	No	3	2	10	0.200	0.224	0.36	62.7	39.4	43.5
JS5	2	Yes	3	2	10	0.200	0.600	0.36	62.7	39.4	43.5
JS6	2	Yes	3	2	10	0.200	0.194	0.32	54.4	39.4	43.5
JL1	--	--	--	--	9.6	--	--	--	--	--	9.6
JL2	1	No	--	--	9.6	0.314	0.224	0.36	18.1	38.8	25.0
JL3	1	No	1	--	9.6	0.314	0.224	0.36	18.1	38.8	25.0
JL4	1	Yes	1	--	9.6	0.314	0.600	0.36	15.1	38.8	22.4

¹ Reduction factor for fiber rupture.

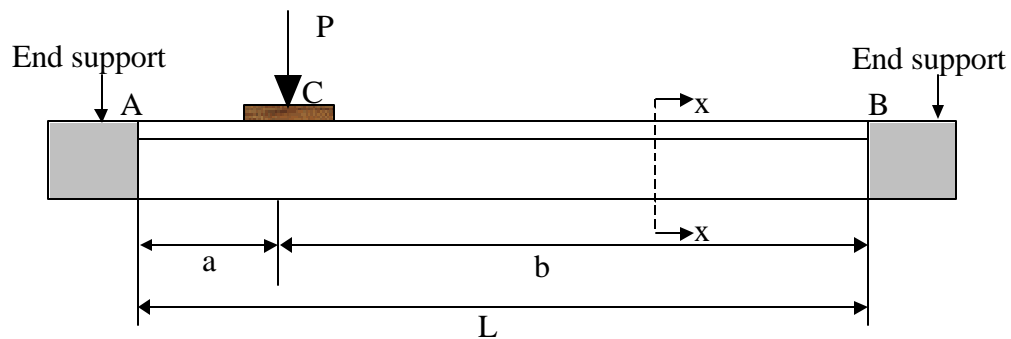
² Reduction factor for cover delamination.

³ Reduction factor for loss of aggregate interlocking.

5. ANALYTICAL MODEL

5.1 GENERAL

In the development of moment-curvature diagrams, only the section's geometric and material properties are required. In order to obtain the load-deflection diagrams, the support and the loading geometry of the member must be clearly known. Figure 5.1 depicts the (assumed) support and known loading pattern for typical experimental beams. The test specimens were part of an existing structure. It was assumed that the joists were completely fixed to the transverse beams. Figure 5.2 depicts the typical cross-section of a short-span member.



1 Figure 5.1: Typical Loading and Support Configuration for Experimental Work

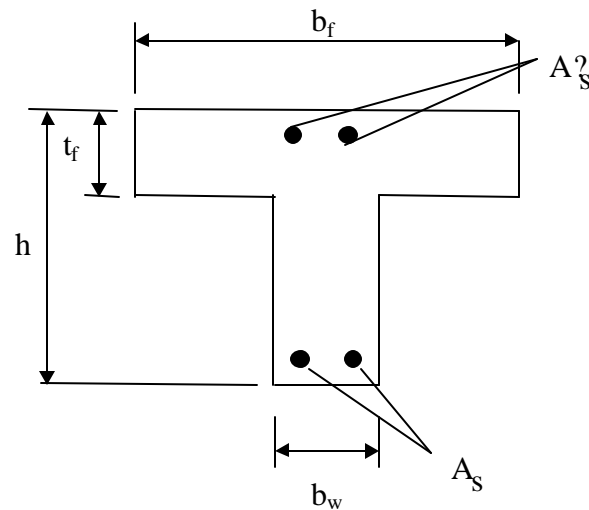


Figure 5.2: Cross Section at x-x

5.2 LOAD DEFLECTION BEHAVIOR

A typical load-deflection curve for a RC beam strengthened with externally bonded FRP sheet can be separated into three distinct piecewise linear stages as illustrated in Figure 5.3.

These three basic stages of load-deflection curve for an FRP-strengthened can be summarized as:

- a.) Precracking stage ($M < M_{cr}$)
- b.) Cracked stage ($M_{cr} < M < M_y$)
- c.) Post yield stage ($M_y < M < 0.9M_u$)

Where M_{cr} , M_y , M_u are the cracking moment, moment corresponding to first yield of steel reinforcement and ultimate moment, respectively. The real challenge to accurately predicting the deflection lies in estimating the extent of cracking in the beam to be considered in deflection computation.

Preracking stage:

In this stage, elastic Equations are used to compute the deflection of the FRP strengthened beams using the gross uncracked transformed moment of inertia, I_g , which includes the contribution of the FRP.

Cracked stage:

If the service moment M is greater than the cracking moment M_{cr} , the flexural stiffness of the beam is affected by this occurrence. In regions of low moments, where the cracking moments has not been exceeded, the moment of inertia remains equal to the gross uncracked transformed moment of inertia I_g . At sections where the discrete cracks are visible, the moment of inertia of the cross section is approximately equal to the transformed cracked moment of inertia, I_{cr} . However between the discrete cracks, the moment of inertia lies somewhere between these two boundary values, I_g and I_{cr} .

Figure 5.4 schematically presents the distribution of reinforcing steel stress, the concrete stress and the variation of moment of inertia between the cracks in the cracking stage. The contribution of the tensile forces, developed in the concrete between the cracks, to the flexural rigidity EI is referred to as tension stiffening. In this stage the

beam no longer has a constant moment of inertia along its length, and an effective moment of inertia I_e is used. The effective moment of inertia has a value less than I_g but greater than I_{cr} , depending on the extent of cracking, distribution of loading, and the contribution of concrete resisting tension. At the first cracking load the flexural rigidity of the beam decreases as the stress is transferred from the cracked concrete to the tension steel, resulting in a corresponding decrease in the slope of the load deflection curve as shown in Figure 5.3. As the load approaches the first yield of the steel reinforcement, the beam flexure stiffness approaches $E_c I_{cr}$. The most widely accepted approach for estimating the effective moment of inertia was developed by Branson and is employed in the ACI code.

The calculated deflections for beams strengthened with FRP using the Branson effective moment of inertia Equation, with transformed section properties for both steel and FRP are usually less than observed experimental values as it will be shown. In other words the effective moment of inertia is overestimated.

Post yield stage:

While conventionally RC beams at this stage are considered to have reached their ultimate load limit, FRP-strengthened beams can exhibit additional load capacity depending on the steel ratio, FRP cross-section area and FRP tensile strength. The ratio between the ultimate moment and yield moment (M_u, M_y) for a conventionally single reinforced section with f'_c less than 5-ksi (35-MPa) and $\rho < 0.03$ is approximately 1.06 as presented schematically in Figure 5.5.

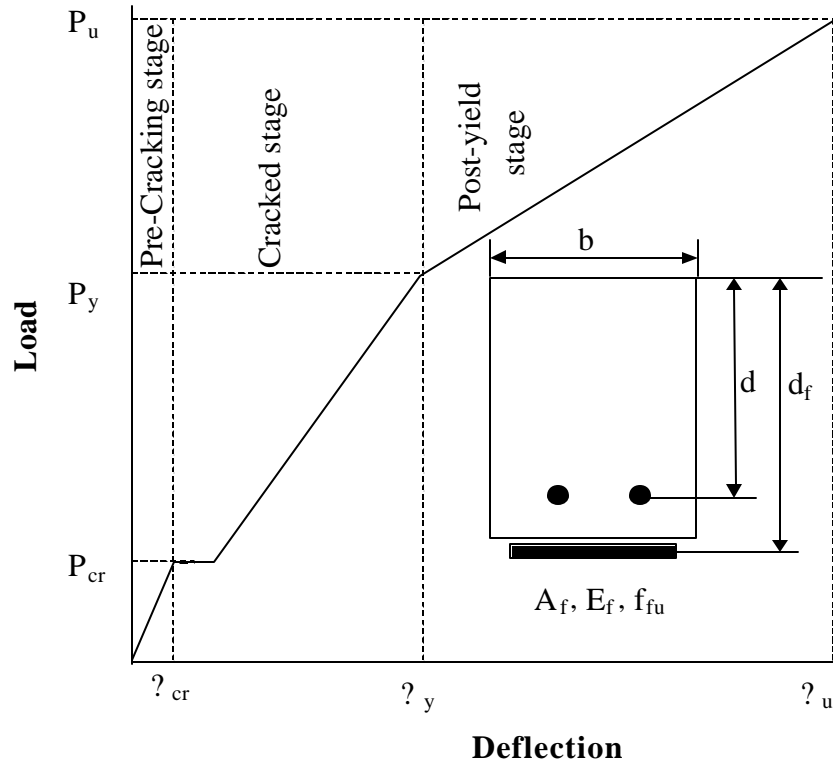


Figure 5.3: Idealized load-deflection curve for FRP-strengthened RC beam

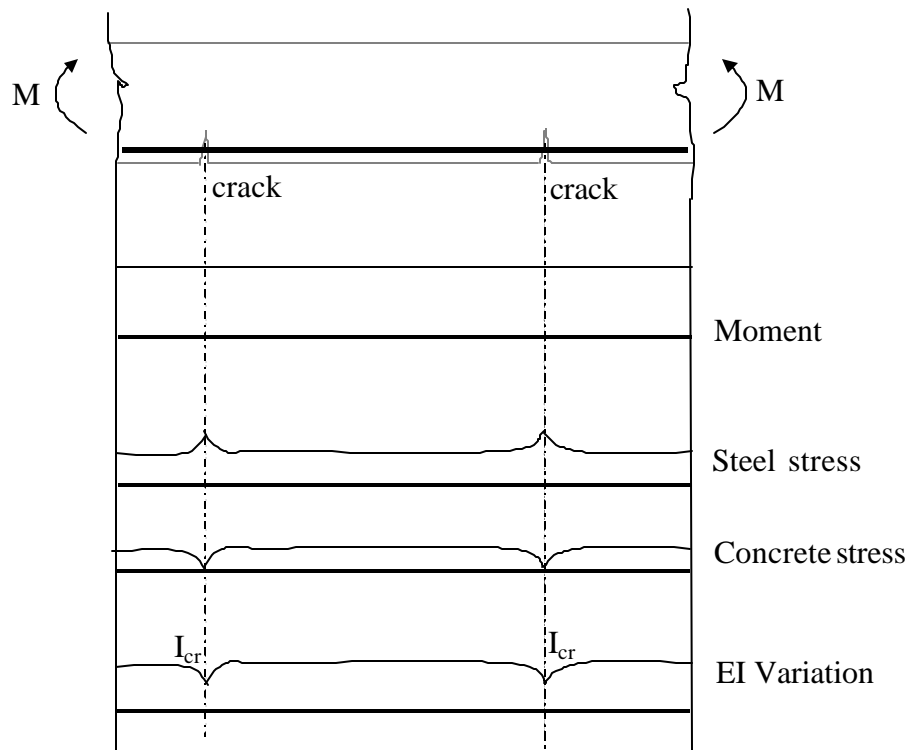


Figure 5.4: Effect of tension cracking on reinforcing steel stress, concrete tension stress and flexural rigidity

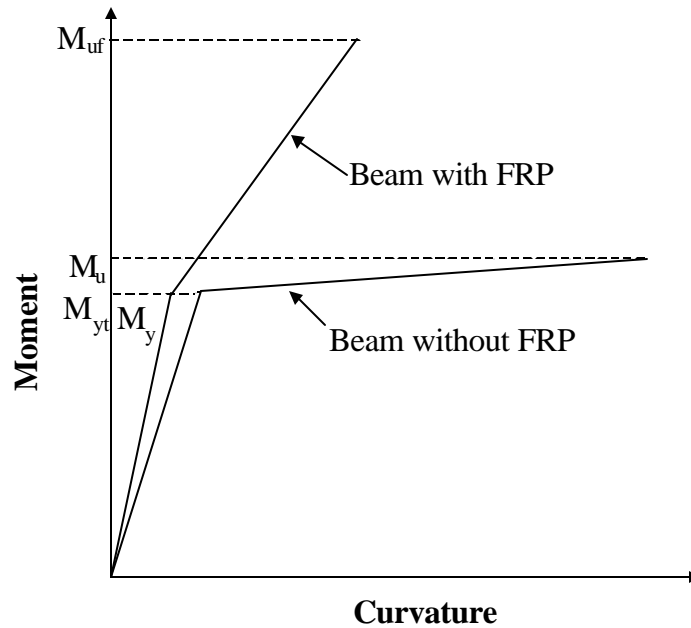


Figure 5.5: Typical moment-curvature curve for RC beams with and without FRP



Figure 5.6: Typical Loading and Support Configuration for Design

5.3 ANALYTICAL BEAM MODEL

Based on the experimental data a beam model (Figure 5.6) was considered for the analytical study. The LVDT and inclinometer measurements were taken into consideration when the model was adopted.

When the beams were tested to failure, the end supports showed settlements. The settlement of support 'A' was higher than the settlement of support B. For analysis a differential settlement of δ_d was considered at support 'A'.

Based on the inclinometer readings (Appendix A) taken during the test, it was observed that inclinometer at support B (Inclinometer #16) recorded negligible reading of end rotation, where as the inclinometer at support 'A' (inclinometer #13), showed a comparatively higher degree of rotation. This clearly indicated that support B behaved as a fixed end, where as support 'A' behaved as a semi rigid connection. In the model, support 'A' was considered with vertical and rotational degrees of freedom only. Support 'B' was considered to be fully fixed.

5.4 DOUBLE INTEGRATION METHOD

Based on the model the Equation for estimation of deflection, bending moment and shear force was derived. For the deflected shape shown in the Figure 5.7, the bending moment and deflection Equations are as follows:

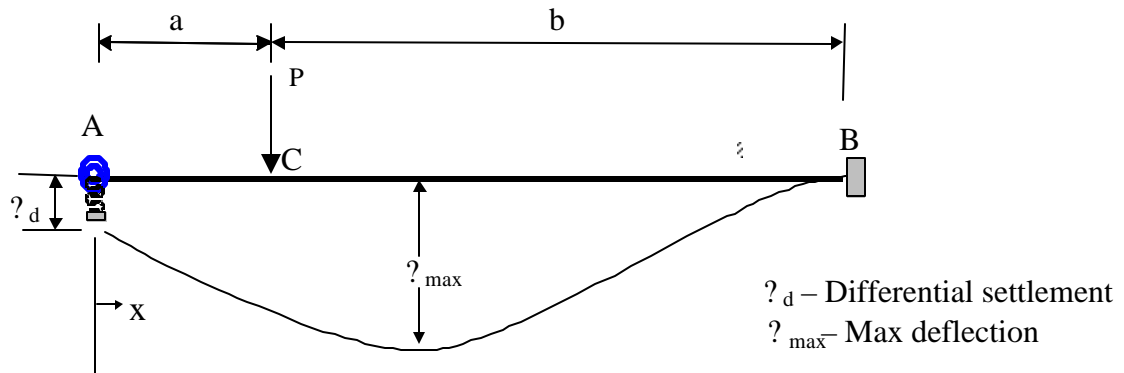


Figure 5.7: Model Beam with Differential Settlement

At any distance 'x' from the support 'A', the bending moment, 'M', is given by:

when $x < a$:

$$EI \frac{d^2 y}{dx^2} = \frac{Pb^2(3a+b)}{L^3}x - \frac{Pab^2}{L^2} + Ma \left[\frac{2x}{L} - 1 \right] \quad (5-1)$$

when $x > a$:

$$EI \frac{d^2 y}{dx^2} = \frac{Pb^2(3a+b)}{L^3}x - \frac{Pab^2}{L^2} + Ma \left[\frac{2x}{L} - 1 \right] - P(x-a) \quad (5-2)$$

where:

$$(5-3)$$

$$Ma = \frac{6EI\Delta_d}{L^2}$$

By integrating the above Equation twice, deflection for the beam for a given load can be determined at any point 'x' along the span of the member.

At any distance 'x' from the support 'A', the deflection, 'y', is given by:

when $x < a$:

$$EI y = \frac{Pb^2(3a+b)}{6L^3}x^3 - \frac{Pab^2}{2L^2}x^2 + Ma \left[\frac{x^3}{3L} - \frac{x^2}{2} \right] \quad (5-4)$$

when $x > a$:

$$EI y = \frac{Pb^2(3a+b)}{6L^3}x^3 - \frac{Pab^2}{2L^2}x^2 + Ma \left[\frac{x^3}{3L} - \frac{x^2}{2} \right] - \frac{P(x-a)^3}{6} \quad (5-5)$$

By differentiating the above Equation thrice, shear force for a given load can be determined at any point 'x' along the span of the member.

At any distance 'x' from the support 'A', the shear force, 'V', is given by:

when $x < a$:

$$EI \frac{d^3y}{dx^3} = \frac{Pb^2}{L^3}(3a+b) - V \quad (5-6)$$

when $x > a$:

$$EI \frac{d^3y}{dx^3} = \frac{Pb^2}{L^3}(3a+b) - V - P \quad (5-7)$$

where,

$$V = \frac{12 EI \Delta_d}{L^3} \quad (5-8)$$

The above set of Equations was used for calculating the values of bending moment, deflection and shear forces. The analysis is complicated by the fact that the value EI is not constant. For example, a portion of the beam may have been loaded in excess to the cracking moment, while the remainder of the beam remains well under the cracking moment. In order to account for this, two moments of inertia must be calculated, I_{cr} and I_g .

The beam model has been divided into equal parts along the length of the member. The elements, which have bending moment in excess to the cracking moment, the moment of inertia values are reduced (Figure 5.8).

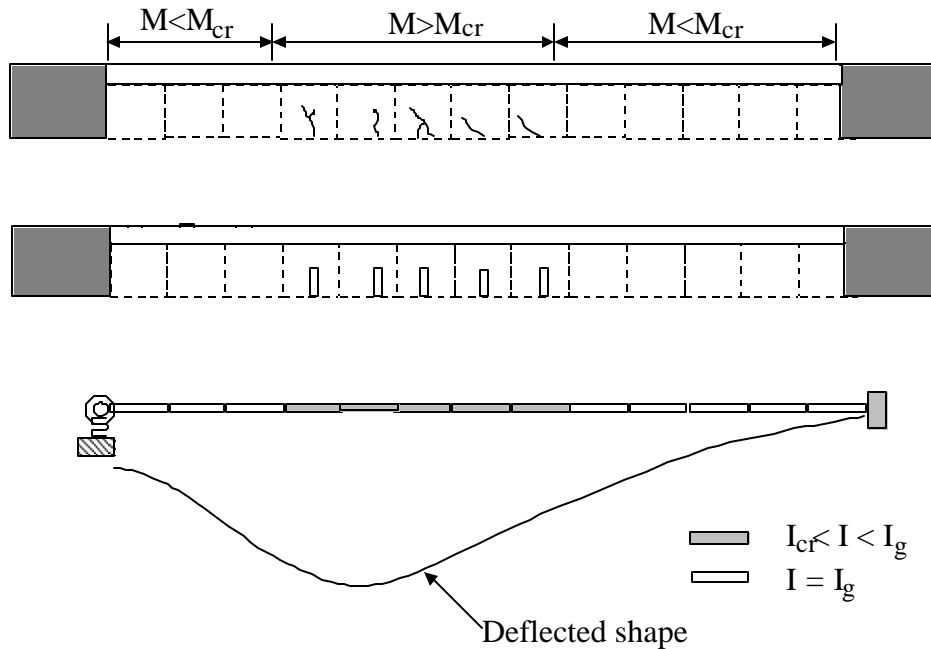


Figure 5.8: Equivalent Model of Cracked Beam with Deflected Shape

5.5 BRANSON EQUATION

In mid 1960's, Branson derived the Equation now used in ACI-318 for the calculation of deflection for RC beams (ACI Committee 435,1966). The expression approximates the effective stiffness of simply supported member as its section transition from I_g to I_{cr} , the moments of inertia of the transformed uncracked sections, respectively. The Equation is written as:

$$I_e = \left(\frac{M_{cr}}{M_a} \right)^a I_{gt} + \left[1 - \left(\frac{M_{cr}}{M_a} \right)^a \right] I_{cr} \quad (5-9)$$

where:

M_a = moment applied at the section.

$$\begin{aligned}
 M_{cr} &= \text{cracking moment} = \frac{f_r I_g}{y_t} \text{ kip-in} \\
 I_g &= \text{moment of inertia of the uncracked concrete section} \\
 f_r &= \text{modulus of rupture} = 7.5 \sqrt{f'_c} \text{ psi} \\
 y_t &= \text{distance from the centroid of the section to the extreme} \\
 &\quad \text{tension fiber}
 \end{aligned}$$

In an attempt to remedy the stated sources of error as well as the difficulty in multiple integration, Branson (1965) proposed a design procedure which accounted for both the residual stiffness between cracks and the number of cracks which may be present. The following section details Branson's proposed Equation and offers insight into the effects of strengthening on member behavior.

For simplicity, the ACI-318 Equation is written in terms of the uncracked or "gross" moment of inertia, which ignore the small increase in the moment of inertia due to steel reinforcement. This expression is expressed in Equation (5-10).

$$I_e = I_{cr} + (I_g - I_{cr}) \left(\frac{M_{cr}}{M_a} \right)^3 \quad (5-10)$$

For a continuous beam, the I_e may be different in the negative and positive regions. In this case, the positive moment value may be assumed to apply between the points of contraflexure and the negative moment values in the end regions.

For beams with two ends continuous:

$$\text{Average } I_e = 0.70 I_{em} + 0.15 (I_{em1} + I_{em2}) \quad (5-11)$$

Where

I_{em} = moment of inertia value at mid-span

I_{em1}, I_{em2} = moment of inertia values at the two ends

In strengthened RC sections with high fiber and steel reinforcements ratios, the transformed section may be significantly larger than the gross section.

5.6 VALIDATION OF THE ANALYTICAL APPROACH

For analytical validation, JS3 member is considered:

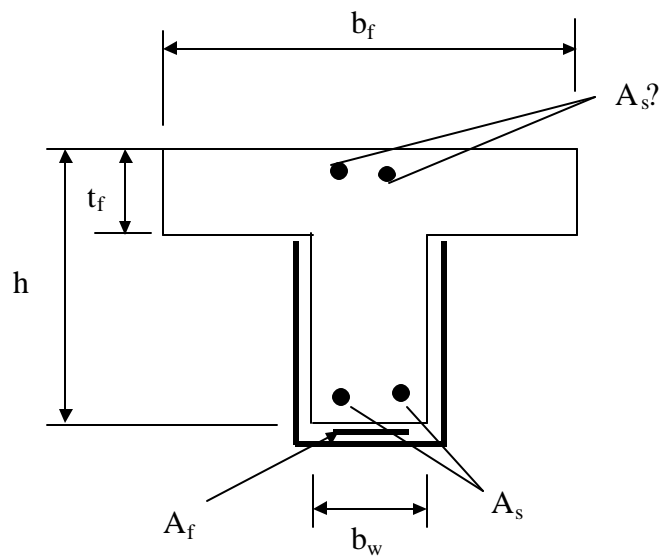


Figure 5.9: Geometry of the Cross Section at Mid-Span used for Validation

The cross-section considered for validation is taken as

The geometric properties are:

$$b_f = 26 \text{ in}$$

$$b_w = 6 \text{ in}$$

$$t_f = 3 \text{ in}$$

$$h = 15 \text{ in}$$

$$A_s = 0.88 \text{ in}^2$$

$$A_s? = 0.4 \text{ in}^2$$

$$A_f = 0.026 \text{ in}^2$$

thickness of carbon fiber = 0.0065 in

The assumed material properties are:

Carbon Fiber:

$$E_f = 33000 \text{ ksi}$$

Epoxy:

$$E_a = 290 \text{ ksi}$$

$$G_a = 107 \text{ ksi}$$

Steel:

$$f_y = 50 \text{ ksi}$$

$$E_s = 29000 \text{ ksi}$$

Concrete:

$$f'_c = 3500 \text{ psi}$$

$$E_c = 57 \sqrt{f'_c} = 3372 \text{ ksi}$$

Step 1: Find the centroid and gross moment of inertia (I_g) of the uncracked section:

The contribution of FRP in compression in increasing the moment capacity is

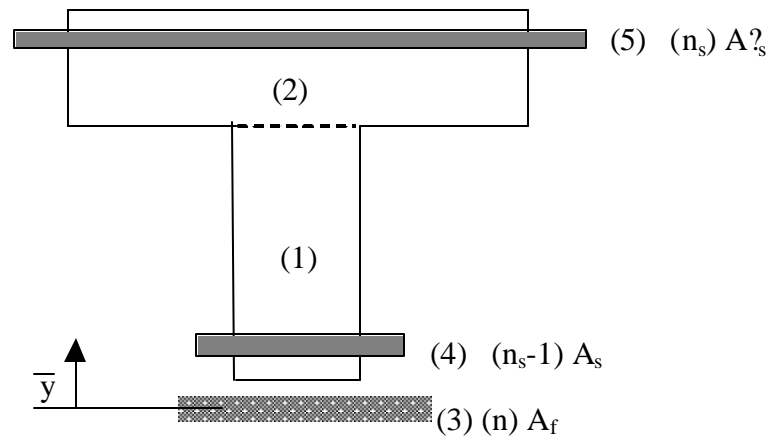


Figure 5.10: Uncracked Transformed Section

negligible; hence it is neglected for validation

where

- (1): area of web concrete
- (2): area of flange concrete
- (3): transformed area of FRP in tension
- (4): transformed area of steel in tension
- (5): transformed area of steel in compression

$$n_s = \frac{E_s}{E_c} = \frac{29000ksi}{3372ksi} = 8.6 \quad (5-12)$$

$$n_f = \frac{E_f}{E_c} = \frac{33000ksi}{3372ksi} = 9.8 \quad (5-13)$$

Table 5.1 was obtained from Figure 5.10:

Table 5.1: Moment of inertia calculations

	A (in ²)	\bar{y} (in)	A. \bar{y} (in ²)	I (in ⁴)	A. ($\bar{y} - \bar{h}$) ²	I+ A. ($\bar{y} - \bar{h}$) ²
1	72.00	6.00	432.00	864.00	922.80	1768.80
2	78.00	13.50	1053.00	58.50	1198.50	1257.00
3	0.25	--	--	--	24.70	24.70
4	6.68	0.75	5.01	--	20.88	139.50
5	3.04	14.25	43.32	--	66.30	66.30

$$\bar{h} = \frac{432 + 1053 + 5.04 + 43.32}{72 + 78 + 0.25 + 6.68 + 3.04} = 9.58in$$

$$I = (1763.8 + 1257.0 + 24.7 + 139.5 + 66.3) = 2349 in^4$$

Step 2: Calculate M_{cr} .

The value positive cracking moment can be calculated as:

$$M_{cr}^+ = \frac{f_r I_g}{y_t} = \frac{7.5\sqrt{3500} (2349)}{9.58} = 108.8 kip-in \quad (5-14)$$

The value of negative cracking moment is calculated as:

$$M_{cr}^- = \frac{f_r I_g}{y_t} = \frac{7.5\sqrt{3500} (2349)}{5.1} = 204.4 kip-in \quad (5-15)$$

Step 3: Calculating the maximum positive and negative bending moment.

For calculating the maximum bending moment capacity of the given cross section the ultimate yield of steel and fiber rupture is taken into consideration.

The depth of the neutral axis is calculated as:

$$c = \frac{(A_s - A_s')f_y + A_f f_{fu}}{\beta_1 f_c b}; \quad (5-16)$$

where, $\beta_1 = 0.85$, $\beta_2 = 0.85$, $f_c = 3.5 \text{ ksi}$, $d = 1 \text{ - in}$

The maximum positive moment is calculated as follows:

$$M^+_{\max} = A_s f_y \left(d - \frac{bc}{2} \right) + A_f f_{fu} \left(h - \frac{bc}{2} \right) + A_s' f_y (d - d') = 1229.6 \text{ kip-in} \quad (5-17)$$

The maximum negative moment is calculated as follows:

$$M^-_{\max} = A_s f_y \left(d - \frac{bc}{2} \right) + A_f f_{fu} \left(h - \frac{bc}{2} \right) + A_s' f_y (d - d') = 2225.5 \text{ kip-in} \quad (5-18)$$

Figure 5.11 schematically represents flow chart of the analytical process used.

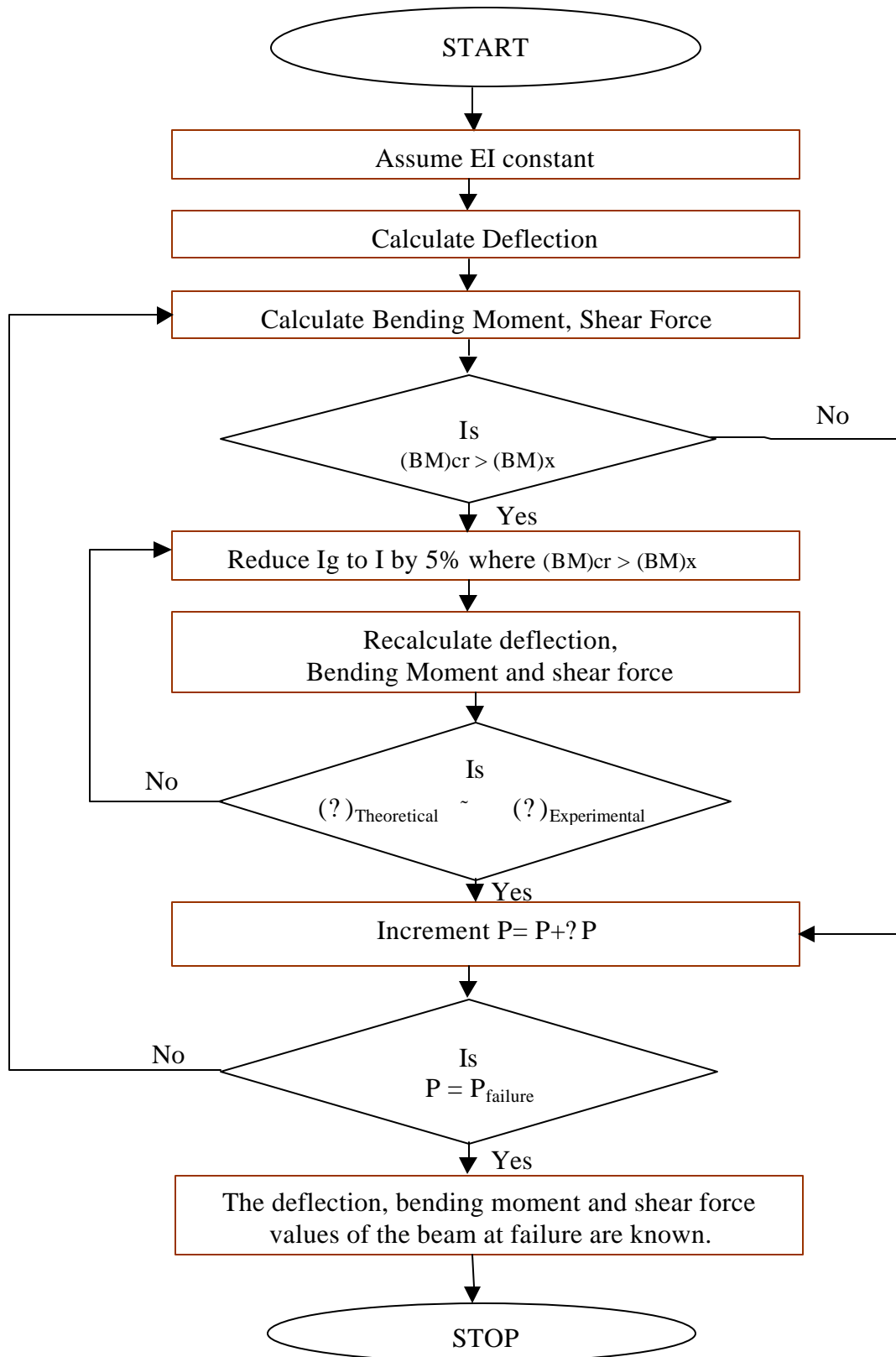


Figure 5.11: Flow chart describing the analytical model approach

VALIDATION BASED ON ACI-318 CODE FOR I_{EQ}

Using the ACI-318 code, I_{eq} of the beam can be calculated for the positive moment and negative moment region. Using Equation 5.8 I_e is used to plot the deflection curve. This curve is in close agreement with the theoretical and the experimental deflection curves.

$$\text{Average } I_e = 0.70 I_{em} + 0.15 (I_{em1} + I_{em2})$$

$$I_{em} = 1234 + (2349 - 1234) \left(\frac{196.7}{524} \right)^3 = 1285 \text{ in}^4$$

$$I_{em1} = 498 + (2349 - 498) \left(\frac{109}{1559} \right)^3 = 498 \text{ in}^4$$

$$I_{em2} = 498 + (2349 - 498) \left(\frac{109}{584} \right)^3 = 500 \text{ in}^4$$

$$I_{eq} = 0.7 (1286) + 0.15 (498+500) = 1050 \text{ in}^4$$

VALIDATION USING FINITE ELEMENT PACKAGE

The validation model was designed using a standard Finite Element package. The moment of inertia values obtained at failure load are used as, I for each member. The analytical model has a spring support at one end. The spring stiffness is adjusted such that the settlement in the spring is equal to the differential displacement (δ_d) observed during the experiment. The deflection curves are thus plotted as shown in Figure 5.12.

Figure 5.14 depicts the shear force in the member at the time of failure. In the span AC, the shear force at the time of failure is much greater than the capacity of the strengthened member. Thus as predicted the member failed in shear at support 'A'.

Table 5.2: Deflection Values of JS3A Using Different Approaches

Span (in)	Experimental (in)	Analytical (in)	FEA (in)	ACI Ieq (in)
0	-0.1133	-0.1133	-0.1134	-0.1133
8	-0.1522	-0.1367	-0.1297	-0.1384
16	-0.2172	-0.1931	-0.1692	-0.1813
24	-0.2830	-0.2610	-0.2185	-0.2333
32	-0.3396	-0.3572	-0.2618	-0.2906
40	-0.3600	-0.3918	-0.2818	-0.3182
48	-0.3396	-0.3844	-0.2726	-0.2960
56	-0.3029	-0.2822	-0.2397	-0.2539
64	-0.2532	-0.2081	-0.1920	-0.2065
72	-0.1675	-0.1269	-0.1382	-0.1438
80	-0.1055	-0.1161	-0.0865	-0.0826
88	-0.0574	-0.0575	-0.0423	-0.0421
96	-0.0252	-0.0158	-0.0116	-0.0072
104	0.0000	0.0000	0.0000	0.0000

Conversion factor: 1-in = 25.4-mm

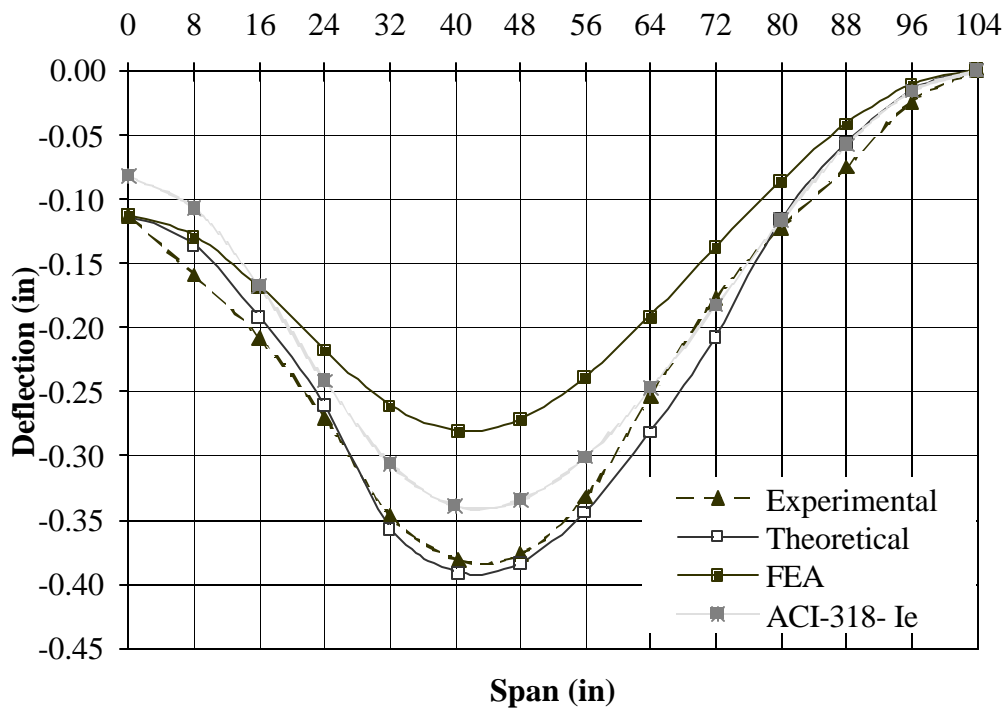


Figure 5.12: Deflection Curves- JS3A

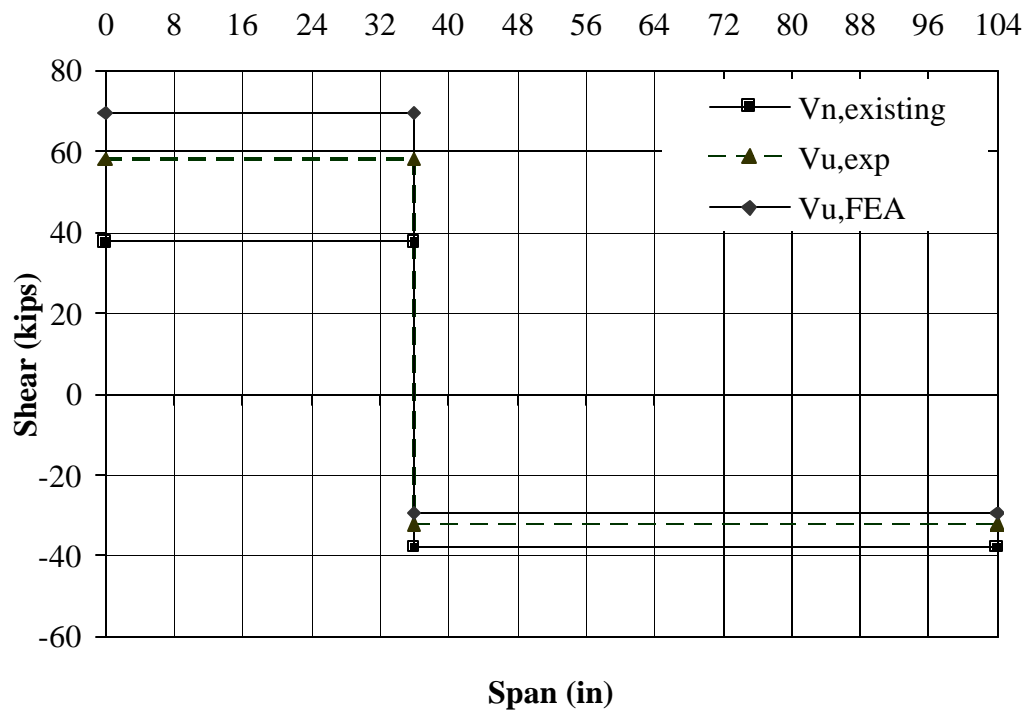


Figure 5.13: Experimental Validation of the Shear Force at Ultimate Load

6. TEST SETUP AND PROCEDURE

All specimens were tested with an unsymmetric load setup. This procedure was implemented to develop high shear at one of the joist ends. The test specimens incorporated elaborate instrumentation to monitor the behavior of the joists under the applied load.

6.1 INSTRUMENTATION

The instrumentation used to monitor the behavior of the test specimens is summarized in Table 6.1. This table includes the names of the devices, their application within this study, their recommended minimum measurable values, and their measuring ranges.

Deflections were measured using linear variable differential transducers (LVDT), shown in Figure 6.1. LVDT's are available in a variety of ranges and accuracy levels. In order to monitor deflection of the test specimens, the LVDT's were mounted on tripods, and extended to reach the bottom of the web of the member undergoing the test.

Inclinometers, shown in Figure 6.2, are used to measure the rotation of a test member as values of slopes can be easily correlated to deflections. The inclinometers used within this study were placed in a horizontal position and were located on the top of the flange of the member undergoing the test.

The most common method for measuring strain is through the use of electrical resistance strain gages, which are bonded directly to the surface of the material for which the strain will be measured.

Table 6.1: Summary of Instrumentation used during the Test

Parameter	Devices	Recommended minimum measurable value	Measuring range
Deflection	LVDT	0.0001 in.	± 2 in.
Rotation	Inclinometer	0.01 deg.	± 3 deg.
Strain	Strain gage Extensometer LVDT	1 <i>me</i> 50 <i>me</i> 50 <i>me</i>	± 3000 <i>me</i> $\pm 10,000$ <i>me</i> $\pm 10,000$ <i>me</i>
Crack width	Extensometer	0.0001 in.	± 0.2 in.
Load	Load Cell Pressure Transducers	10 lbs. 100 lbs.	0 – 200,000 lbs. 0 – 200,000 lbs.

Conversion Factor: 1 in = 25.4 mm, 1 lb. = 4.448 N

Electrical resistance strain gages (Figure 6.3) are ineffective when they are intersected by a crack or bridge a crack. To measure strain over a crack, LVDT's or extensometers can be used. An extensometer, as shown in Figure 6.4, is attached directly to the surface on two knife-edges, which straddle an anticipated crack or an existing crack. An extensometer can then be used to either measure the average strain over the gage length between the two knife-edges or the change in width of an intersecting crack. LVDT's can be used to determine the average strain over a larger gage length than that provided by the extensometer. The horizontal LVDT is placed into a bracket that is attached to the test specimen. Another bracket is attached to the test specimen such that the apparatus spans an existing crack or an anticipated location of a crack. The distance between the two brackets is the gage length over which the average strain is computed.

A device used to monitor the level of load application is a load cell. Load cells can be in a variety of shapes, sizes and capacities. The hydraulic jacks are used for the application of load. Pressure transducers can be used to measure fluid pressures in the hydraulic system, which can be calibrated to a specific level of load.



Figure 6.1: LVDT setup



Figure 6.2: Inclinator



Figure 6.3: Location of strain gages



Figure 6.4: Extensometer

6.2 TEST SETUP

For the testing of specimens of series JS, which had a span length of 104-in (2641-mm), the point of loading was 36-in (914-mm) from the near end support. For testing of specimens of series JL, which had a span length of 341-in (8475-mm), the point of loading was 60-in (1524-mm) from the near end support. Figure 6.5 schematically illustrates the push down test setup. The load was applied by means of two 100-ton (220-kip) hydraulic jacks.

In the pushdown test (Mettemeyer, 1999), two 100-ton (220-kip) hydraulic jacks with extensions was used to apply a downward concentrated load on the test member as illustrated in Figure 6.6. The extensions attached to the jacks reacted against the upper floor when the jacks extended. Shoring was installed on the floor above to share/distribute the reactions over several floors. A load cell was placed on top of the extensions over the hydraulic jacks to read the load that was applied by the jack. LVDT's were placed along the length of the specimen being tested, to collect deflection data of the joist as the load was applied.

Figures 6.7 and 6.8 show a schematic representation of the instrumentation that was used to collect data during the test for short and long-span members, respectively. The inclinometers were used to measure the rotation or the slope of the test member. Strain gages were applied on the CFRP sheets to measure the strain in the sheets. They

were also applied to the concrete surface to measure the compressive strain in the concrete. Extensometers were used to read strain over cracked sections. A data acquisition system was used to collect data simultaneously as the load was applied.

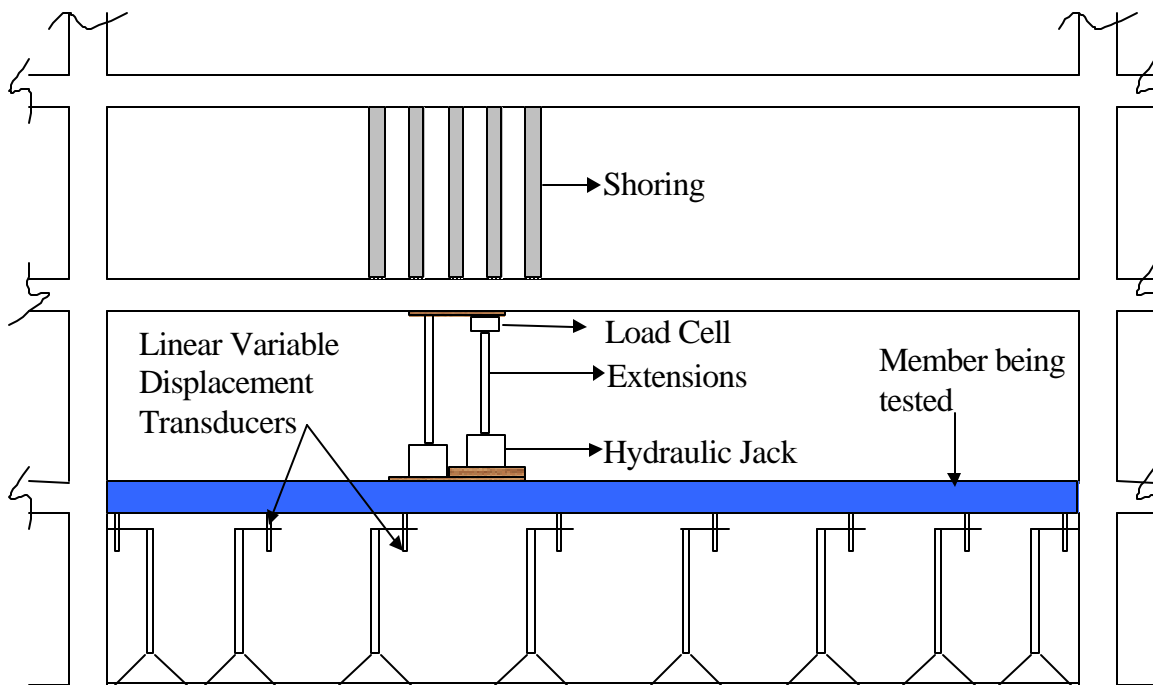
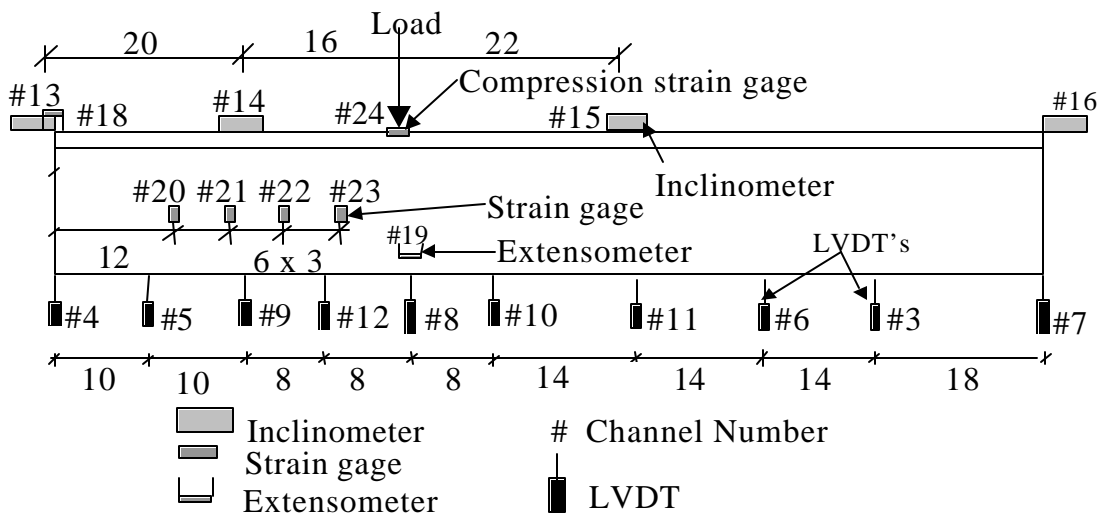


Figure 6.5: Schematic representation of the pushdown test.

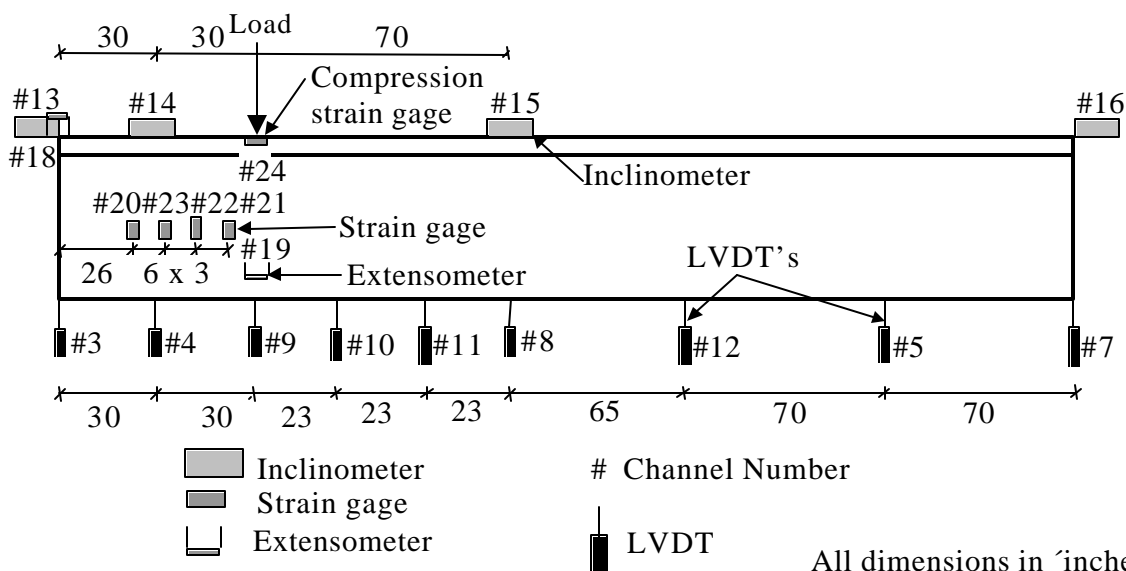


Figure 6.6: Load setup



All Dimensions in 'inches'
1 in = 25.4 mm

Figure 6.7: Instrumentation setup for short-span member



All dimensions in 'inches'
1 in = 25.4 mm

Figure 6.8: Instrumentation setup for long-span member

7. TEST RESULTS

7.1 SHORT-SPAN MEMBERS

In the following sections, in-situ test results will be discussed for each series of component testing in terms of load deflection, cracking behavior and failure mode. The experimental test results of the short-span members (JS series) are tabulated in Table 7.1.

Table 7.1: Experimental Results of Short-Span Joists

Member	Strengthening systems		Experimental			
	No of plies	End anchors	Experimental failure mode	Max CFRP strain (in/in)	Total load applied at failure P (kips)	Estimated V_u (kips)
JS1A	None	No	Shear	---	71	48
JS1B			Shear		72	
JS2A	1	No	Peeling	-NA-	80	53
JS2B			Peeling		79	
JS3A	1	Yes	APO ²	0.00075	99	66
JS3B			APO ²		93	
JS4A	2	No	Peeling	0.0003	82	57
JS4B			Peeling		70	
JS5A	2	Yes	APO ²	0.0005	94	67
JS5B			APO ²		90	
JS6A ¹	2	Yes	APO ²	0.0005	91	55
JS6B ¹			APO ²		81	

¹Aramid sheets

²Anchor pullout

Conversion Factor: 1 in = 25.4 mm, 1 kip = 4.448 kN

7.1.1 DISCUSSION OF FAILURE MODES

Control Specimen (JS1):

When the control specimens JS1 (A/B) were loaded to failure, they exhibited inclined flexural shear failure.

For beam JS1A, initial shear cracks were formed in the shear span between the applied load and support-‘A’ at a load of 30-kips (133-kN). The widening of this shear crack at its middle, and its propagation at its ends led to eventual failure of the beam in the left shear span at a load of 71-kips (316-kN), as shown in Figure 7.1. Beam JS1B exhibited similar failure and failed in shear in the left shear span at a load of 72-kips (320-kN). The shear failure of the control specimen is illustrated in Figure 7.2.

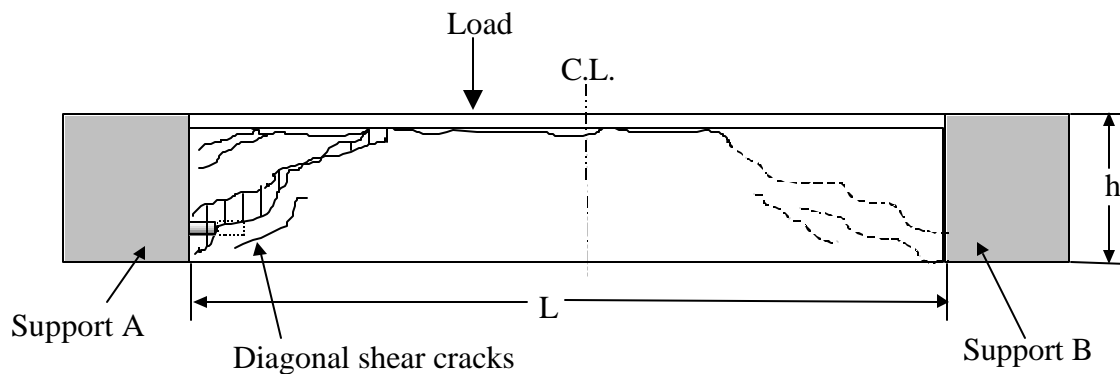


Figure 7.1: Schematic representation of shear cracks in unstrengthened member

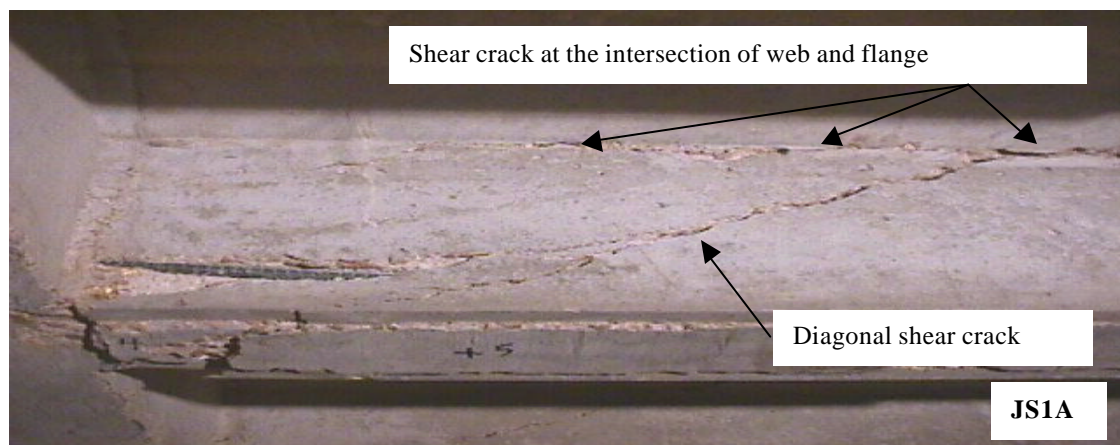


Figure 7.2: Shear cracks in unstrengthened member at failure

Unanchored specimens (JS2 & JS4):

Beams JS2 and JS4 were strengthened by applying CFRP sheets in the form of a jacket around the bottom and side faces of the entire joist as described in chapter 3 and previously shown in Figure 3.10 and Figure 3.14. The failure of these unanchored specimens was due to cover delamination of the CFRP sheets. For JS2 and JS4, the maximum load attained was 80-kips (335-kN) and 82-kips (364-kN), respectively. The failure was a gradual process. This could be identified by the cracking sound as the load was being applied. To identify the possible locations of delamination, the load was kept constant, and the sides of the joist were gently tapped. Close to failure load the deflection increased rapidly and the beam failed with a loud noise. The crack pattern of the strengthened specimen could be observed by peeling of the sheets after the test was concluded (Figure 7.3). The peeling failure of an unanchored member is shown in Figure 7.4. The unanchored specimens exhibited a similar crack pattern at the near end support as that of the control specimen as illustrated in Figure 7.5.

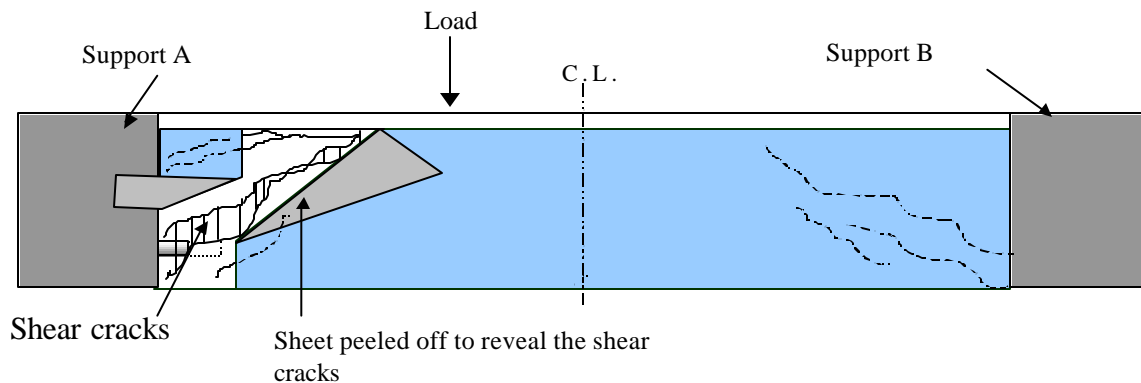


Figure 7.3: Sheets peeled off to reveal the shear cracks in unanchored members

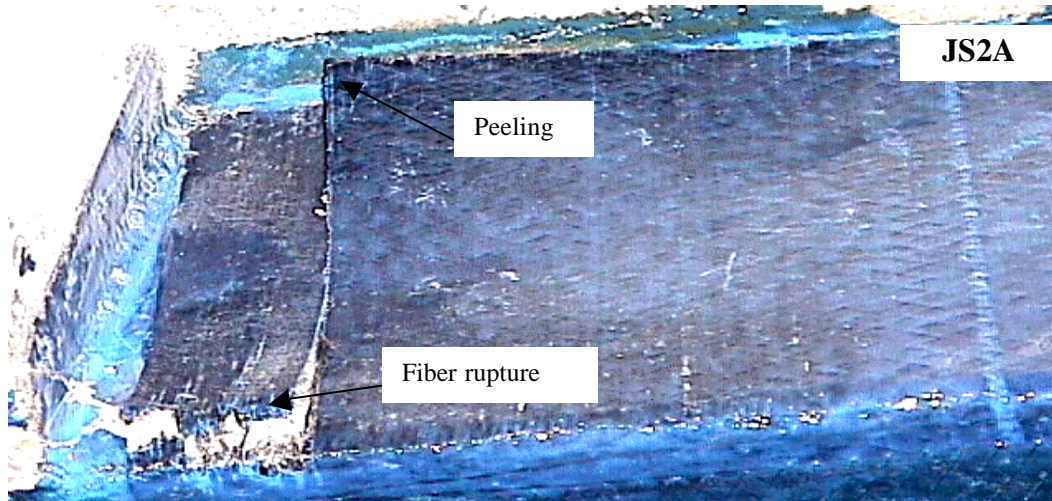


Figure 7.4: Peeling in unanchored members

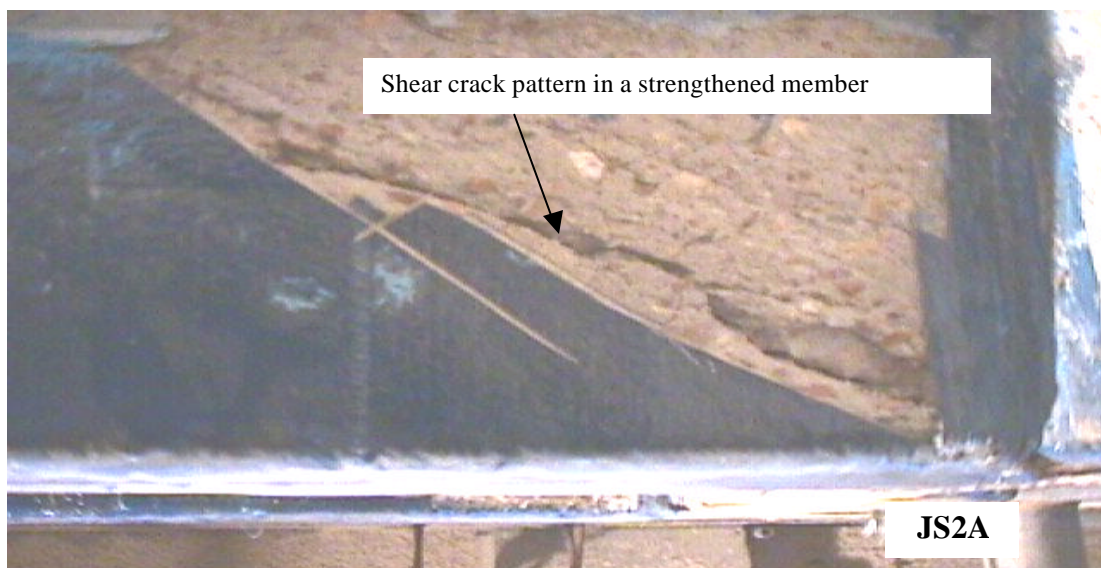


Figure 7.5: Sheets peeled off to reveal the shear cracks in a strengthened member

End-Anchored Systems (JS3, JS5 & JS6):

Beams JS3, JS5 and JS6 were strengthened by applying fiber sheets in the form of a jacket around the bottom and side faces of the shear span. These sheets were anchored using deformed #4 GFRP rods. For JS3, JS5 and JS6 the maximum load attained was 99-

kips (440-kN), 94-kips (420-kips) and 91-kips (404-kN), respectively. The failure of the anchored members was due to anchor pull out, as shown in Figure 7.6. The failure of the beam was sudden and accompanied by a loud noise. The crack pattern of the specimens could be observed by peeling of the sheets after the test was concluded. Each of these strengthened specimens showed a similar crack pattern as that of the control specimen. The diagonal shear cracks formed on the left-end shear span of the member. These cracks widened and propagated to the top of the beam and then into the flange. The anchor pullout failure can be attributed to the propagation of diagonal shear cracks to the intersection of web and flange (Figure 7.6), thus weakening the bond.

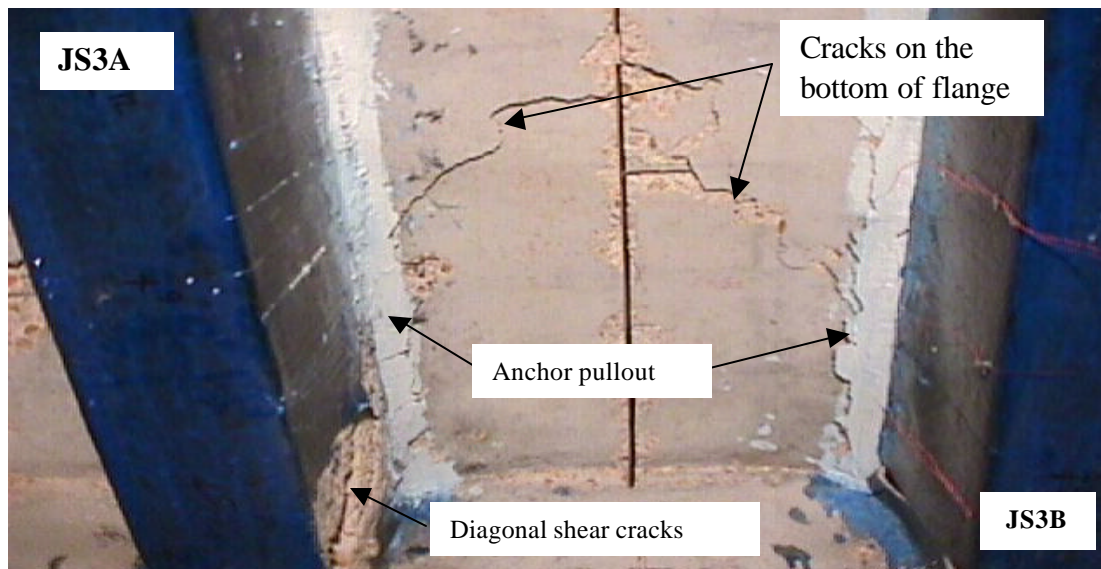


Figure 7.6: Failure of the end anchored member due to anchor pull out

Comparison of the strains:

Figure 7.7 illustrate the strains that developed in the FRP sheets during the load testing of members JS3A, JS5A, and JS6A respectively. JS1 being the unstrengthened member no strain gages were used on that specimen. The strain data for members JS2 and JS4 was lost due to faulty instrumentation.

As illustrated in Figure 7.7, it is clearly visible that beyond point Q, a sudden increase in the strain readings in the FRP sheets occurred. This is attributed to the formation of diagonal shear cracks on the near end support of the beam (support 'A').

The strain that developed in JS3A prior to failure of the strain gage instrumentation was 7429- μe , which was equivalent to 46% of the ultimate strain (16,000- μe) of the FRP sheets. The actual load of failure of JS3A was 99-kips (440-kN), but the strain gage failed to register data after 60-kips (267-kN). Four strain gages were used for all the members. Strain gage channel-#21 located at a distance of 14-in (355-mm) from support 'A' recorded the highest strain. This indicates the possibility of shear cracks close to support 'A'. Strain gages are very sensitive, and are susceptible to damages when cracks pass at close proximity to them. The loss of strain data (channel-#21) after 60-kips (267-kN) for JS3A/JS6A and 70-kips (311-kN) for JS5A could be attributed due to the shear cracks passing through the strain gage.

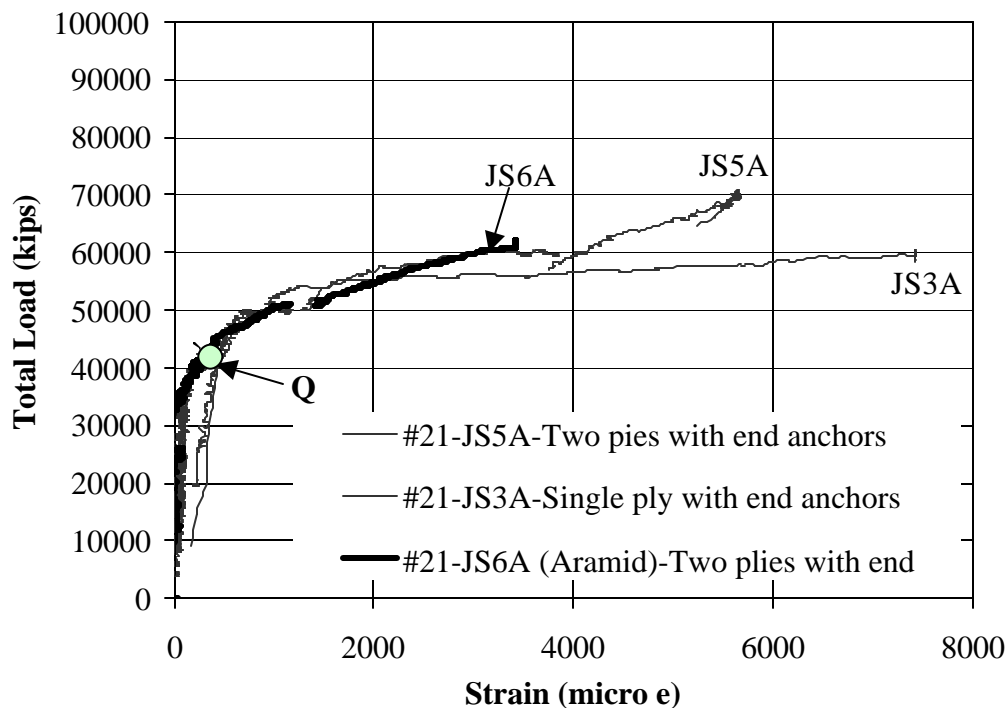


Figure 7.7: Load vs. strain diagram of JS3A, JS5A and JS6A specimens.

Strain developed in specimen JS5A was 5575- $\mu\epsilon$, corresponding to 35% of the ultimate strain on the FRP sheet. The actual load of failure for JS5A was 94-kips (418-kN), but the strain gage failed to register data after 70-kips (311-kN).

Strain developed in specimen JS6A was 3487- $\mu\epsilon$, corresponding to 22% of the ultimate strain on the FRP sheet. The actual load of failure for JS6A was 91-kips (404-kN), but the strain gage failed to register data after 61-kips (271-kN).

7.1.2 COMPARISON OF RESULTS

Single and Double plies:

Without End-Anchors (JS2A & JS4A):

Load-deflection curves of specimen JS2A and JS4A are given in Figure 7.8. Both of the specimens failed due to cover delamination.

The use of FRP sheets increased the stiffness of the member. This is clearly evident from the load-deflection curve presented in Figure 7.8. Up to an applied load of 60-kips (267-kN), beams (JS2A/JS4A) exhibited similar stiffness. Shear cracks appeared in the joists at 60-kips (267-kN). Beyond 60-kips (267-kN), the member strengthened with two-ply of CFRP retained the same stiffness, while the member with one ply (JS2A) exhibited a considerable degradation in the stiffness.

For JS2A a maximum deflection of 0.43-in (10-mm) was observed at an applied load of 80-kips (355-kN), which corresponded to a maximum shear force of 53-kips (236-kN) on support 'A' (Figure 7.1). For JS4A, a maximum deflection of 0.26-in (6-mm) was observed at an applied load of 82-kips (365-kN), which corresponded to a maximum shear force of 57-kips (256-kN) at support 'A'. JS4A showed an increase of 61% in stiffness. The increase in the shear capacity was approximately 8.5%.

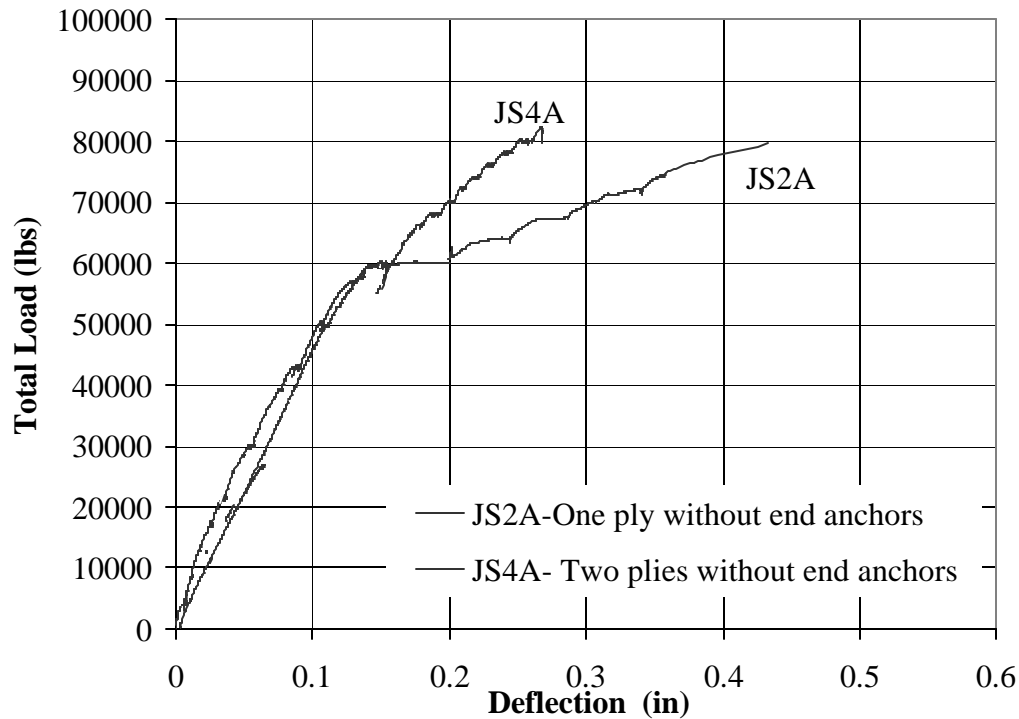


Figure 7.8: Load vs. deflection curves of JS2A and JS4A

With End-Anchors (JS3A & JS5A):

Load-deflection curves for JS3A and JS5A are presented in Figure 7.9. Both these members exhibited failure due to anchor pullout.

Figure 7.10 shows load-strain readings for each member at a distance of 14-in (355-mm) from the end support (support 'A'). The strain in JS3A and JS5A increased rapidly beyond an applied load of 45-kips (178-kN), represented by point 'Q' in Figure 7.10. This sudden increase in the strain can be attributed to the appearance of diagonal shear cracks in the left end shear span. As the load increased the strain in the members also increased. The strain reading for JS3A and JS5A was 7500 $\mu\epsilon$ and 5600 $\mu\epsilon$, respectively.

The deflected shape of JS3A and JS5A is illustrated in Figure 7.11. Up to an applied load of 45-kips (200-kN), JS3A and JS5A exhibited similar stiffness. As the applied load increased beyond 45-kips (200-kN), the member strengthened with two plies (JS5A) exhibited slightly higher stiffness than the member with one ply (JS3A)

Figure 7.12, illustrates the load-rotation curves for members JS3A and JS5A until failure. Inclinator #13 was placed at the near end support (support 'A'). Inclinator #13, for JS3 showed a maximum rotation of 0.10-deg at failure. Member JS5A showed a maximum rotation of 0.07-deg at failure.

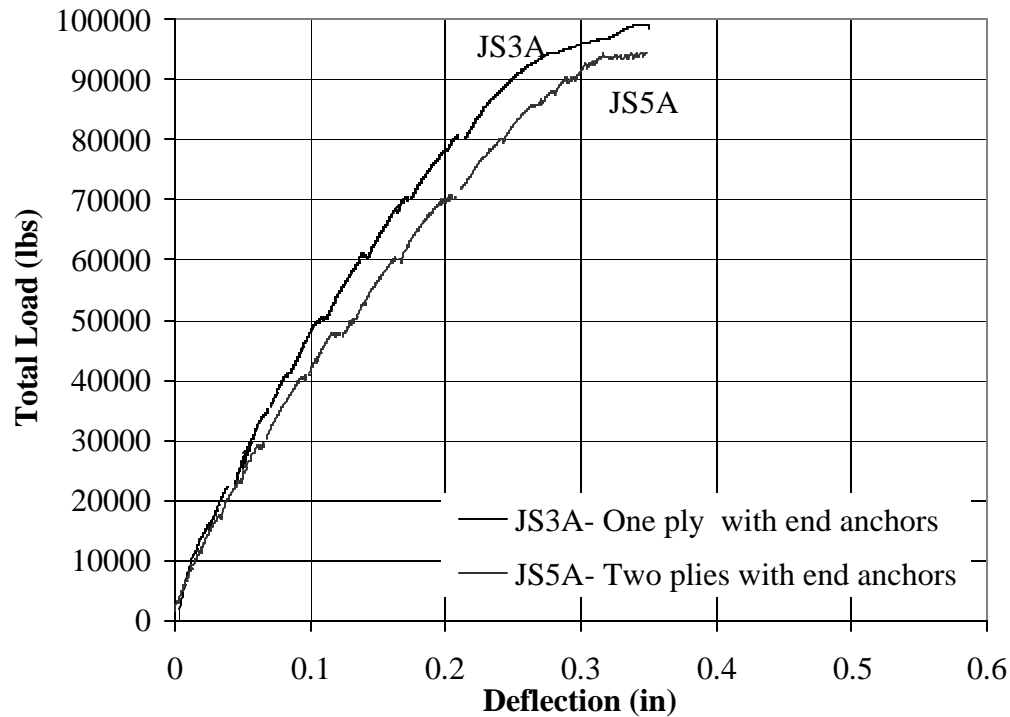


Figure 7.9: Load vs. deflection curves of JS3A and JS5A

Beams JS3A and JS5A underwent shear failure followed by anchor pullout. For JS3A, a maximum deflection of 0.35-in (8.9-mm) was recorded for a applied load of 99-kips (440-kN). This corresponded to a maximum shear force of 66-kips (295-kN) on support 'A'. In JS5A, a maximum deflection of 0.34-in (8.86-mm) was observed at an applied load of 94-kips (418-kN), which corresponded to a maximum shear force of 67-kips (298-kN) at support 'A'. No significant increase in stiffness or shear capacity of the member was observed.

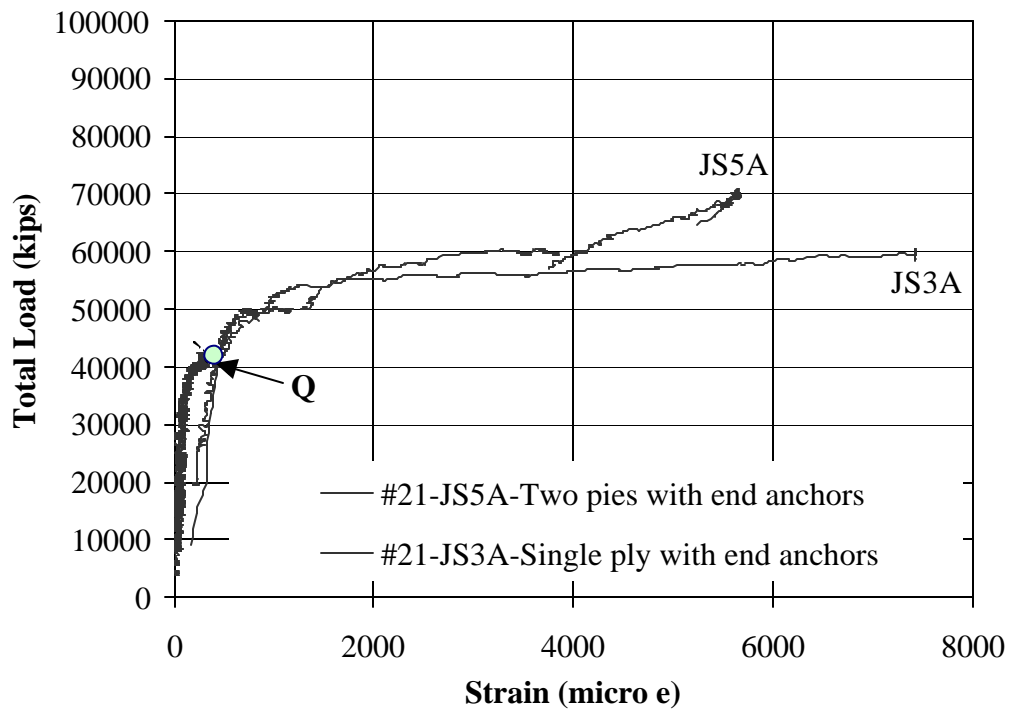


Figure 7.10: Load vs. strain curves of JS3A and JS5A

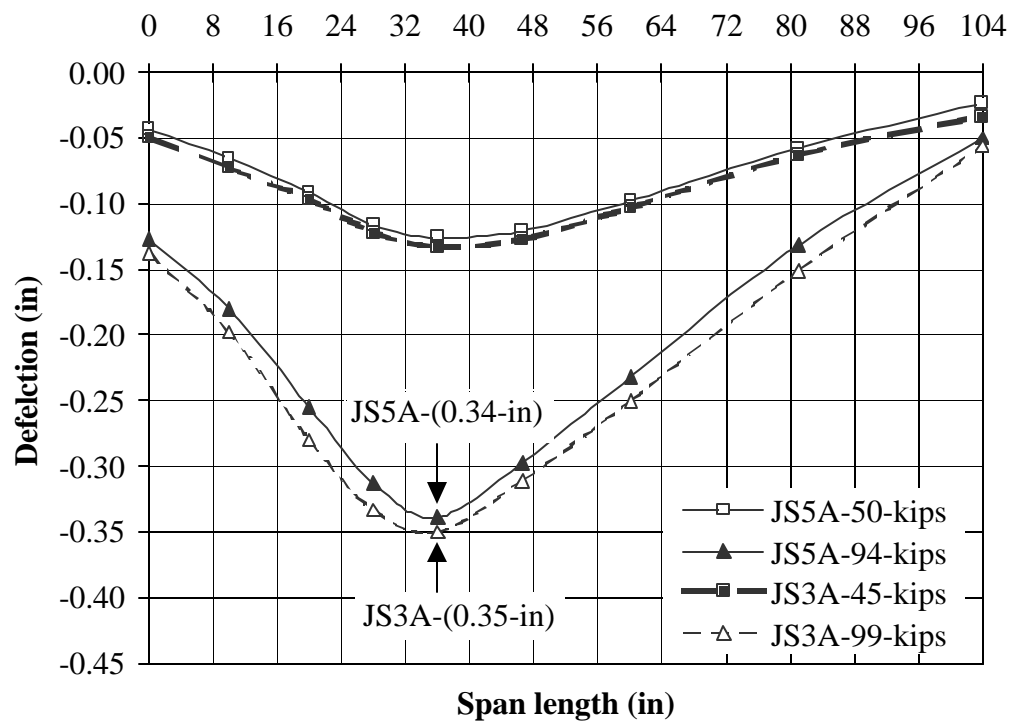


Figure 7.11: Deflection curve of JS3A and JS5A

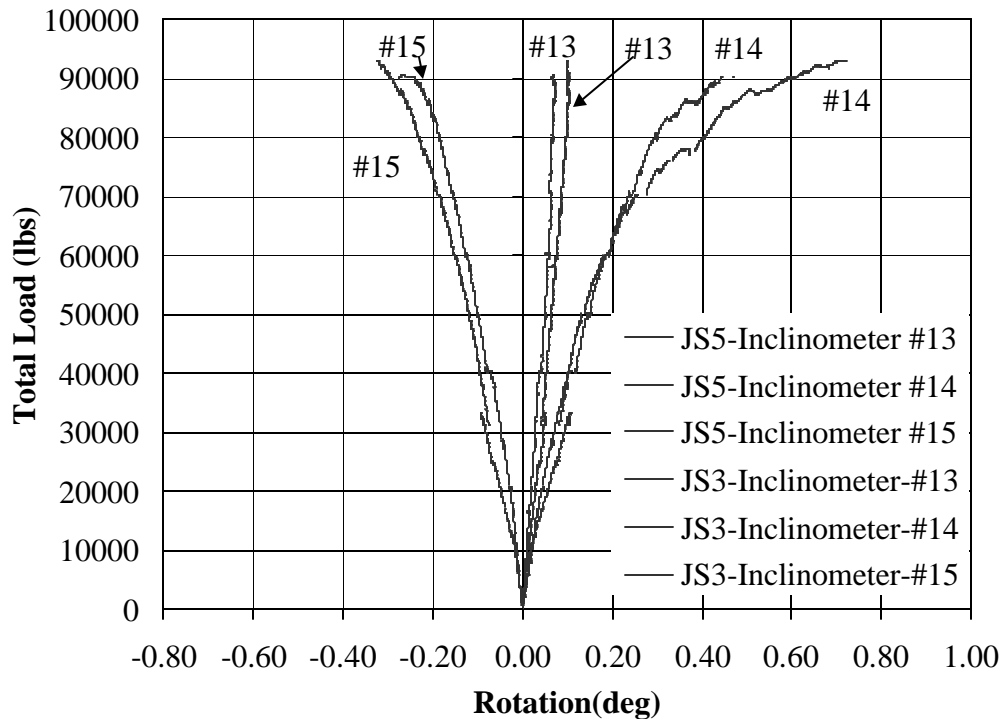


Figure 7.12: Load vs. rotation of JS3A and JS5A

Same number of plies:

One ply - with and without end anchors (JS2A & JS3A):

Figure 7.13 illustrates the relationship between applied load and deflection under load for members JS2A and JS3A. Both these members had the same amount of FRP, however, JS3A included an end anchor.

As exhibited in Figure 7.13 both members had a similar stiffness up to point 'A' (60-kips). Beyond an applied load of 60-kips (267-kN), there was considerable decrease in the stiffness of JS2. This decrease can be attributed to the formation of diagonal shear cracks. The single ply unanchored members (JS2) were less effective in retaining the stiffness of the beam after the formation of shear cracks, when compared to the single ply end anchored members (JS3).

The diagonal shear cracks observed in the beams after failure were similar in both the cases. The shear force was greater in the beam with end anchorage. In JS2A, a maximum deflection of 0.43-in (11-mm) was observed for a load of 79-kips (359-kN),

which corresponded to a maximum shear force of 53-kips (236-kN) on support 'A'. In JS3A, a maximum deflection of 0.35-in (9-mm) was observed for a load of 99-kips (440-kN), which corresponded to a maximum shear force of 66-kips (295-kN) on support 'A'. JS3A showed a gain in stiffness of 20% and increase in shear capacity by 25%.

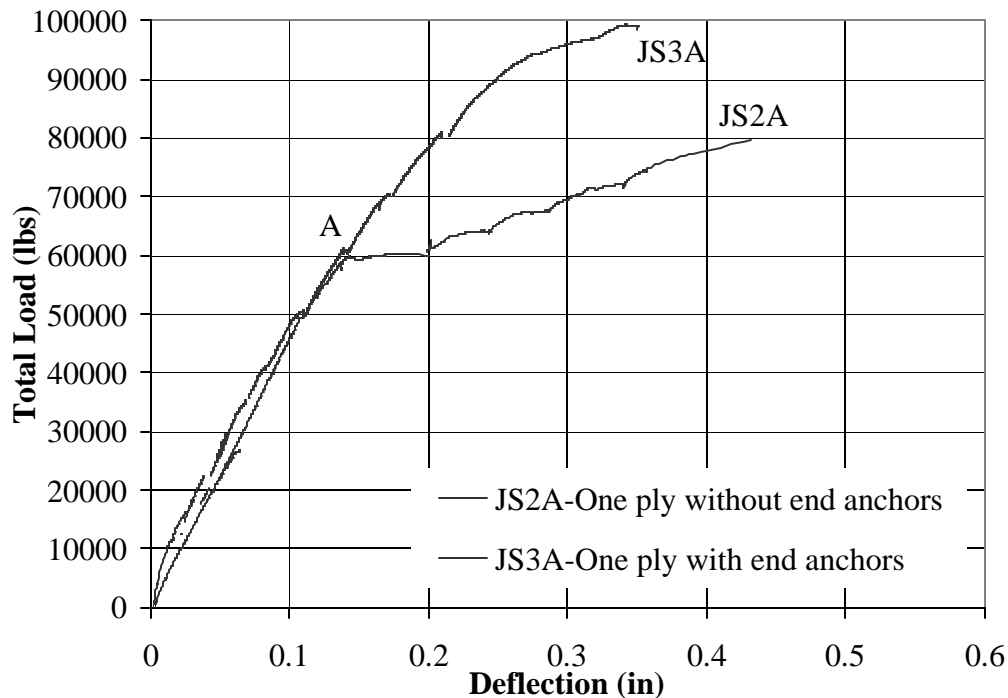


Figure 7.13: Load vs. deflection curves of JS3A and JS2A

Two ply-with and without end anchors (JS4A & JS5A):

Figure 7.14 illustrates the relationship between applied load and deflection under load for members JS4A and JS5A. Both these members were strengthened with the same amount of FRP, however, JS5A included an end anchor.

As illustrated in Figure 7.14, it is clearly visible that both specimens exhibited similar stiffness, however, the joist strengthened with an end anchor (JS5A) exhibited an increase in strength compared to the unanchored (JS4A) member. In JS4A, a maximum deflection of 0.26-in (6.8-mm) was observed at an applied load of 80.6-kips (358-kN), which corresponded to a maximum shear force of 57.6-kips (236-kN) at support 'A'. For JS5A, a maximum deflection of 0.35-in (6.6-mm) was observed at an applied load of

88.4-kips (393-kN), which corresponded to a maximum shear force of 67-kips (298-kN) on support 'A'. JS5A showed a gain in shear capacity was 17%.

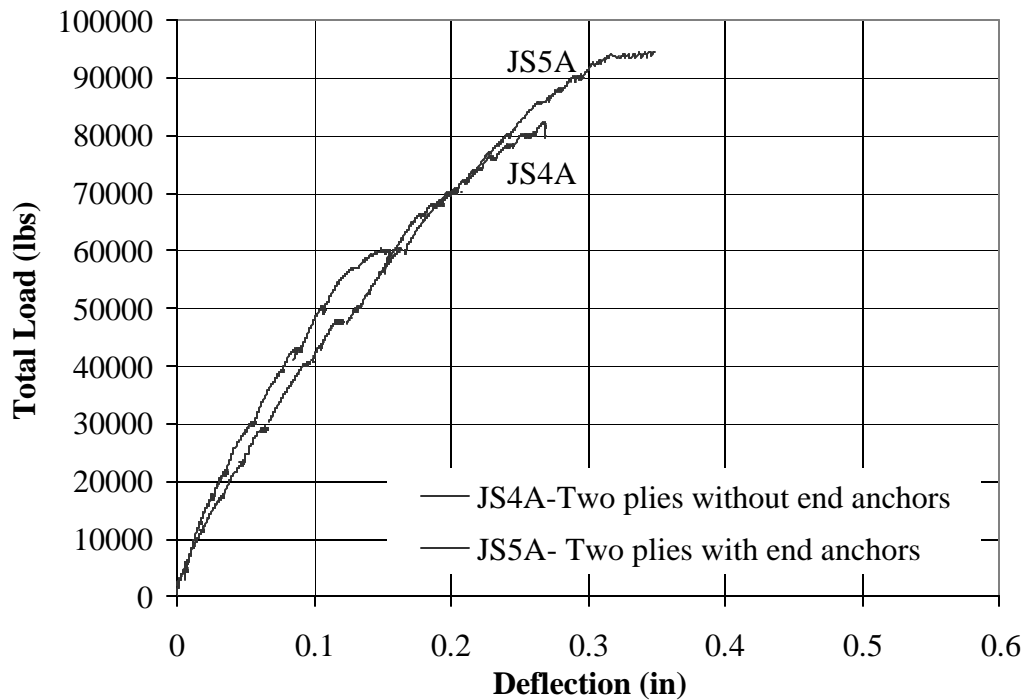


Figure 7.14: Load vs. deflection curves of JS4A and JS5A

Different fiber types:

Two ply - with end anchor (JS5A & JS6A):

Figure 7.15 illustrates the relationship between applied load and deflection under load for members JS5A and JS6A. Both these members had the same amount of FRP. JS5A was strengthened with two plies of CFRP sheets and JS6A was strengthened with two plies of AFRP sheets. The member strengthened with CFRP sheet exhibited a slight increase in the shear capacity.

For JS5A, a maximum deflection of 0.35-in (8.6-mm) was observed at an applied load of 94-kips (418-kN), which corresponded to a maximum shear force of 55-kips (243-kN) on support 'A'. For JS6A, a maximum deflection of 0.39-in (10-mm) was observed at an applied load of 91-kips (408-kN), which corresponded to a maximum

shear force of 67-kips (298-kN) on support 'A'. JS5A showed a gain in stiffness of about 17% and a gain in shear capacity by 22% compare to the unstrengthened members.

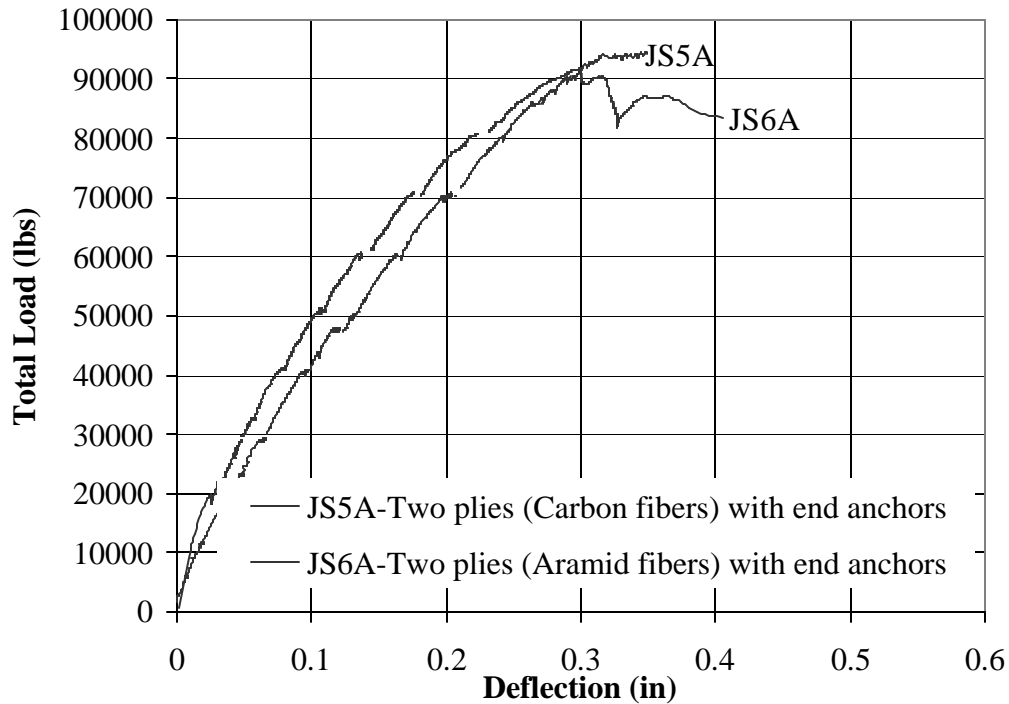


Figure 7.15: Load vs. deflection curves of JS5A and JS6A

7.2 LONG-SPAN MEMBERS

In the following sections, results of members of the long-span series in terms of load deflection, cracking behavior and the mode of failure will be discussed in detail. The test results of all the long-span members are tabulated in Table 7.2.

7.2.1 DISCUSSION OF FAILURE MODES

Control Specimen:

When the control specimens JL1 (A/B) were loaded to failure, they exhibited inclined shear failure as represented pictorially in Figure 7.16.

For beam JL1A, at a point load of 16-kips (72-kN), the initial cracks were formed at the end of the flare, at a distance of 36-in (914-mm) from the near end support (support 'A'). The initial cracks were formed as negative flexure cracks in the flange. These cracks widened and propagated through the flare along the direction of the reinforcing steel, ultimately resulting in failure at a peak load of 45-kips (248-kN). JL1B showed similar failure mode, and failed in shear at an ultimate load of 56-kips (200-kN). The shear failure of the control specimens is illustrated in Figure 7.17.

Table 7.2 Experimental Results of Long-Span Members

Member	Strengthening Systems			Experimental			
	No. of plies	End anchor	No. of neg. plies	Experimental failure mode	Max CFRP strain (in/in)	Total load applied at failure P (kips)	Estimated V_u (kips)
JL1A	None	No	0	Shear	---	45	39
JL1B				Shear		56	
JL2A	1	No	0	Peeling	-NA-	72	66
JL2B				Peeling		64	
JL3A	1	Yes	1	NFF ¹	0.0071	60	62
JL3B				NFF ¹		70	
JL4A	2	No	1	NFF ¹	0.0062	49	59.2
JL4B				NFF ¹		65	

¹ Negative flexure failure

Conversion Factor: 1-in = 25.4-mm, 1-kip = 4448-N

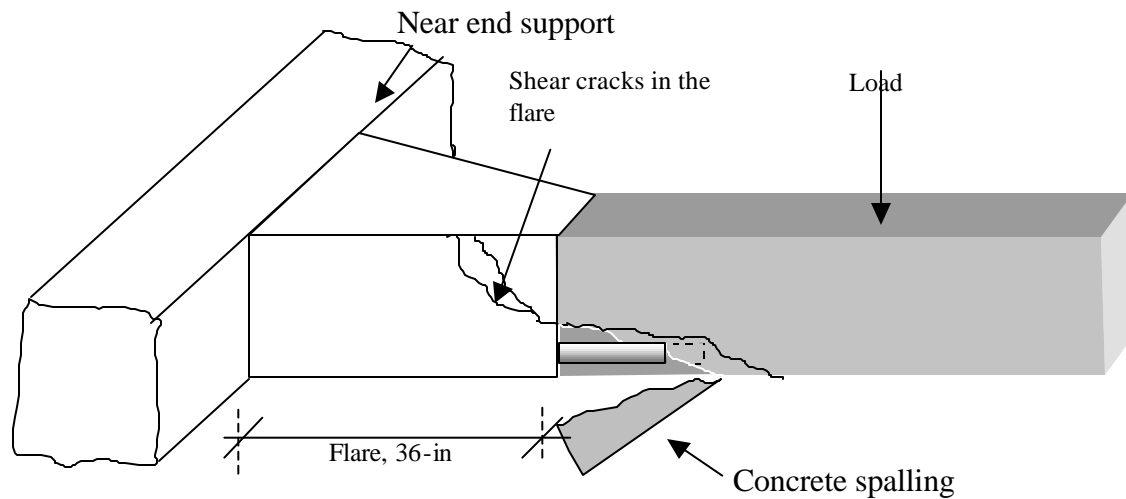


Figure 7.16: Pictorial representation of shear crack in unstrengthened member

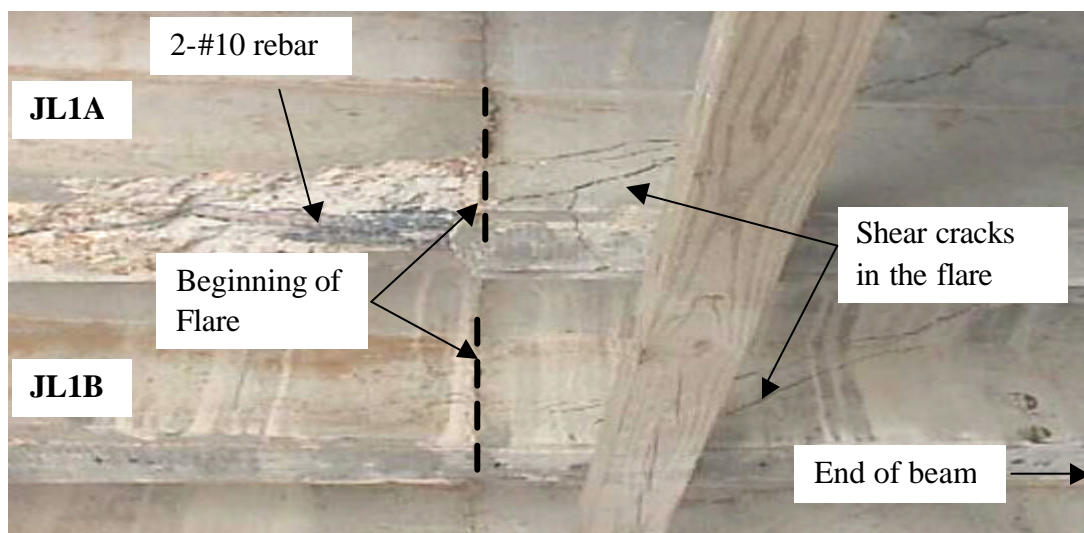


Figure 7.17: Shear failure of unstrengthened members

Unanchored specimens (JL2 & JL3):

Beams JL2 and JL3 were strengthened by applying CFRP sheets in the form of a jacket around the bottom and the side faces of the shear span as discussed in Chapter 3.

For JL2, with a continuous shear wrap was applied up to a distance of 96-in (2438-mm). The failure of unanchored member was due to cover delamination of CFRP

sheets. For JL2 the maximum load attained was 72-kips (320-kN). The failure of the member due to peeling is illustrated in Figure 7.18.

The failure of JL3 was due to negative flexure. This was an unexpected failure mode. This was attributed to excessive rotation of the weakened near-end support caused by excessive saw cutting. Each of the joists spanned between two end girders. These girders were assumed to act as fixed end supports for the joists. The joists were isolated by saw cutting the floor, along the longitudinal direction. In the case of JL3, this saw cut extended a distance of 14-in (356-mm) into the end support beam. The FRP sheets extended a distance of 12-in (304-mm) onto the end support. The negative flexure cracks were initiated beyond the FRP sheets, as illustrated in Figure 7.19. Figures 7.20 and 7.21 illustrate the negative flexure failure mode.

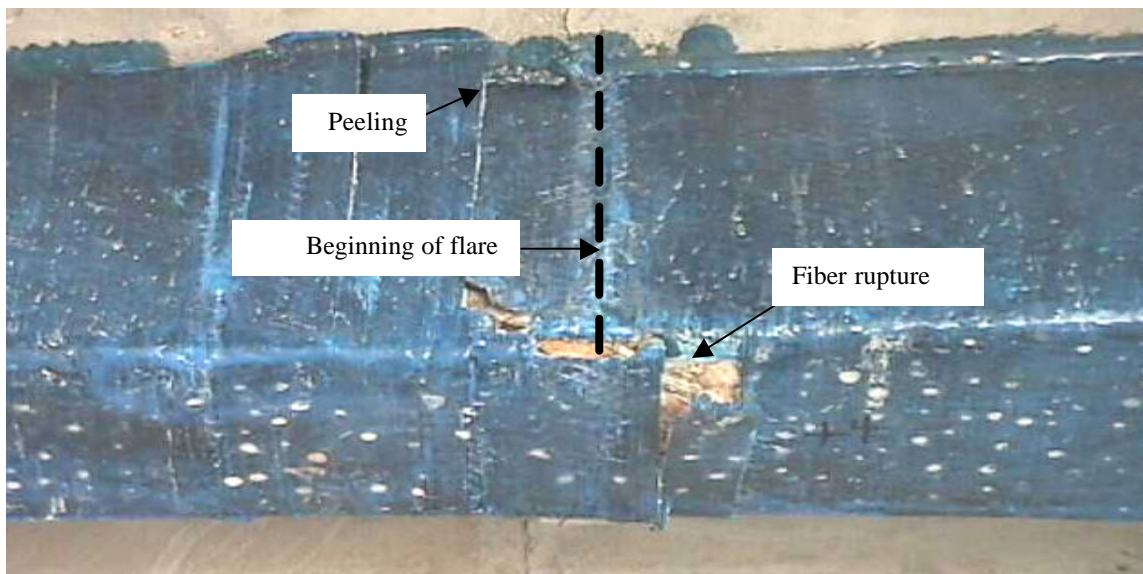


Figure 7.18: Peeling failure in an unanchored member

End-Anchored Systems:

The specimens of JL4 (A/B) were strengthened with a single U-wrap of CFRP sheet and end anchors. Specimens of JL4B failed at an ultimate applied load of 65-kip (292-kN). The failure of the members of system JL4 was similar to that of JL3. This failure mode is illustrated in Figure 7.20 and Figure 7.21.

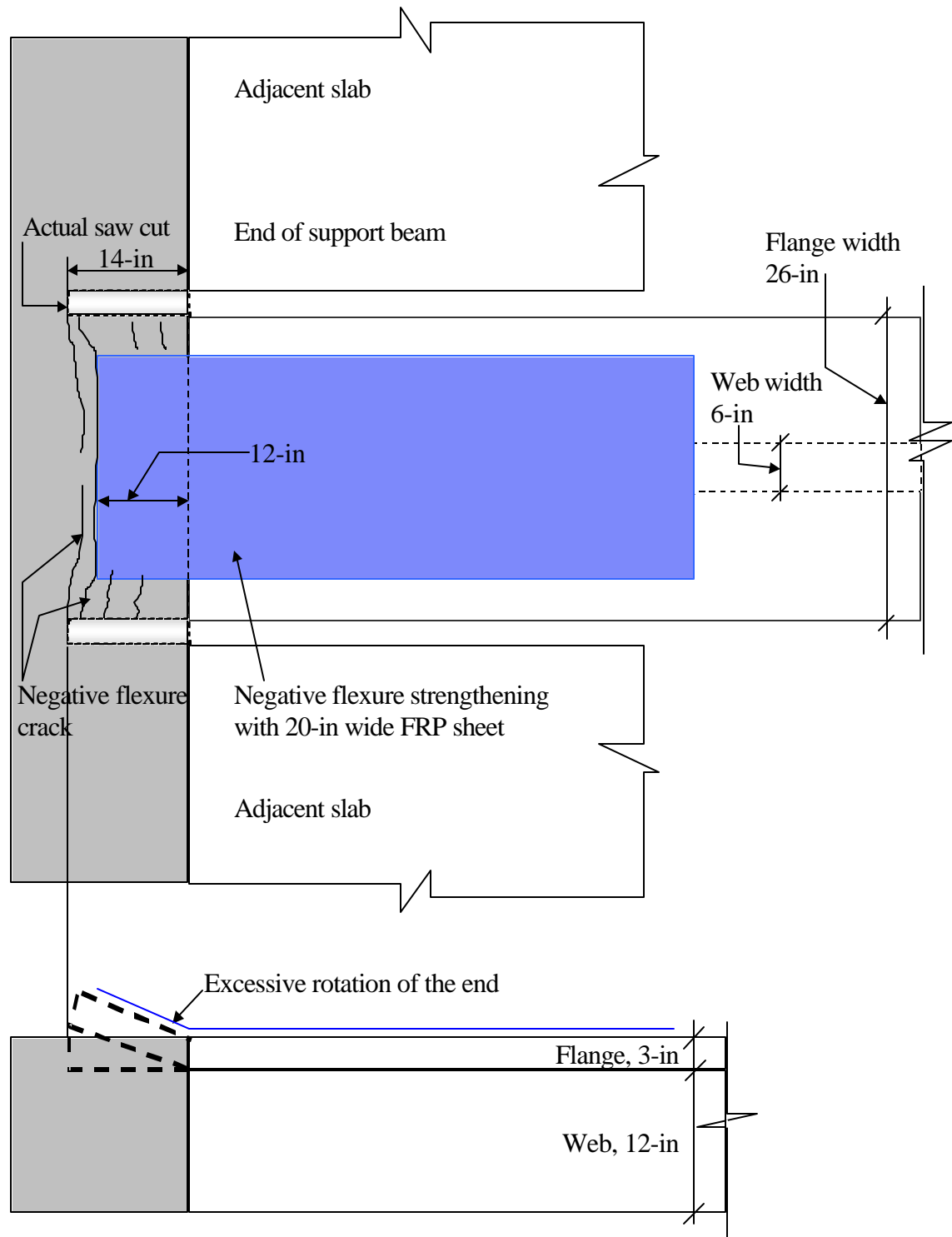


Figure 7.19: Schematic representation of negative flexure cracks

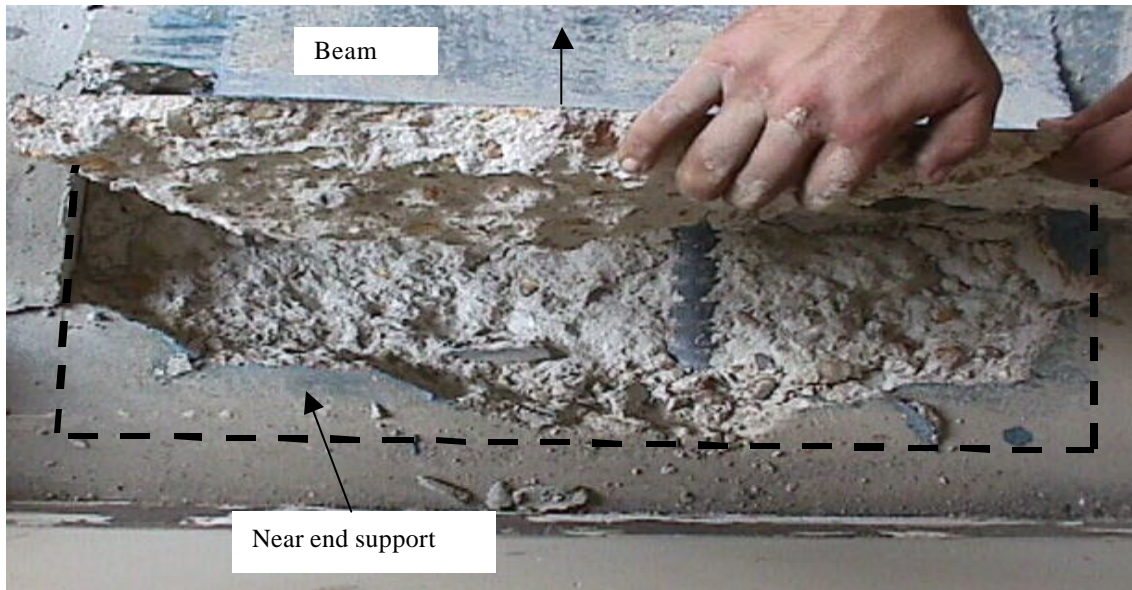


Figure 7.20: Negative flexure failure - view from top slab looking down

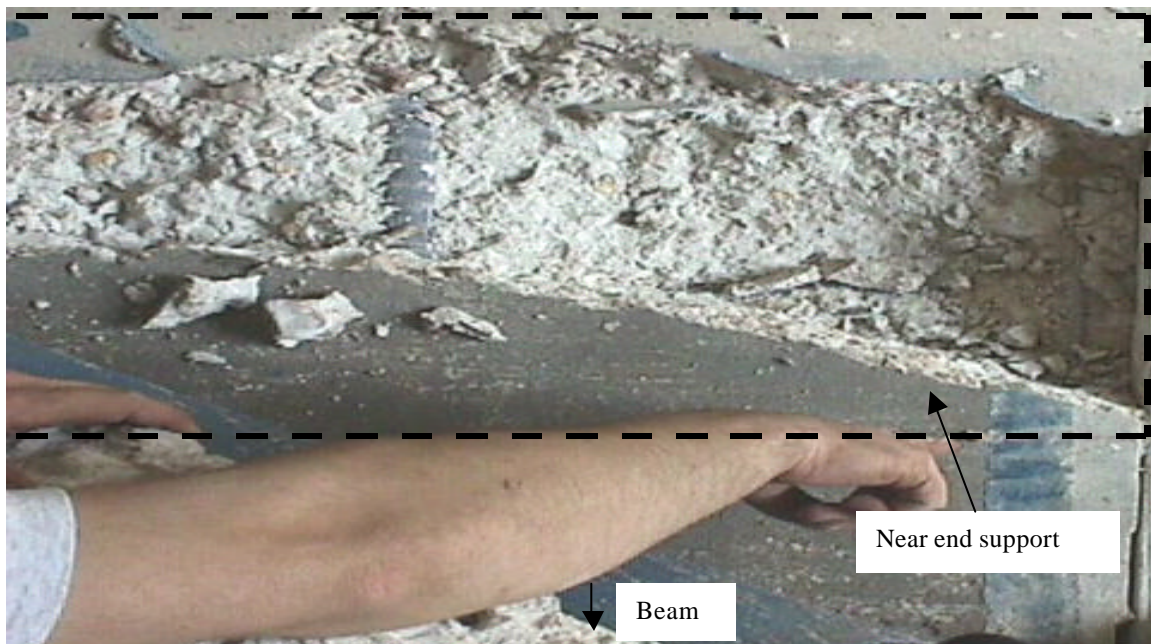


Figure 7.21: Negative flexure Failure

7.2.2 COMPARISON OF RESULTS:

Same number of plies:

One ply –with and without negative flexure strengthening:

Figure 7.22 illustrates the relation between the applied load and the deflection under load for member JL2A and JL3B. Both members had the same amount of shear strengthening, however, JL3B was strengthened in negative flexure. Specimen JL2A failed at an ultimate load of 72-kips (320-kN), that corresponded to a maximum shear force of 66-kips (278-kN) on support ‘A’. The specimen JL3B failed at an ultimate load of 70-kips (312-kN), that corresponded to a maximum shear force of 62-kips (293-kN) at support ‘A’. There was no gain in the shear capacity as predicted due to the unexpected mode of failure of the member.

The maximum deflections for JL2A and JL3B were 1.66-in (42.3-mm) and 1.10-in (28-mm) respectively. Load-deflection curves of the specimens of JL2A and JL3B are shown in Figure 7.22.

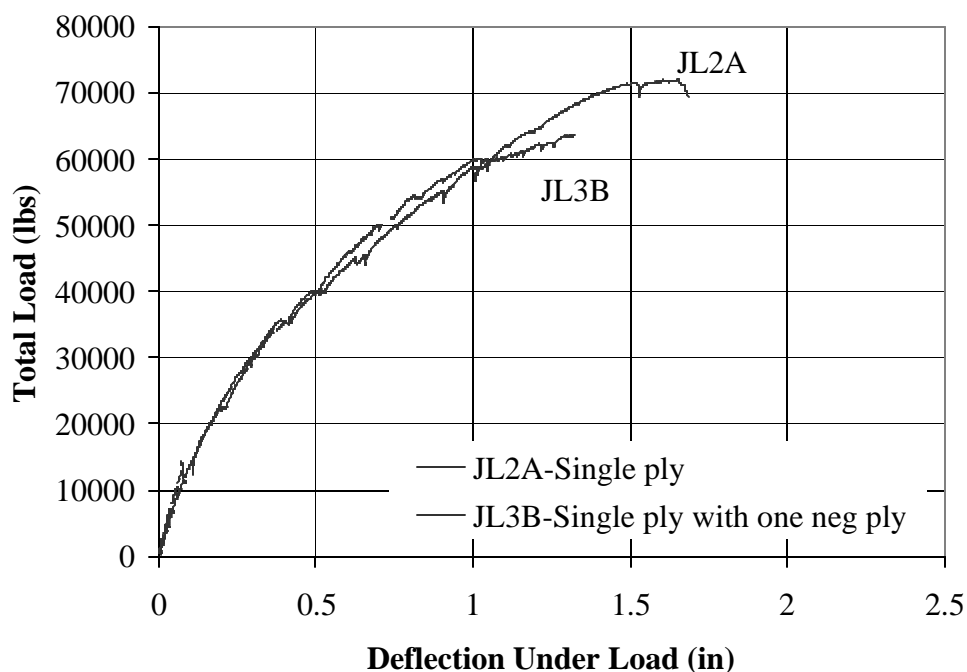


Figure 7.22: Load vs. deflection behavior of specimens JL2A and JL3B

All strengthened and unstrengthened members:

Figure 7.23 illustrates the load-deflection curves for all the long-span specimens excluding JL3. JL3 members failed in negative flexure, thus their results are not reported in Figure 7.23.

The strengthened members exhibited considerable increase in the load carrying capacity compared to the unstrengthened member. The strengthened members displayed better stiffness in relation to the unstrengthened member.

JL1B failed at an ultimate load of 56-kips (249-kN), the maximum displacement for the unstrengthened member was 1.25-in (31.7-mm). The displacement in the strengthened members at that load was 0.85-in (21.6-mm), which corresponded to an increase of 47% in the stiffness of the member.

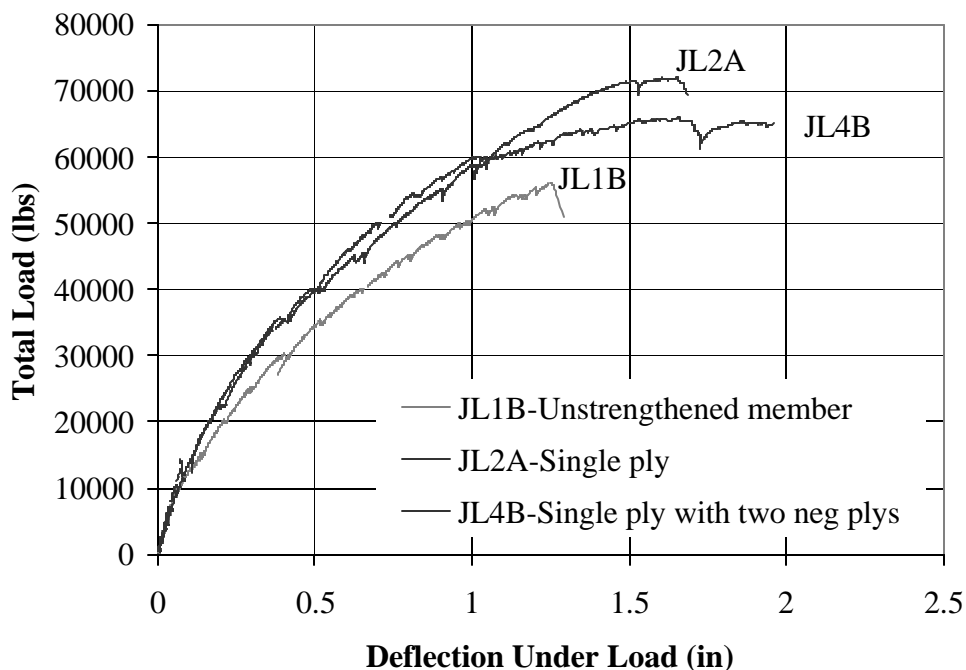


Figure 7.23: Comparison of load vs. deflection behavior for long span specimens

8. SUMMARY, CONCLUSIONS AND RECOMMENDATIONS

8.1 SUMMARY

The main objectives of this research study were:

- (a) To investigate the shear performance and modes of failure of RC joists strengthened with externally bonded CFRP sheets.
- (b) To validate design procedures.

In order to fulfil these objectives, an experimental program consisting of twenty full size RC joists was performed at the Malcolm Bliss Hospital, St. Louis, Missouri. The joist specimens were grouped into two series based on their span lengths. The first series consisted of twelve specimens, which were strengthened with different strengthening schemes and were tested to failure. The variable considered in this series was the number of plies used for shear strengthening. In addition to this, a novel end-anchor system that allowed for better exploitation of the strengthening system was also validated. The second series consisted of eight members that were strengthened with different strengthening systems. This series was used to validate the shear strengthening technique with and without end-anchors.

The design approach used for computing the shear strength of the RC joists with externally bonded FRP composites was also validated. The experiments addressed the two modes of failure of FRP reinforcement, namely: FRP fracture and FRP debonding.

8.2 CONCLUSIONS

Due to deterioration, age, or modifications in usage of RC structures, there is a growing demand for effective means of repair and strengthening of RC structures. Because of their outstanding mechanical, physical, and chemical properties, in addition to simplicity and effectiveness, advanced composite materials show promise in this area. The tests results described in this study indicated that for the strengthening techniques investigated externally bonded CFRP composites can be used to significantly increase shear capacity of RC beams. It was evident from the study conducted herein that the

efficiency of the strengthening technique varied depending on several variables. For the beams investigated in the experimental program, increases in shear strength ranged from 10 to 172% when compared to the control specimens.

Based on the experimental and analytical results, the following conclusions were drawn:

- Externally bonded FRP reinforcement can be used to enhance the shear capacity of RC beams in positive and negative moment regions.
- The test results confirmed that the strengthening technique of FRP system was applicable and can increase the shear capacity of rectangular as well as T-beams.
- The experimental verification of the end anchor system illustrated its effectiveness in increasing the shear capacity of RC beams. This anchor is recommended where bond and/or development length of FRP is critical according to the design procedure.
- Existing evidence clearly indicated that the end anchor system can make FRP strengthening even more attractive and economical for concrete repair and strengthening.
- The recorded FRP strain of the tested beams indicated that the failure of a FRP system occurs at an average effective stress level below nominal strength due to stress concentration or debonding of FRP from concrete surface.
- Increasing the amount of FRP may not result in a proportional increase in the shear strength especially if debonding of FRP controls the failure. A proportional increase in shear capacity with increasing FRP amount may be achieved when debonding is prevented such in the case of beams with end anchor.
- Shear strengthening schemes may not be effective for beams having short-span lengths, as was observed within the study. A splitting failure between the slab and beam (joist) can occur before the shear strengthening can be effective.

8.3 RECOMMENDATIONS FOR FUTURE WORK

Based on the findings and conclusions of the current study, the following recommendations are made for future study in FRP shear strengthening:

- Research is needed to further develop an analytical model to predict the shear behavior and failure mode of RC members strengthened with externally bonded FRP composites and to evaluate the influences of different parameters on the overall behavior of the member.
- Experimental and analytical investigations are required to link the shear contribution of FRP with the load condition.
- Research is needed to characterize the roughness of the concrete surface to link the bond capacity of FRP with the degree of concrete surface roughness and concrete strength.
- To optimize the design algorithm, additional in-situ members need to be tested with different FRP reinforcement levels and configurations.

APPENDIX A

TEST RESULTS

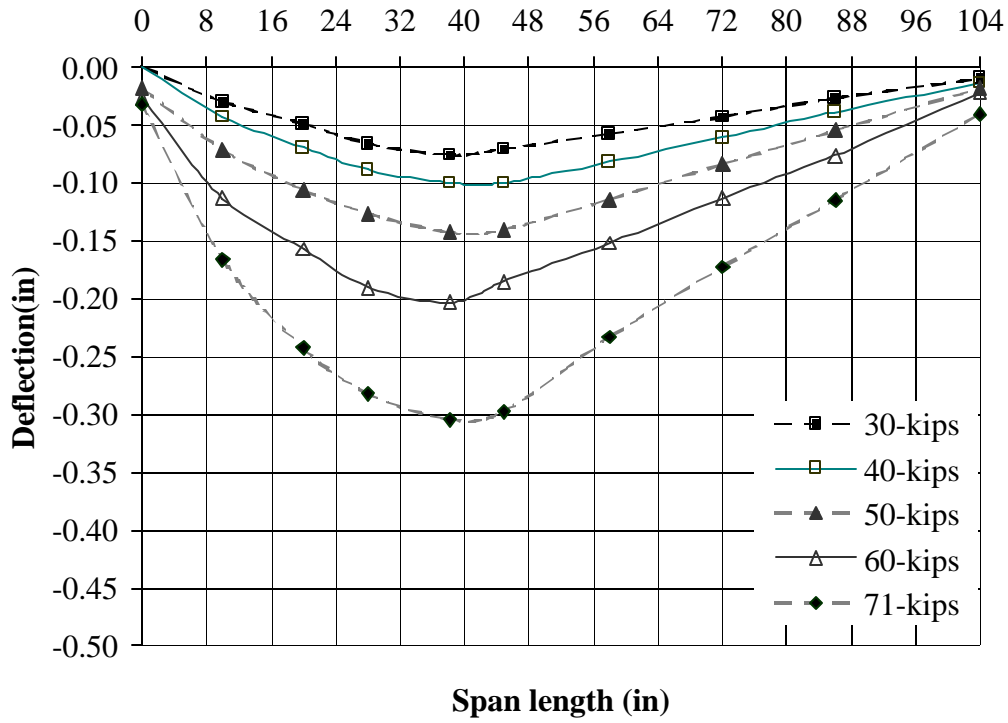


Figure A1: Deflected shape of joist JS1A

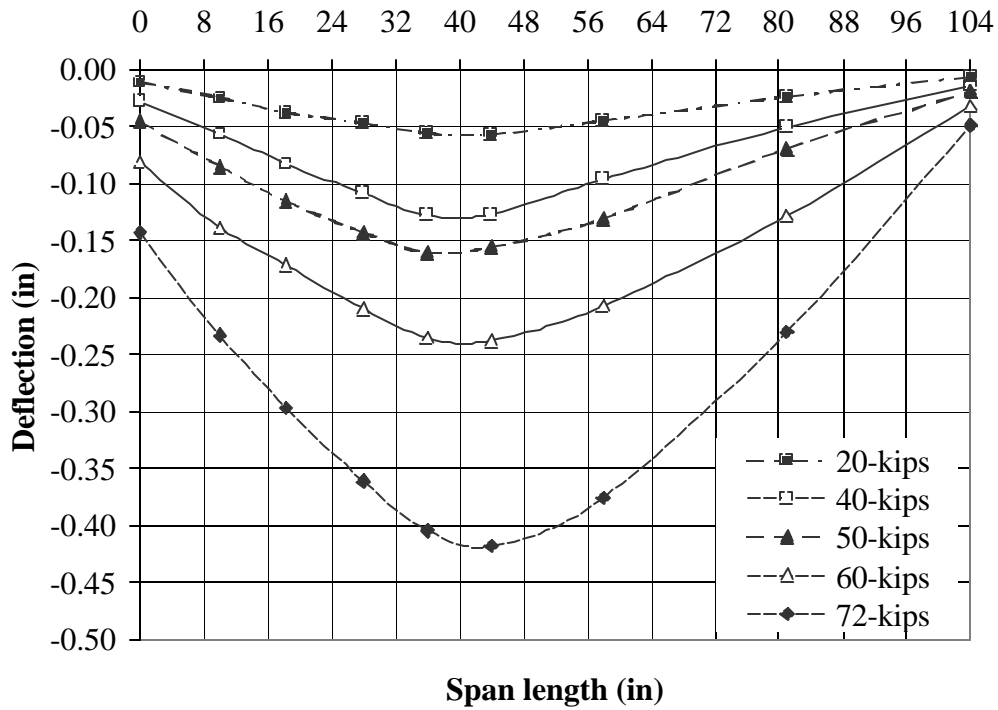


Figure A2: Deflected shape of joist JS1B

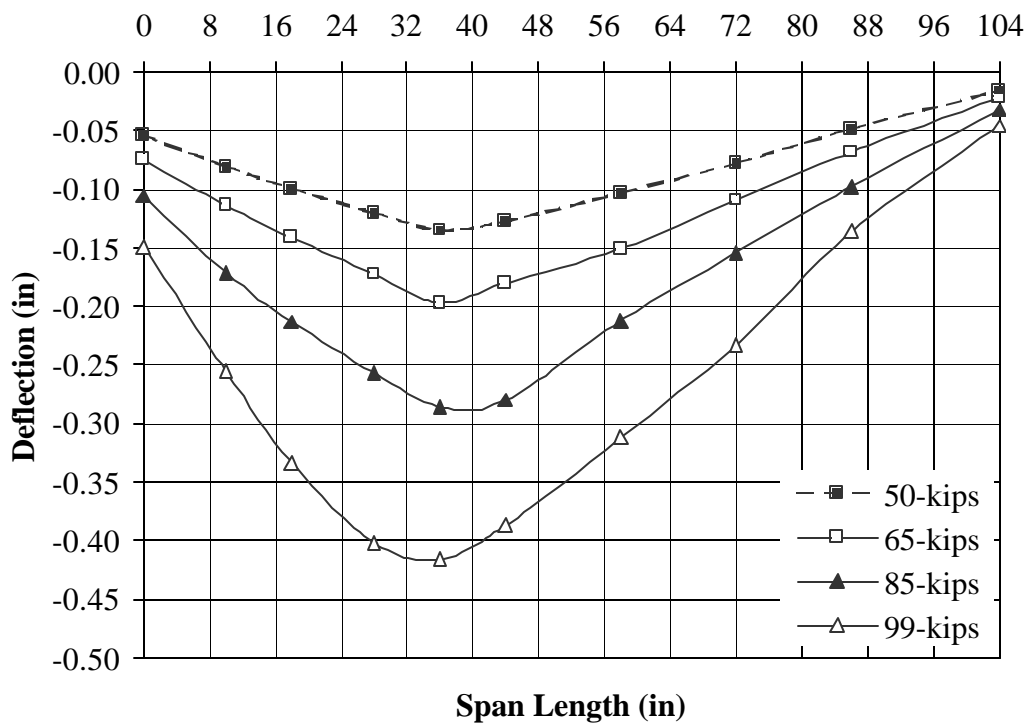


Figure A3: Deflected shape of joist JS3A

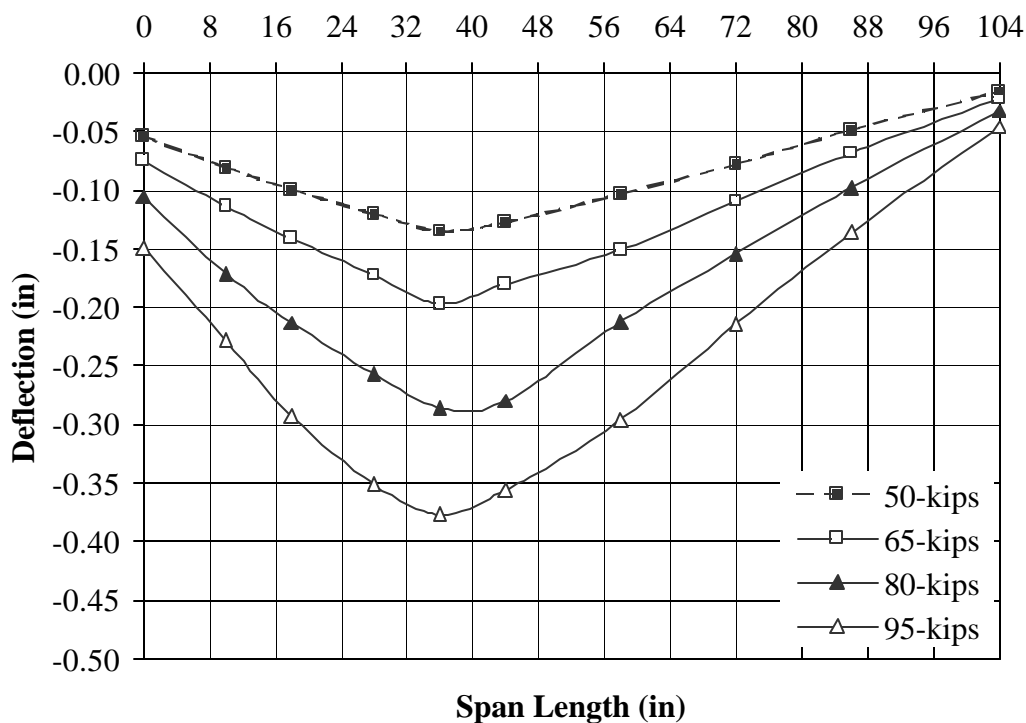


Figure A4: Deflected shape of joist JS3B

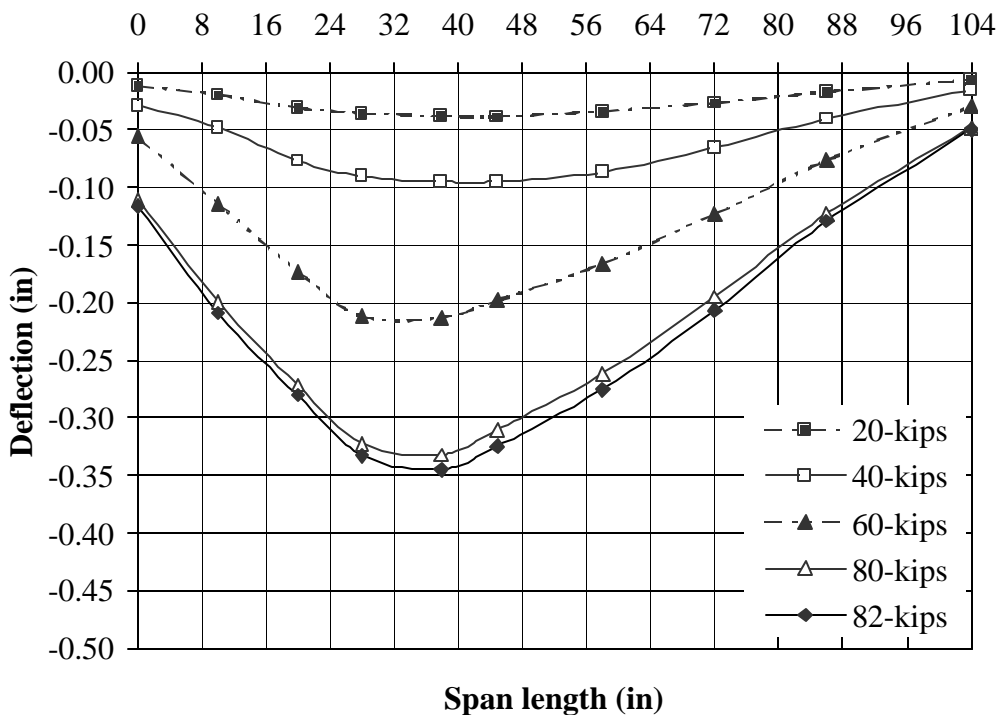


Figure A5: Deflected shape of joist JS4A

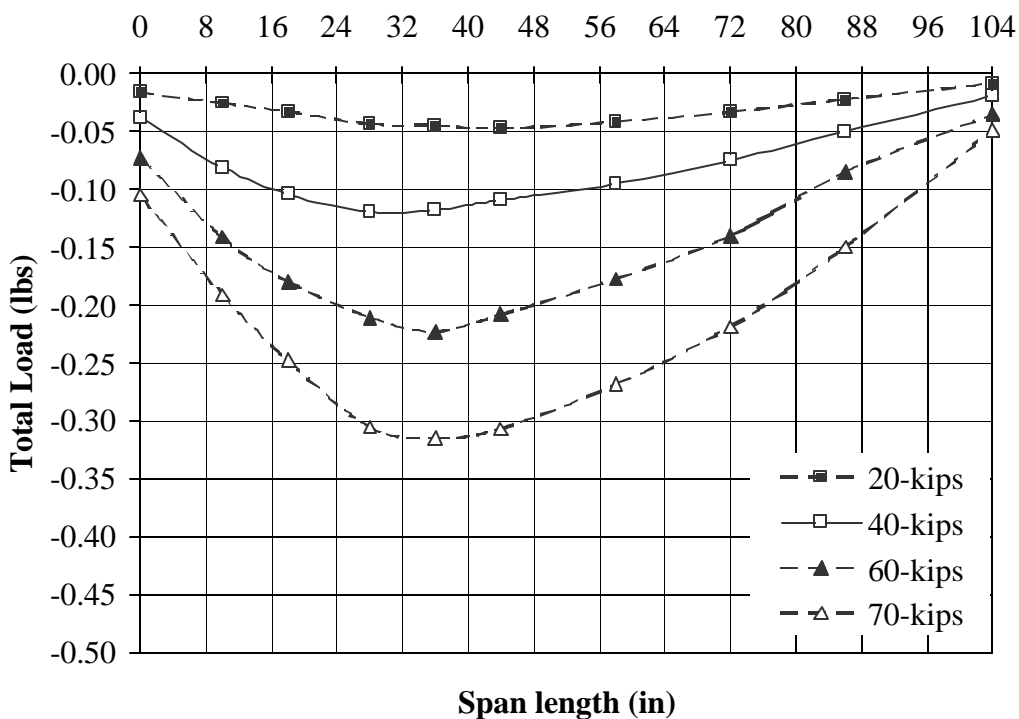


Figure A6: Deflected shape of joist JS4B

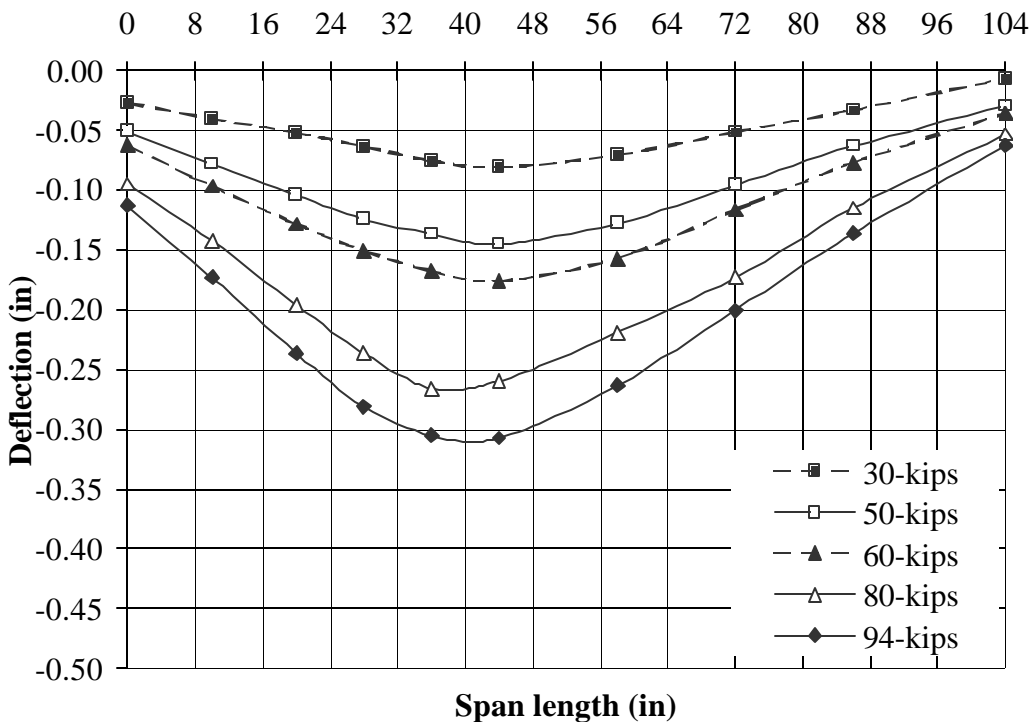


Figure A7: Deflected shape of joist JS5A

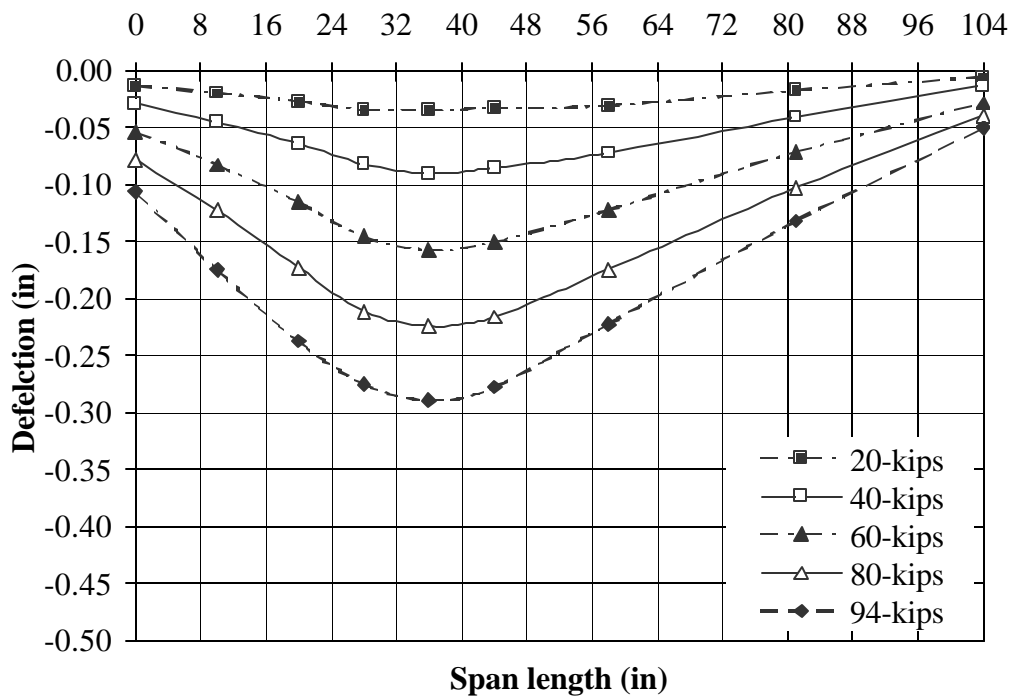


Figure A8: Deflected shape of joist JS5B

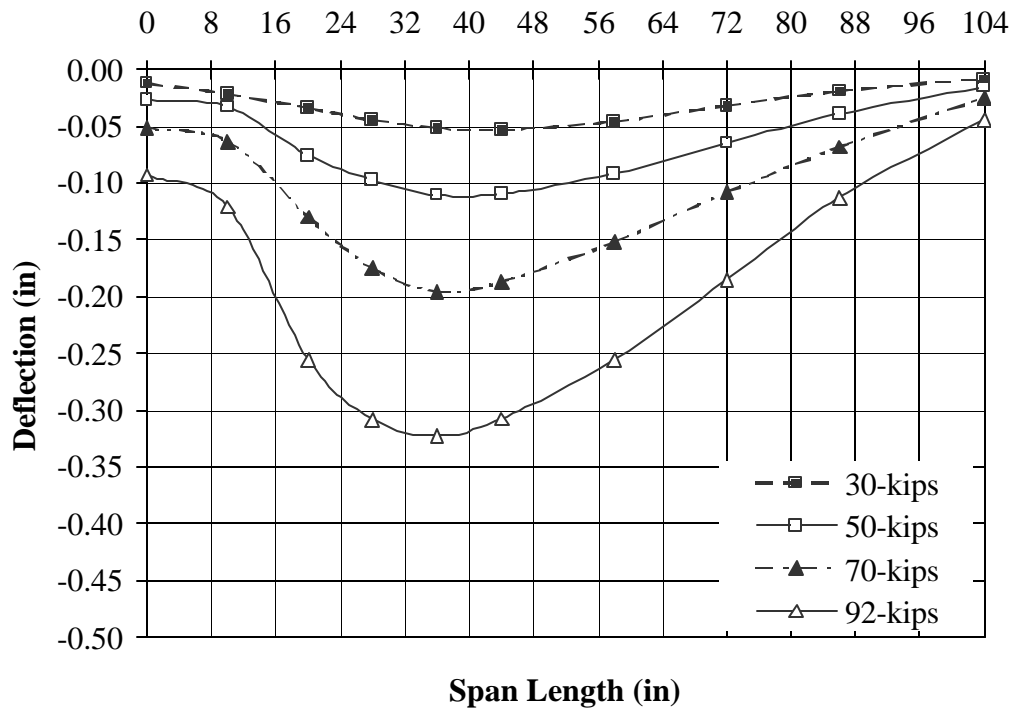


Figure A9: Deflected shape of joist JS6A

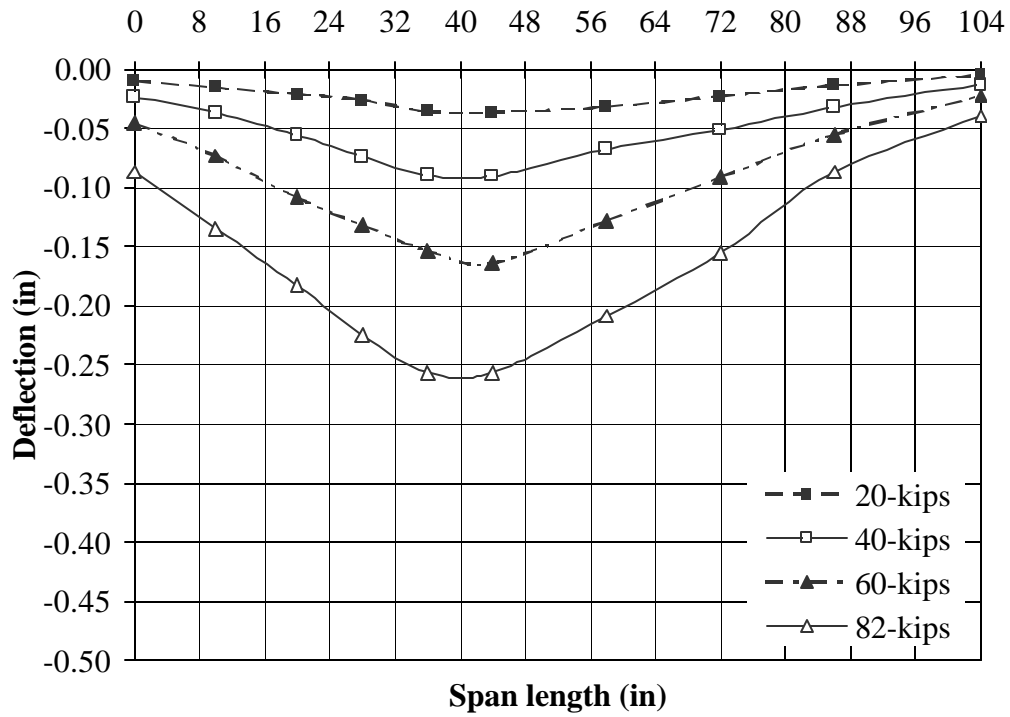


Figure A10: Deflected shape of joist JS6B

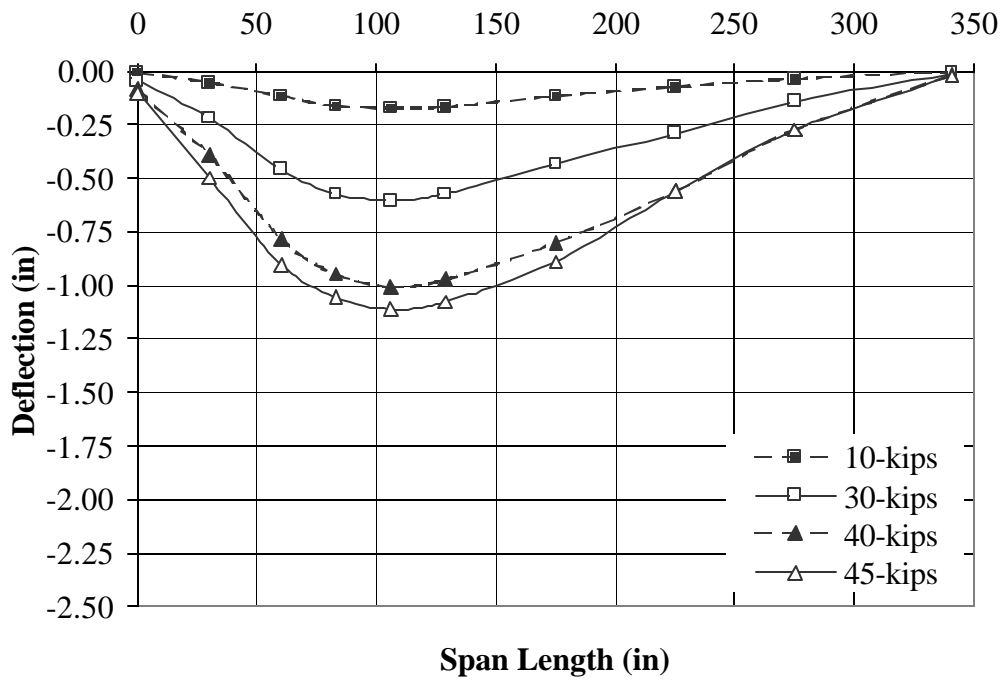


Figure A11: Deflected shape of joist JL1A

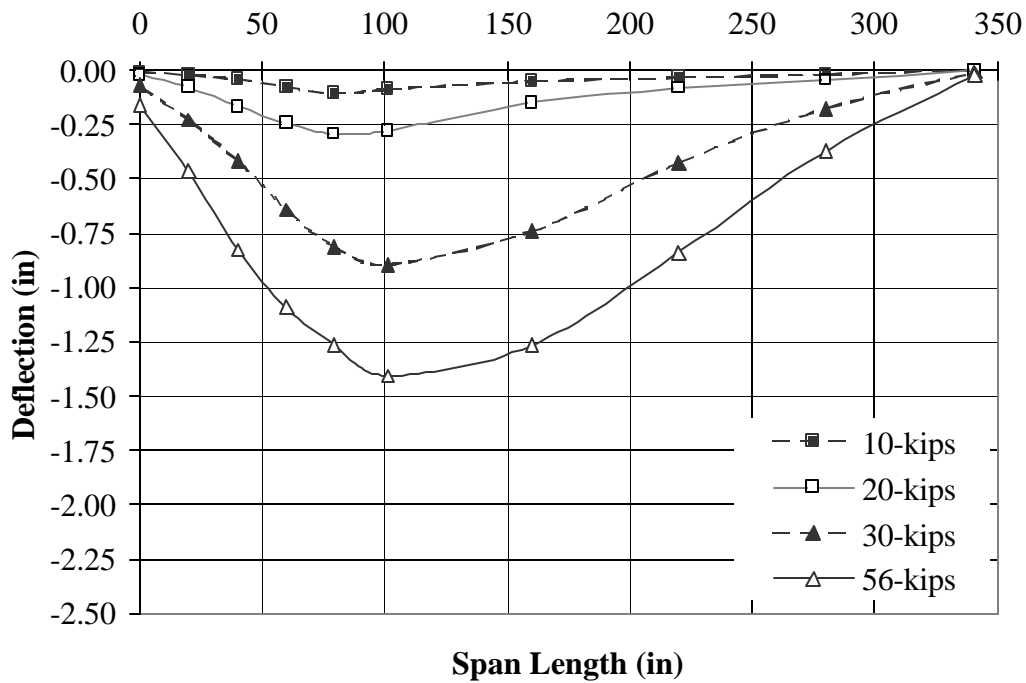


Figure A12: Deflected shape of joist JL1B

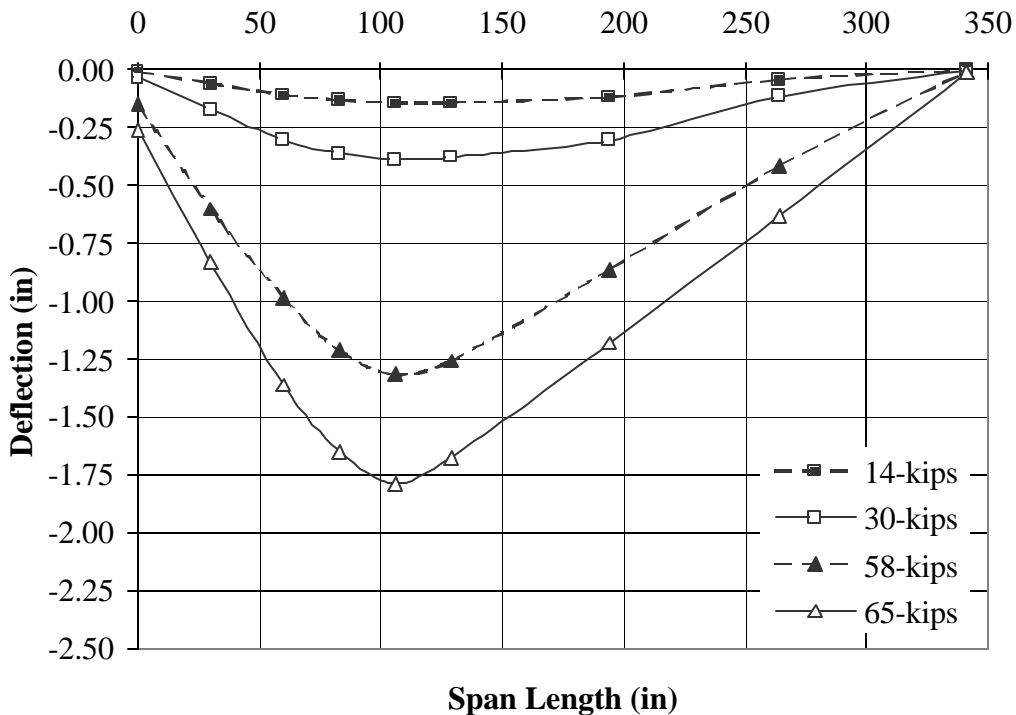


Figure A13: Deflected shape of joist JL2A

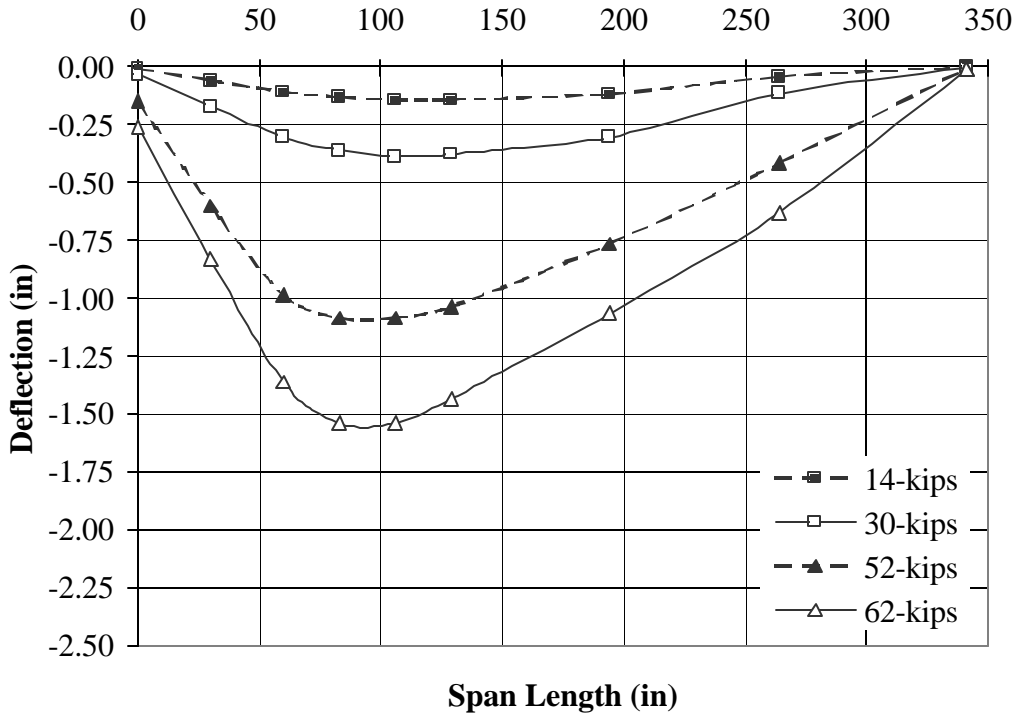


Figure A14: Deflected shape of joist JL2B

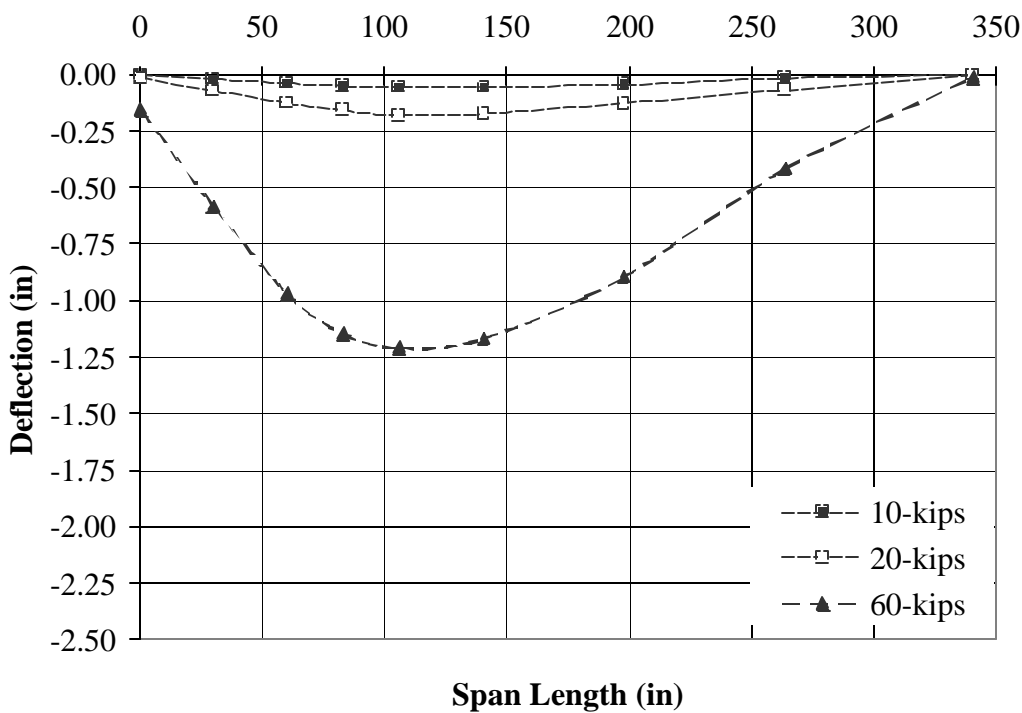


Figure A15: Deflected shape of joist JL3A

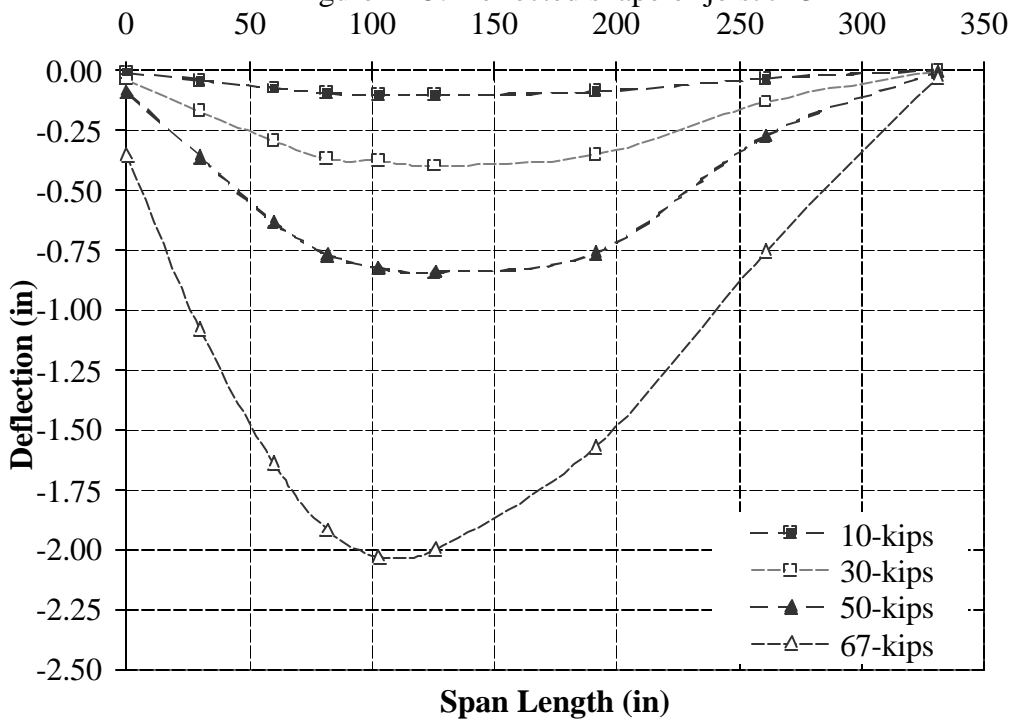


Figure A16: Deflected shape of joist JL3B

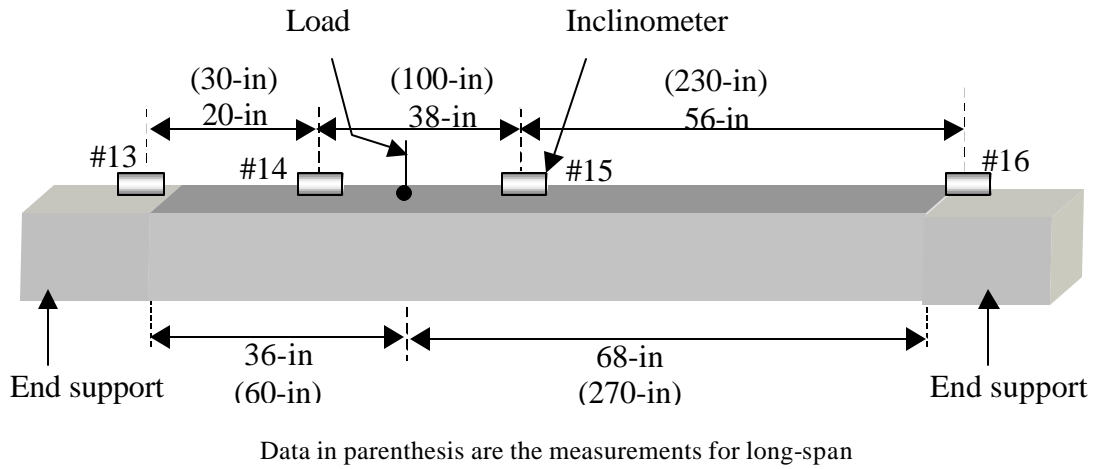


Figure A17: Locations of inclinometers for short and long-span members.

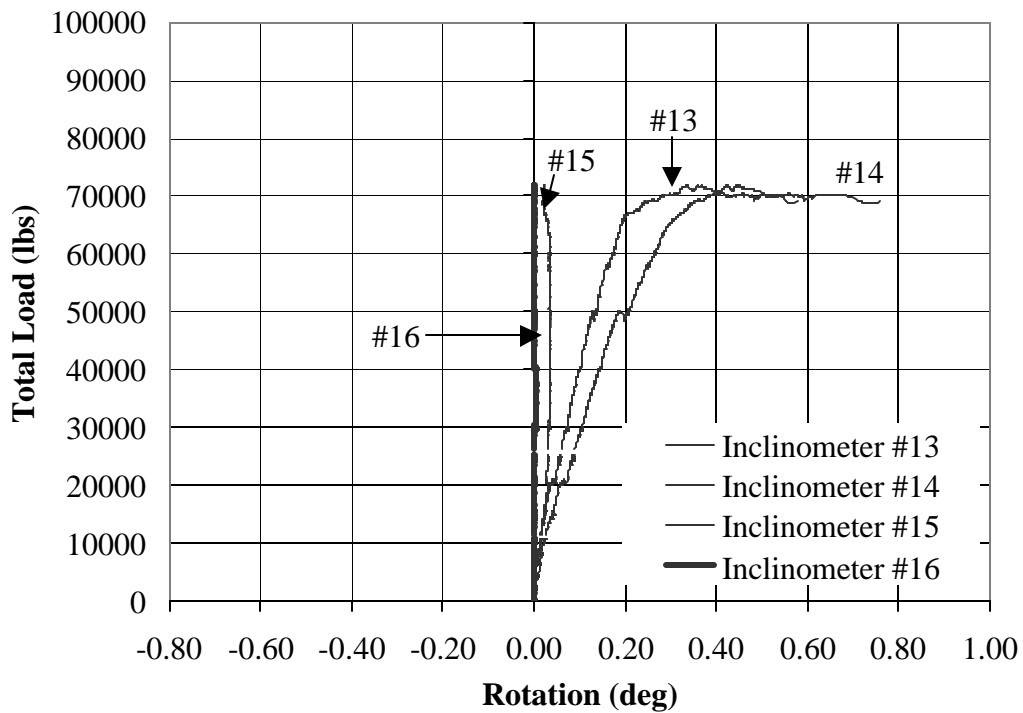


Figure A18: Inclinometer readings for JS1A

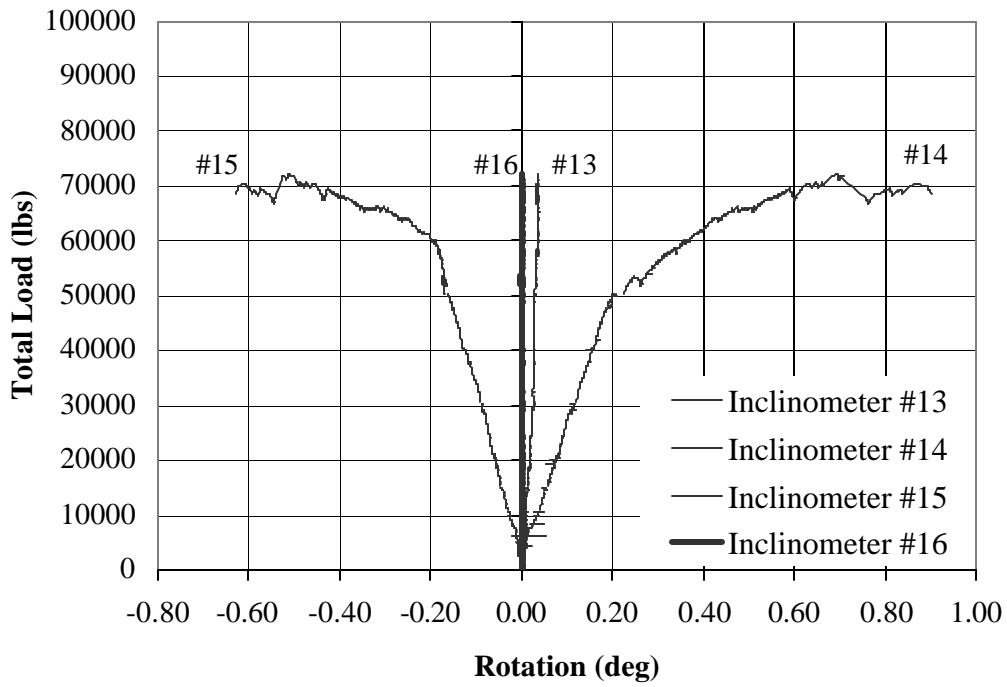


Figure A19: Inclinometer readings for JS1B

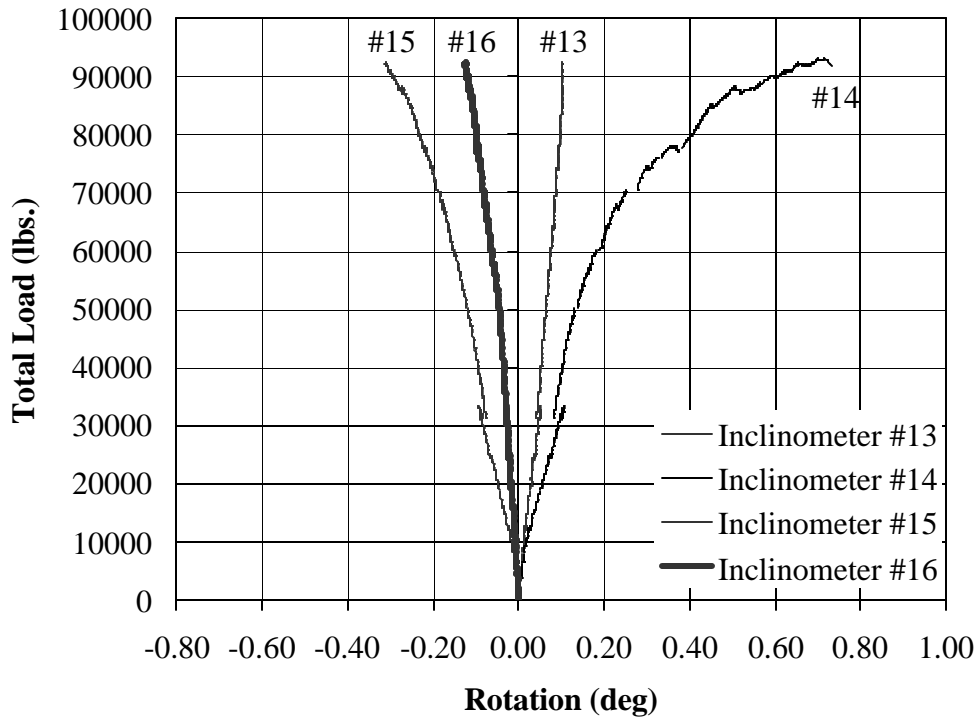


Figure A20: Inclinometer readings for JS3B

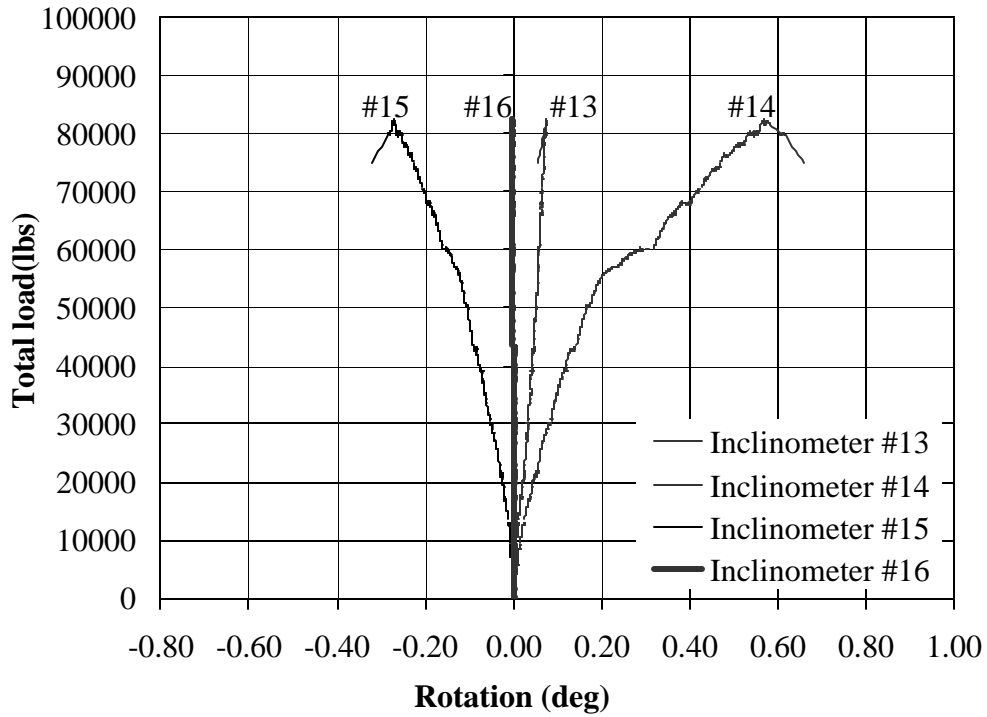


Figure A21: Inclinometer readings for JS4A

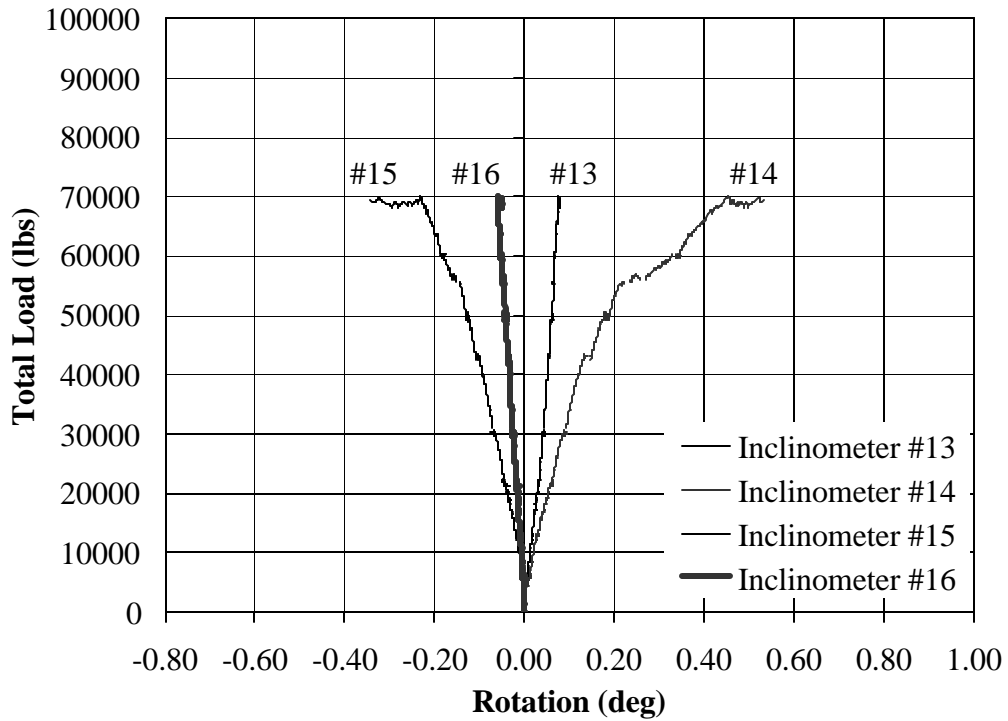


Figure A22: Inclinometer readings for JS4B

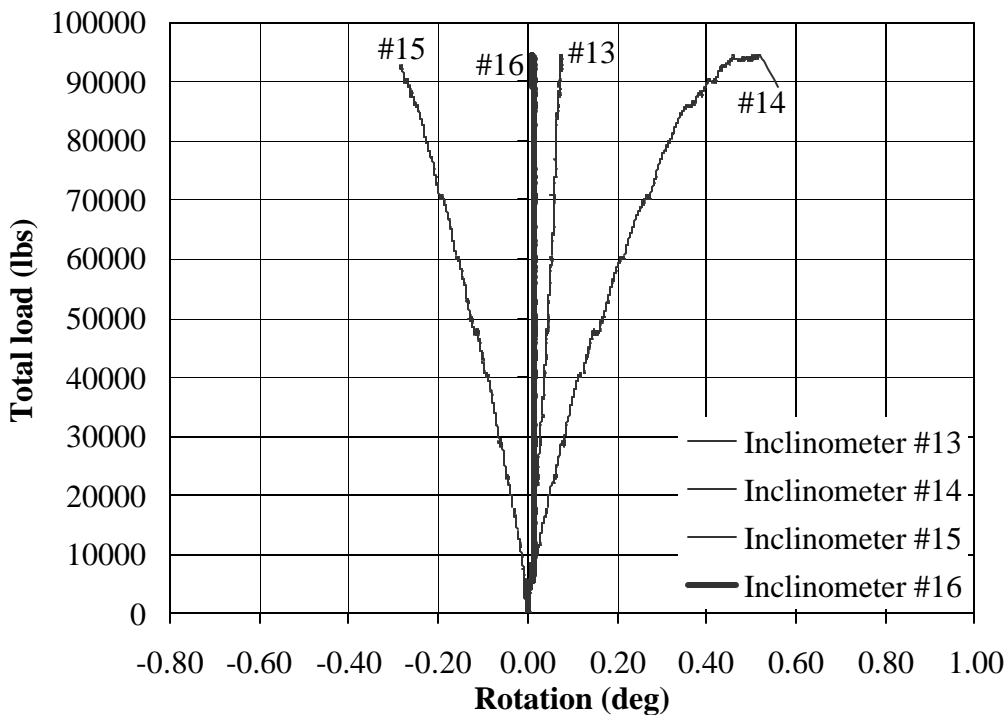


Figure A23: Inclinometer readings for JS5A

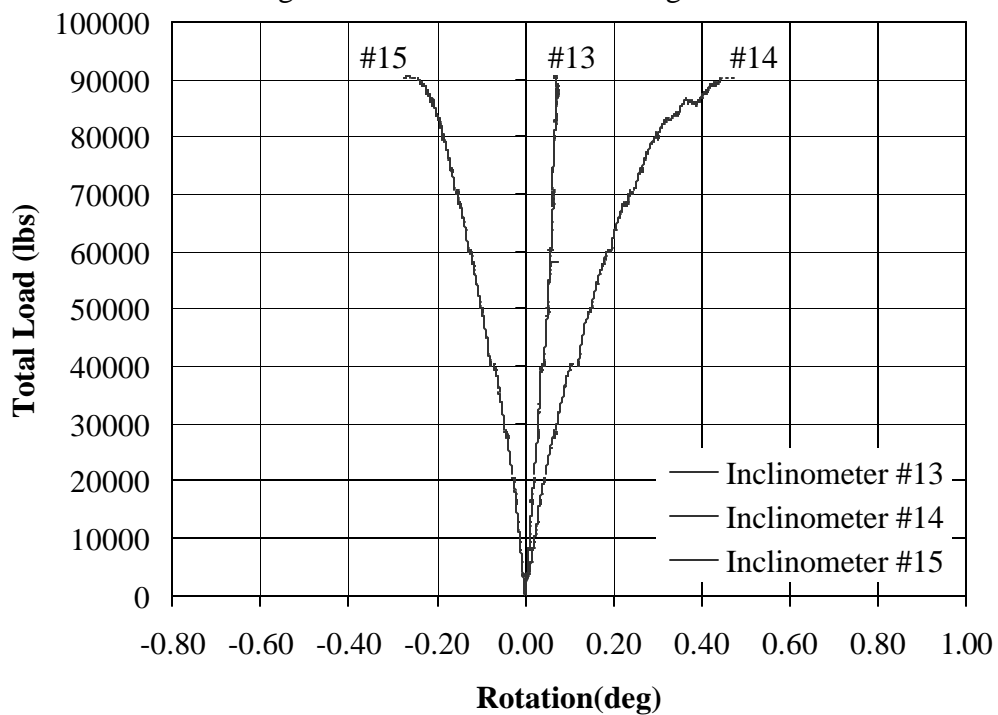


Figure A24: Inclinometer readings for JS5B

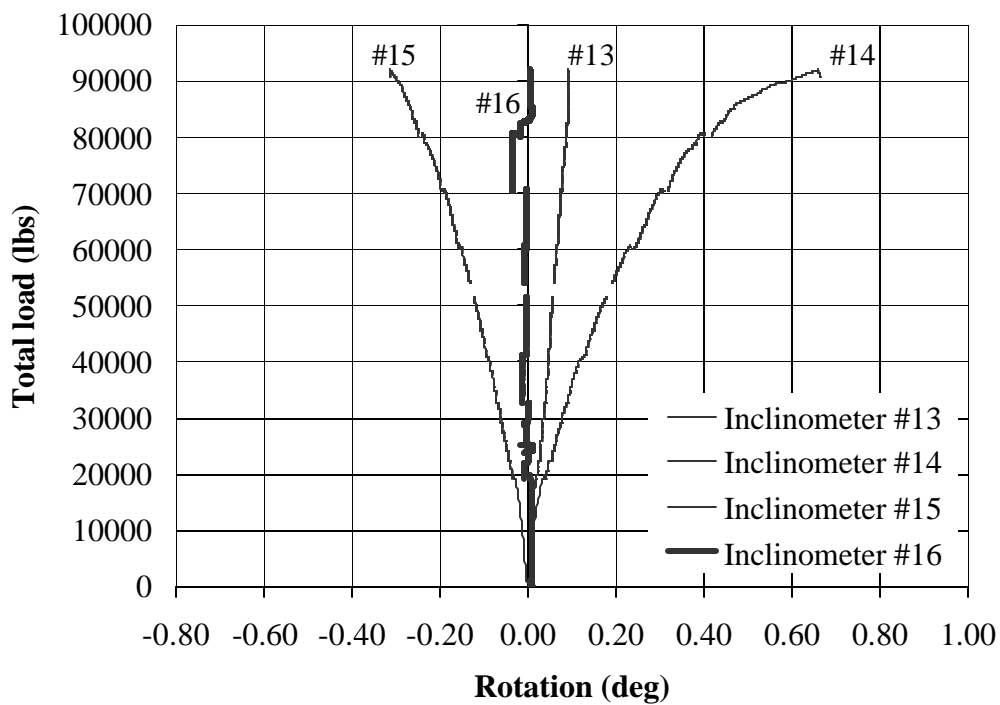


Figure A25: Inclinometer readings for JS6A

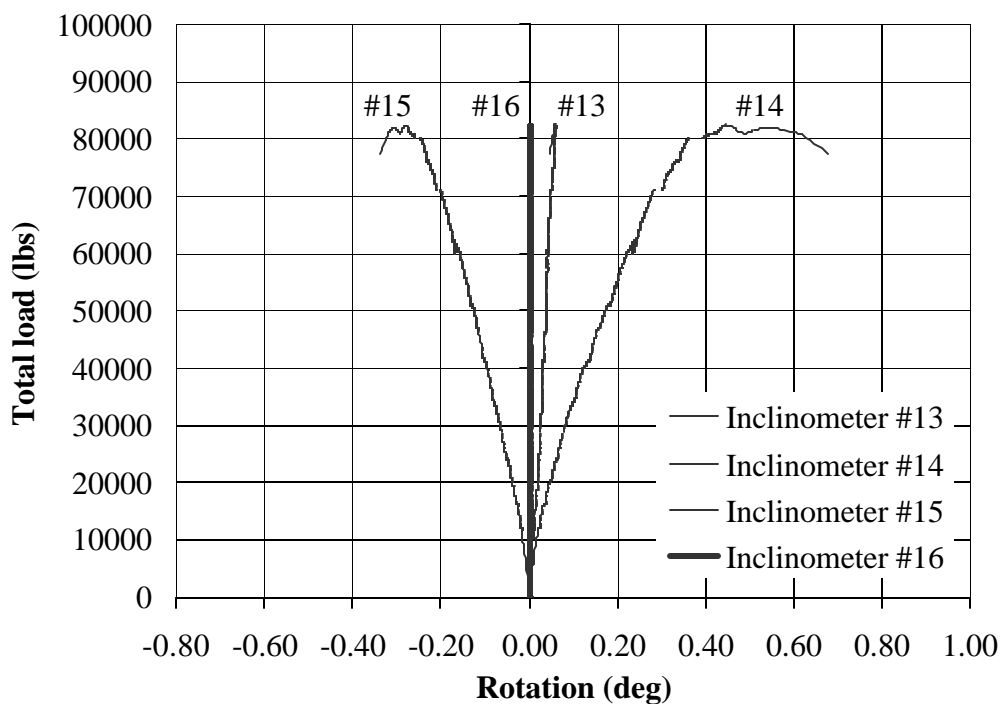


Figure A26: Inclinometer readings for JS6B

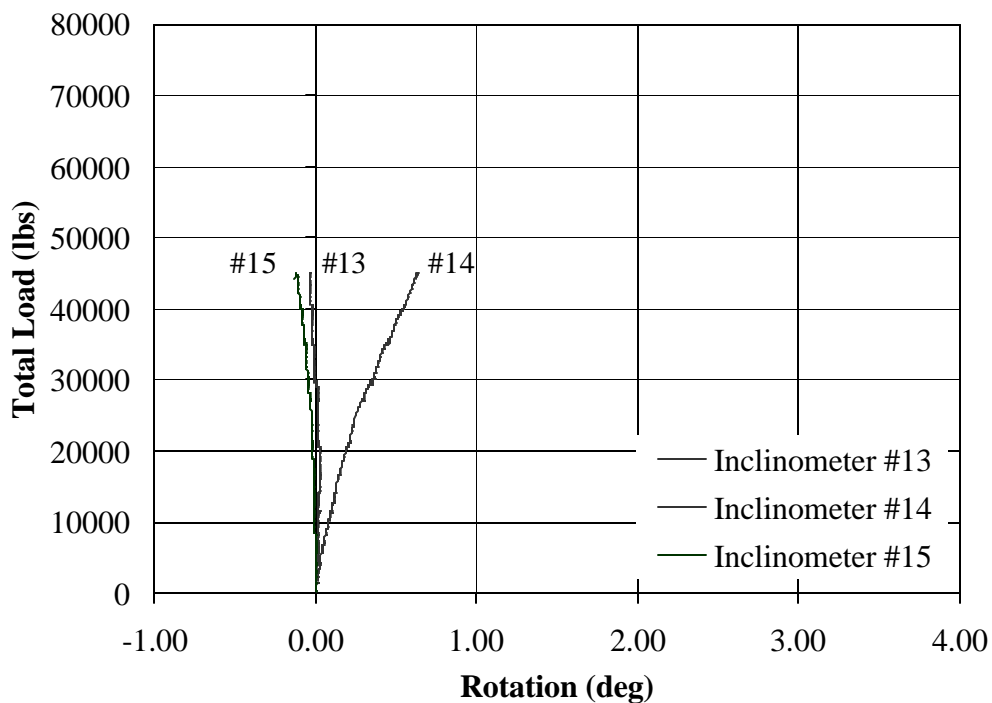


Figure A27: Inclinometer readings for JL1A

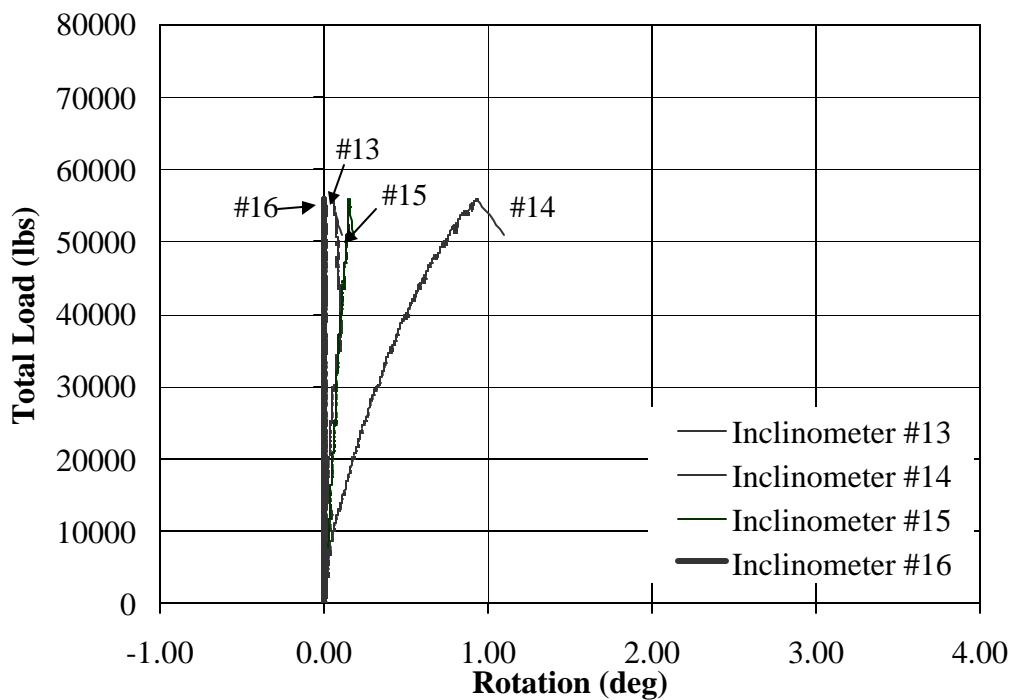


Figure A28: Inclinometer readings for JL1B

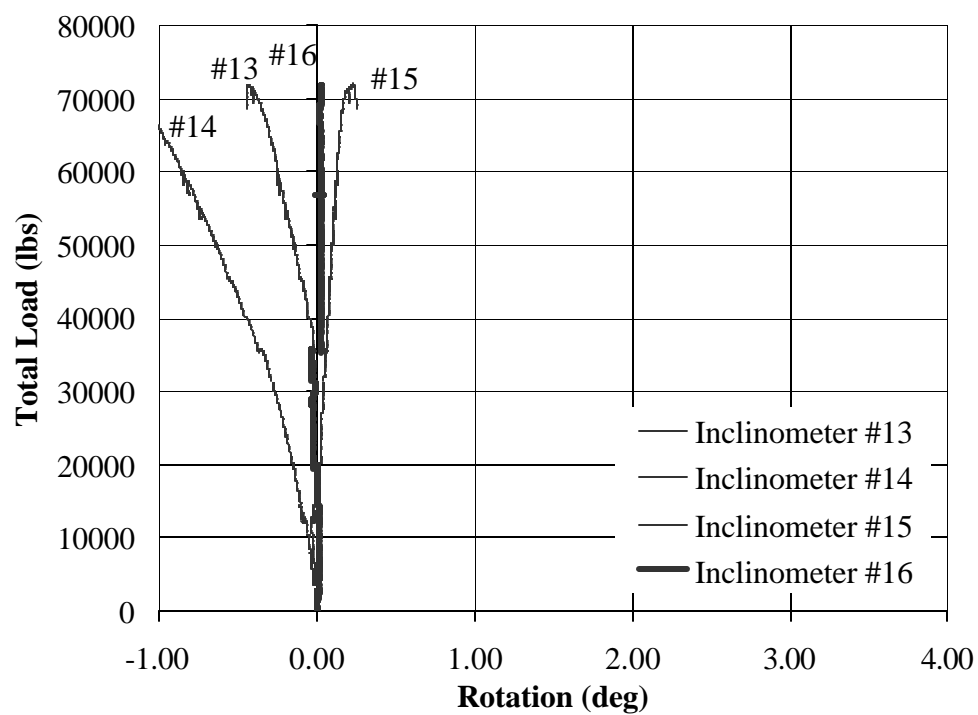


Figure A29: Inclinometer readings for JL2A

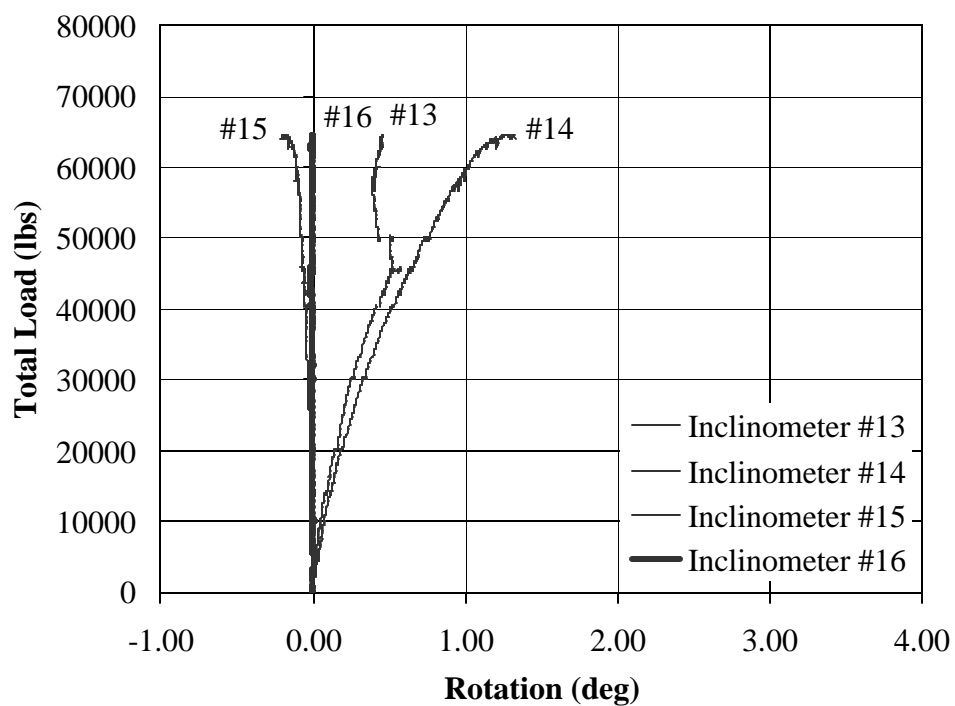


Figure A30: Inclinometer readings for JL2B

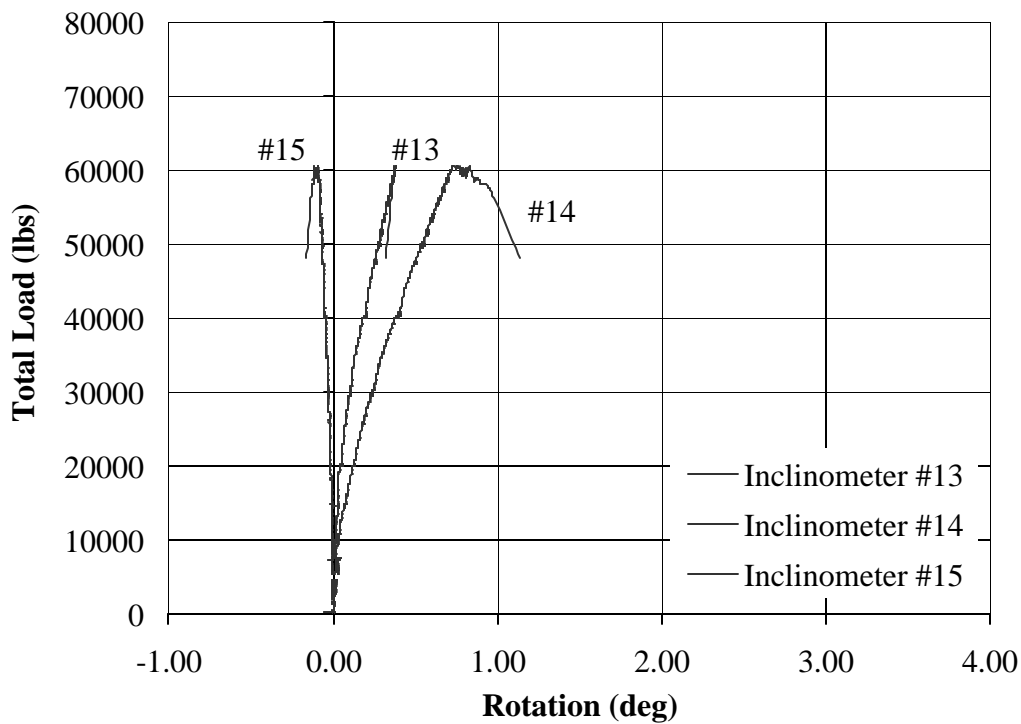


Figure A31: Inclinometer readings for JL3A

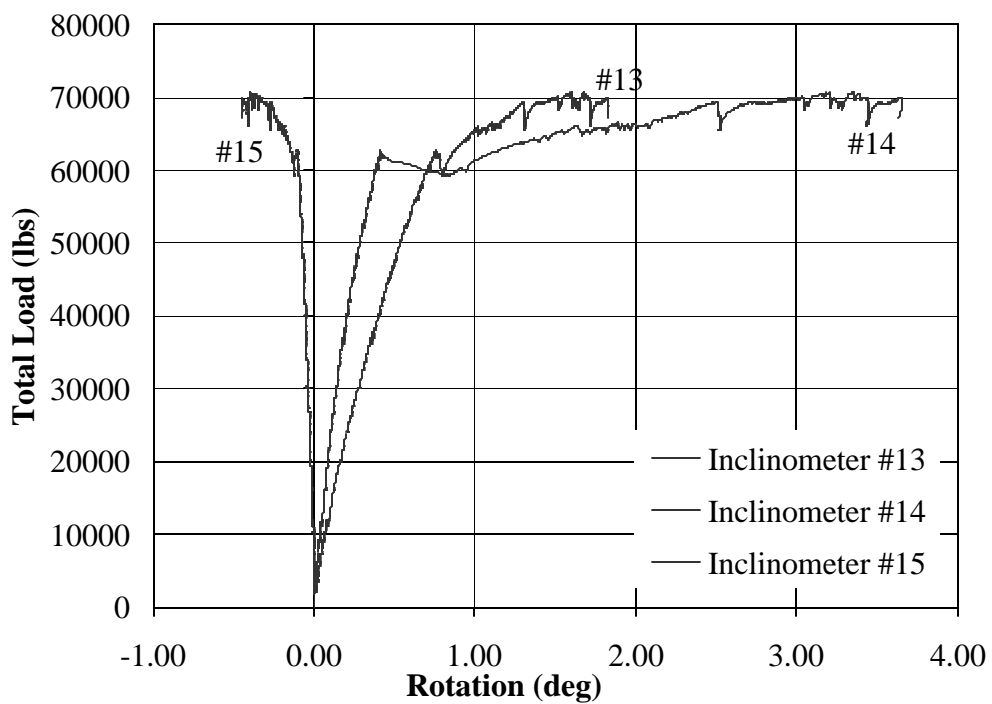


Figure A32: Inclinometer readings for JL3B

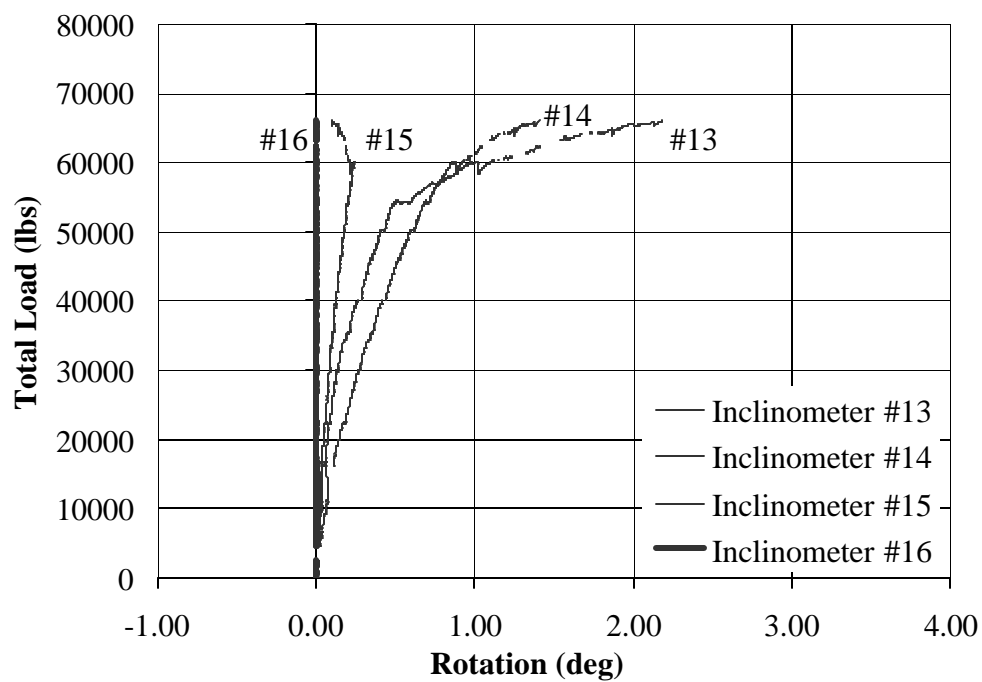


Figure A33: Inclinometer readings for JL4A

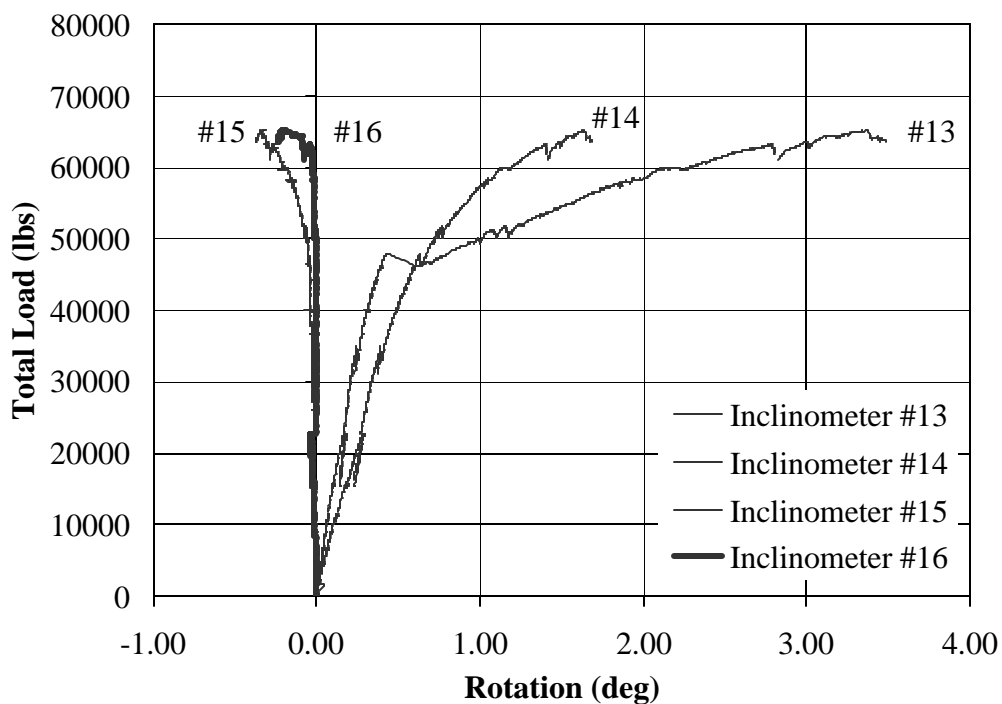


Figure A34: Inclinometer readings for JL4B

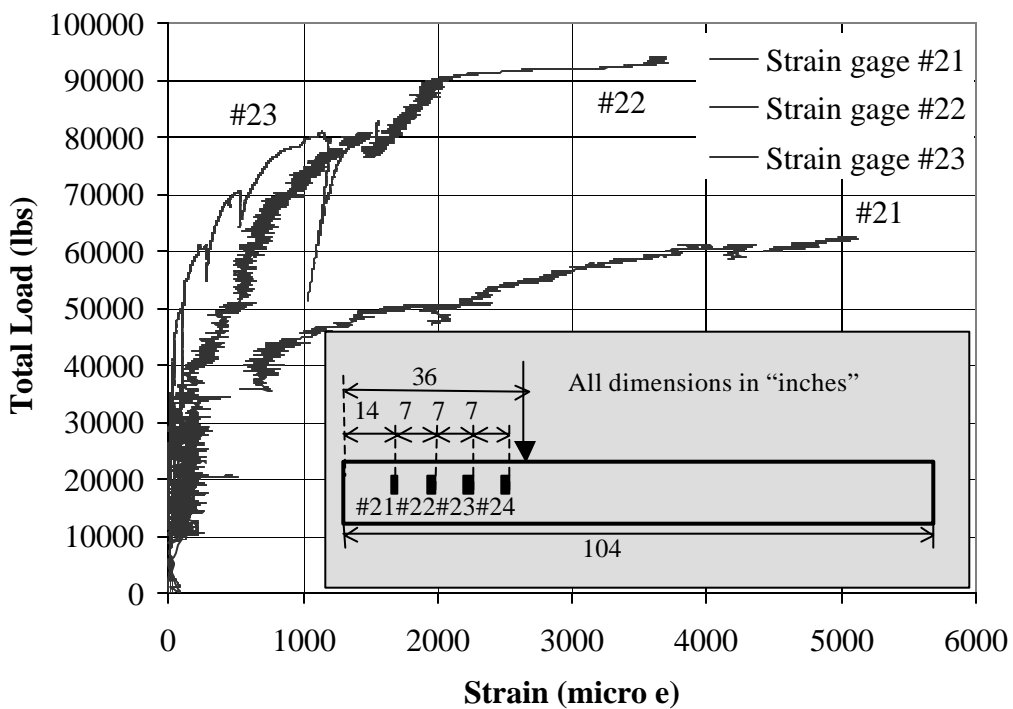


Figure A35: Strain gages reading for JS3A

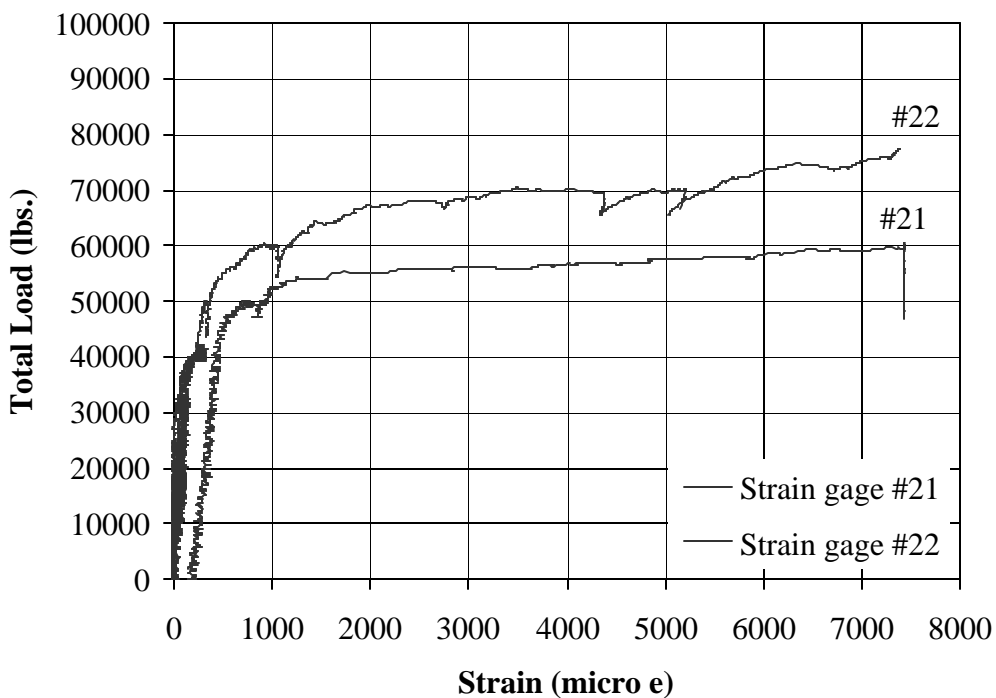


Figure A36: Strain gages reading for JS3B

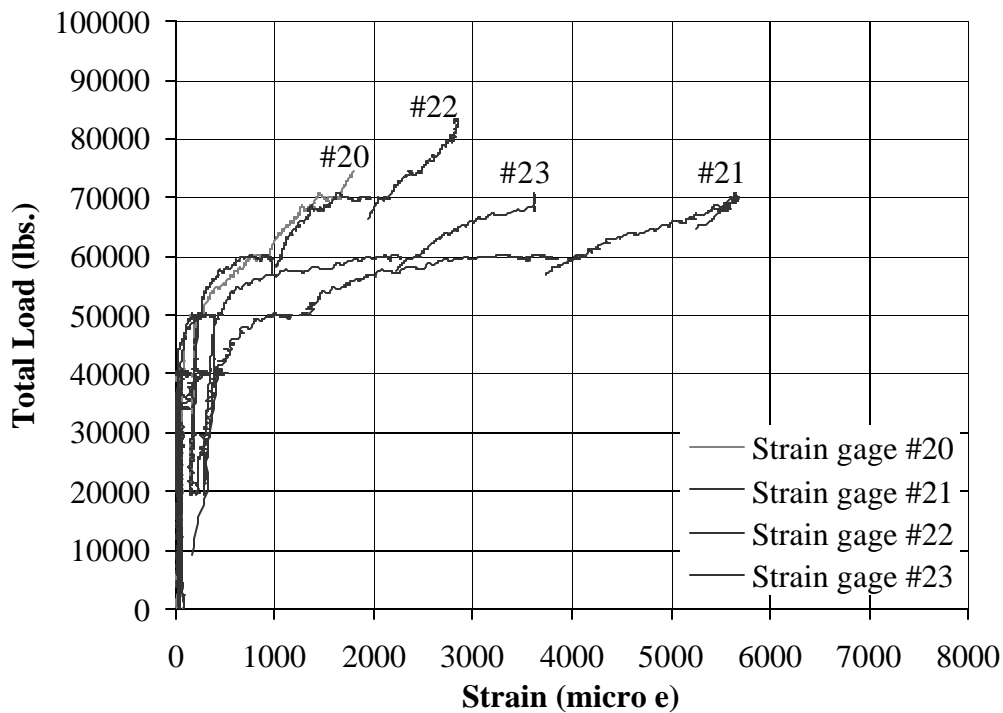


Figure A37: Strain gages reading for JS5B

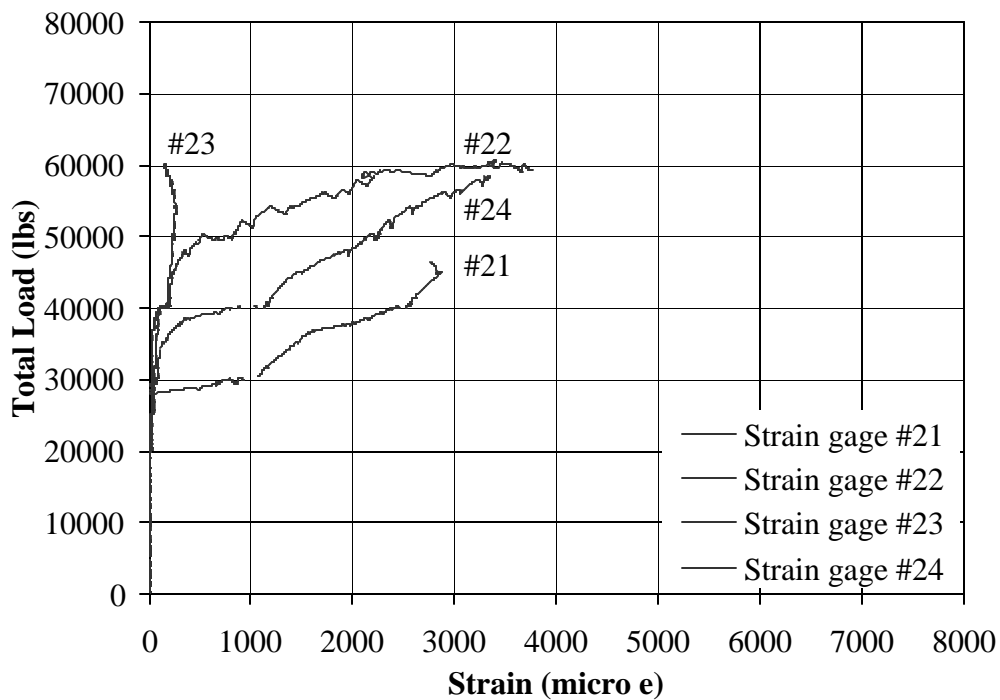


Figure A38: Strain gages reading for JL3A

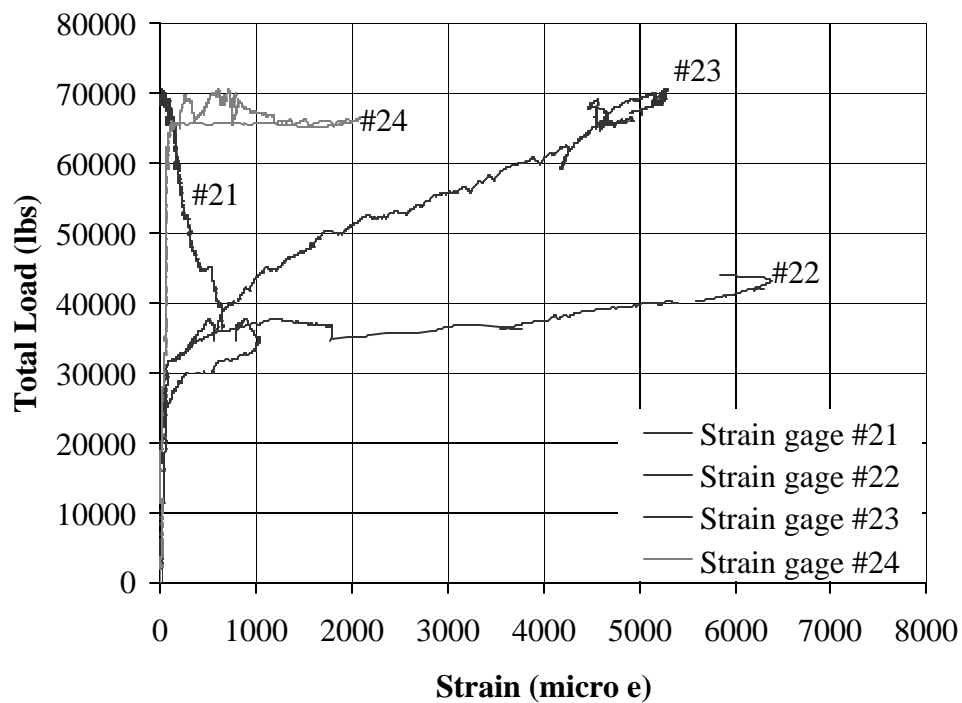


Figure A39: Strain gages reading for JL3B

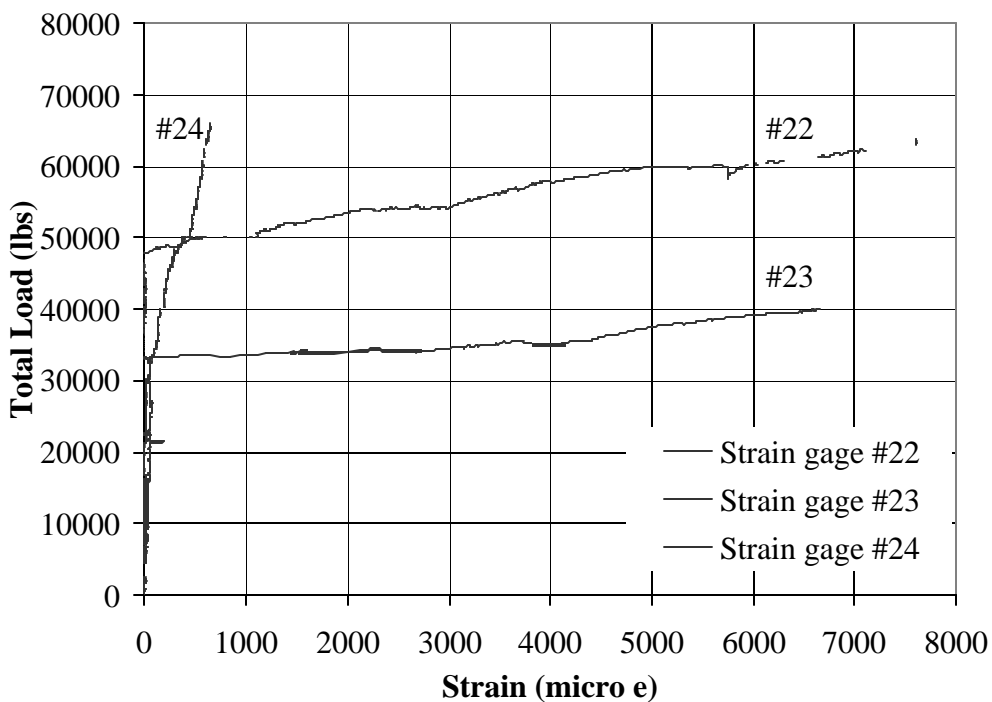


Figure A40: Strain gages reading for JL4A

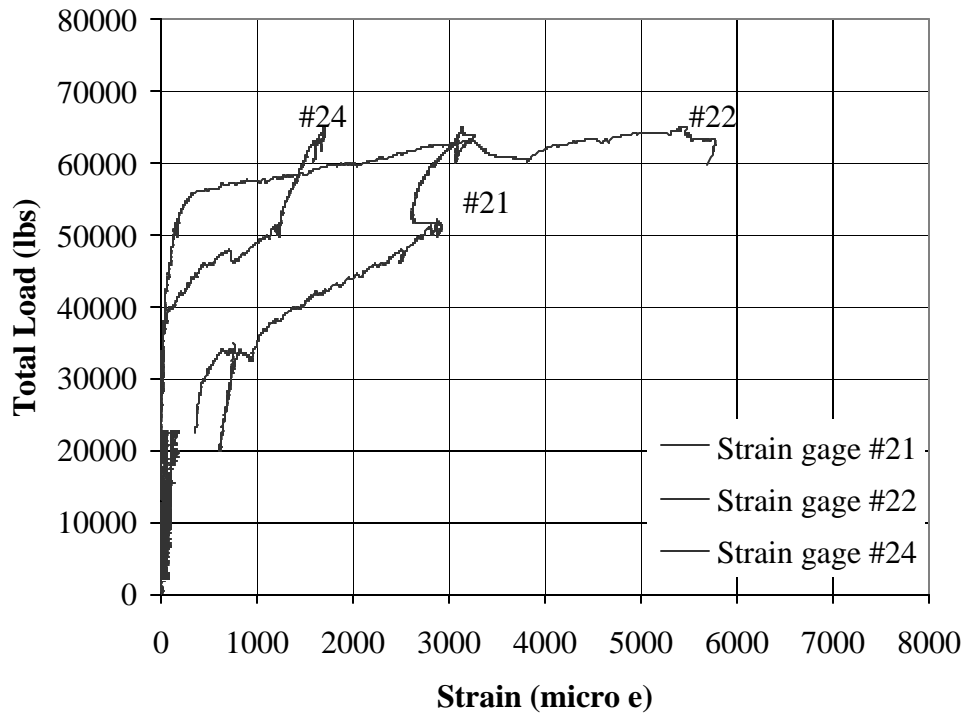


Figure A41: Strain gages reading for JL4 B

APPENDIX B
ANALYTICAL CURVES

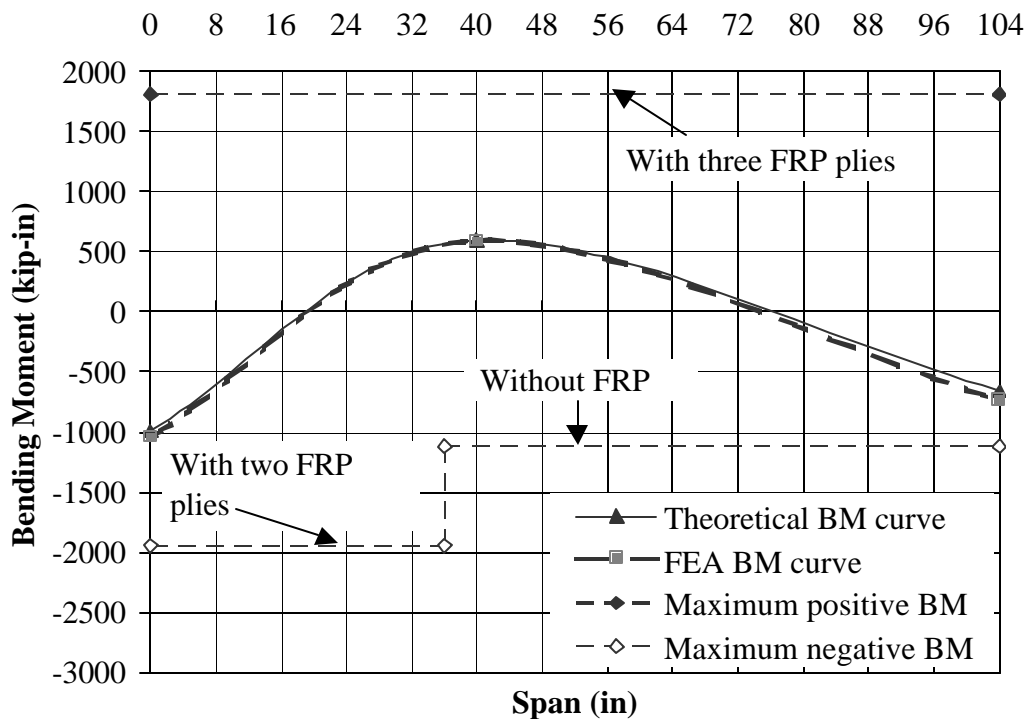


Figure B1: Model bending moment curves - JS1

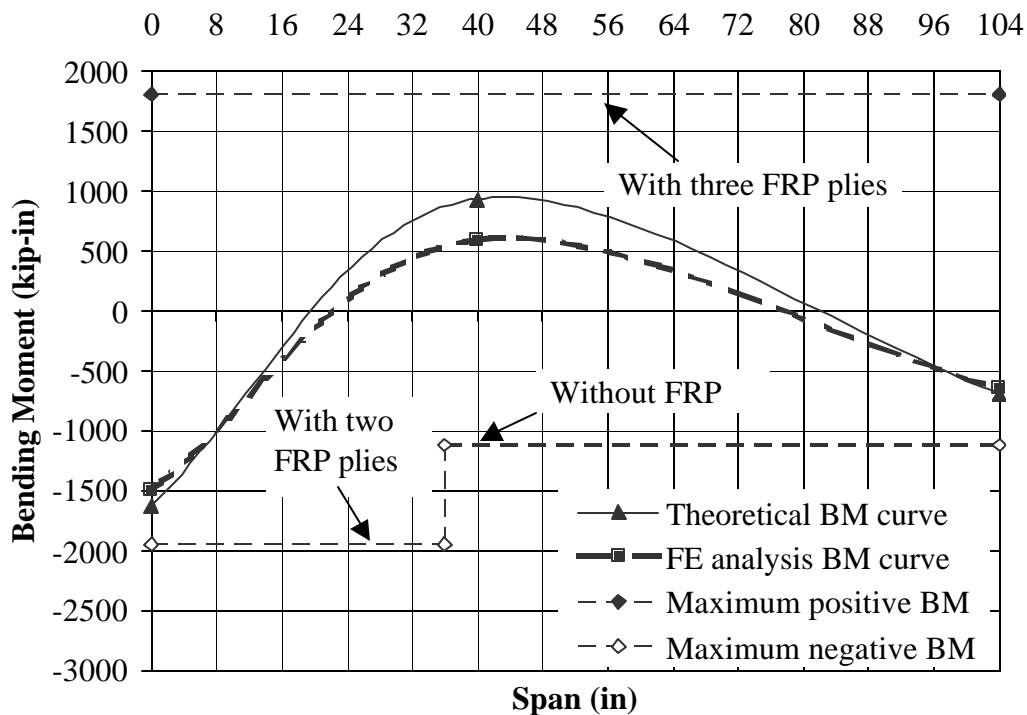


Figure B2: Model bending moment curves - JS3

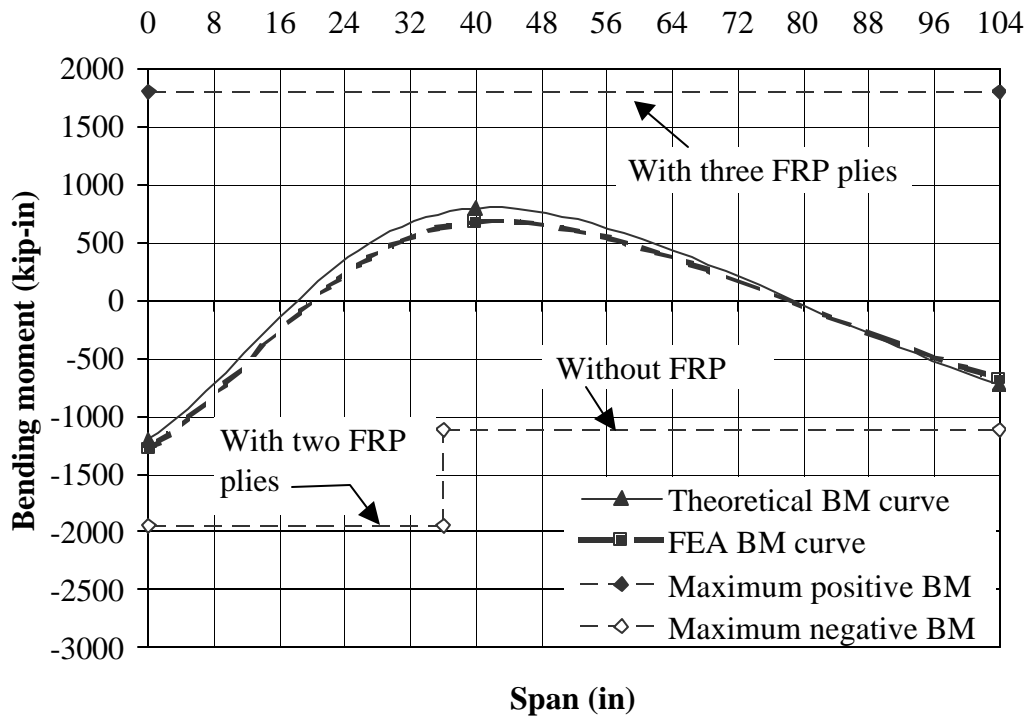


Figure B3: Model bending moment curves - JS4

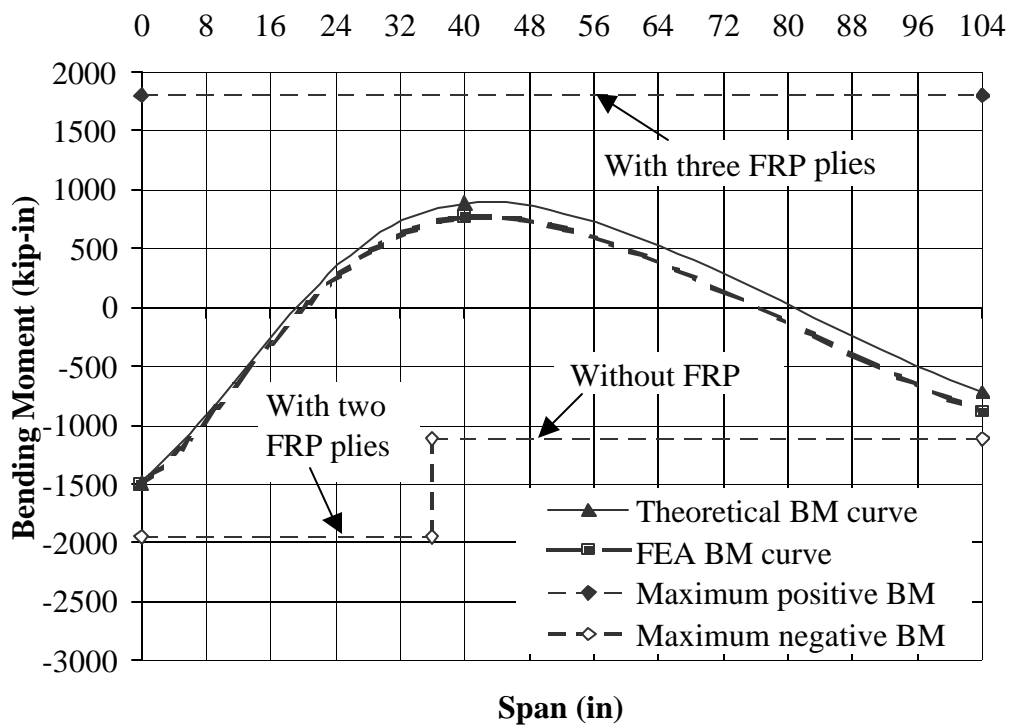


Figure B4: Model bending moment curves - JS5

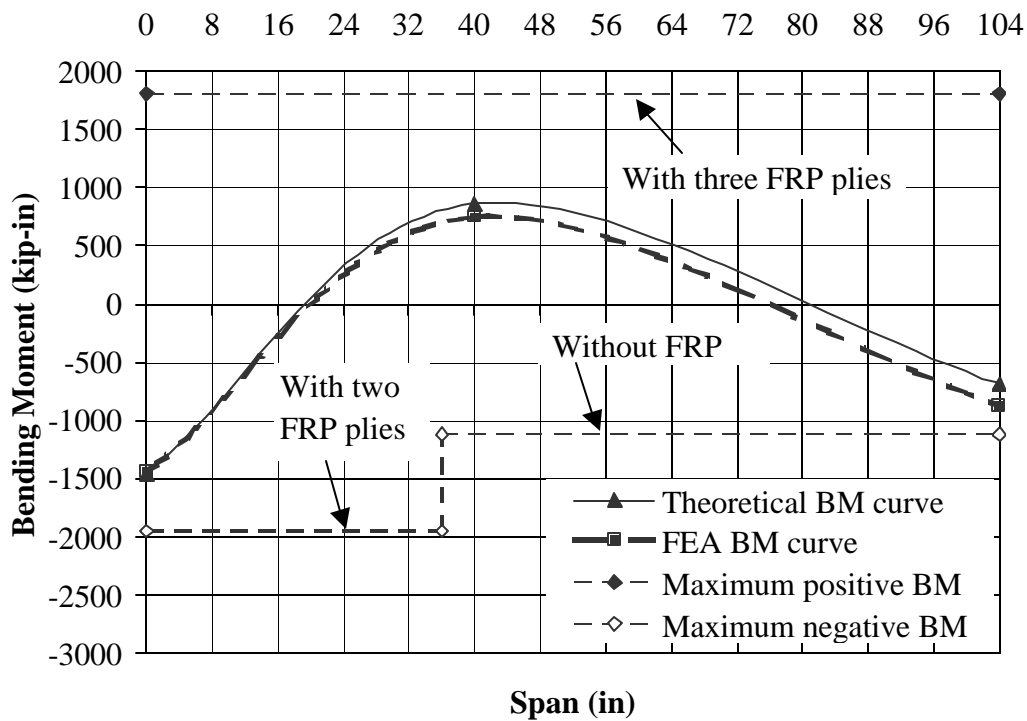


Figure B5: Model bending moment curves - JS6

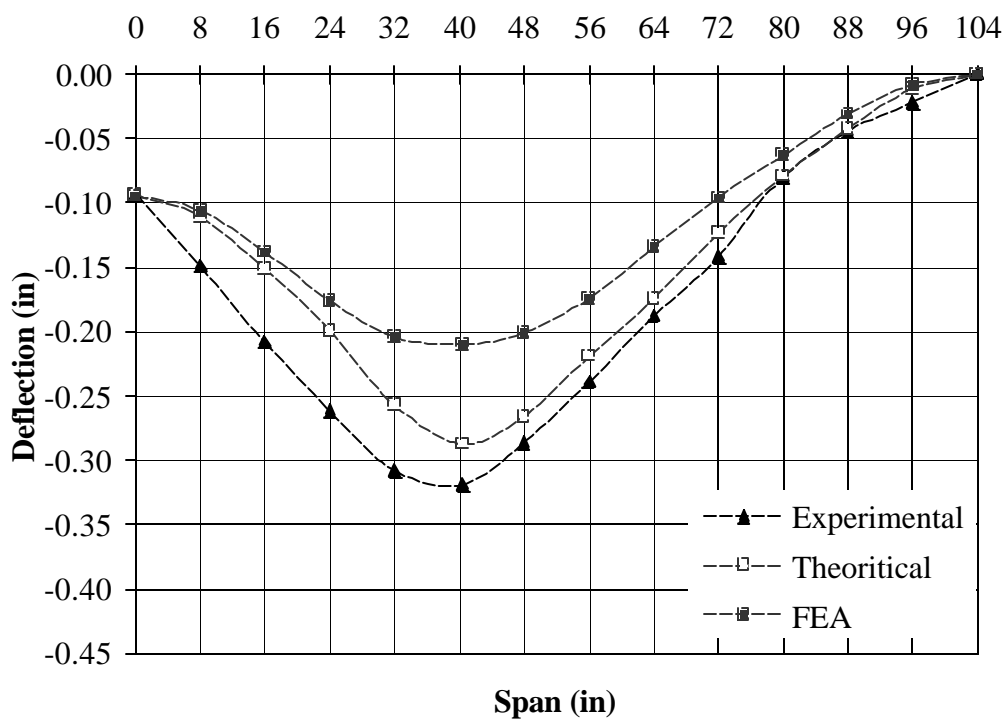


Figure B6: Deflection curves - JS1

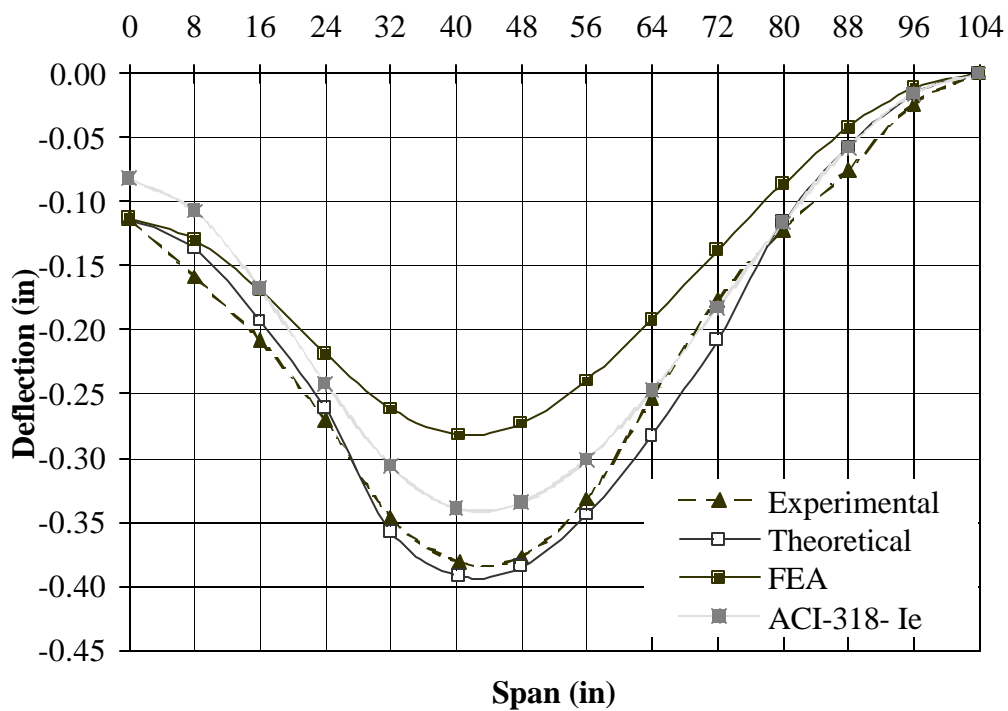


Figure B7: Deflection curves - JS3

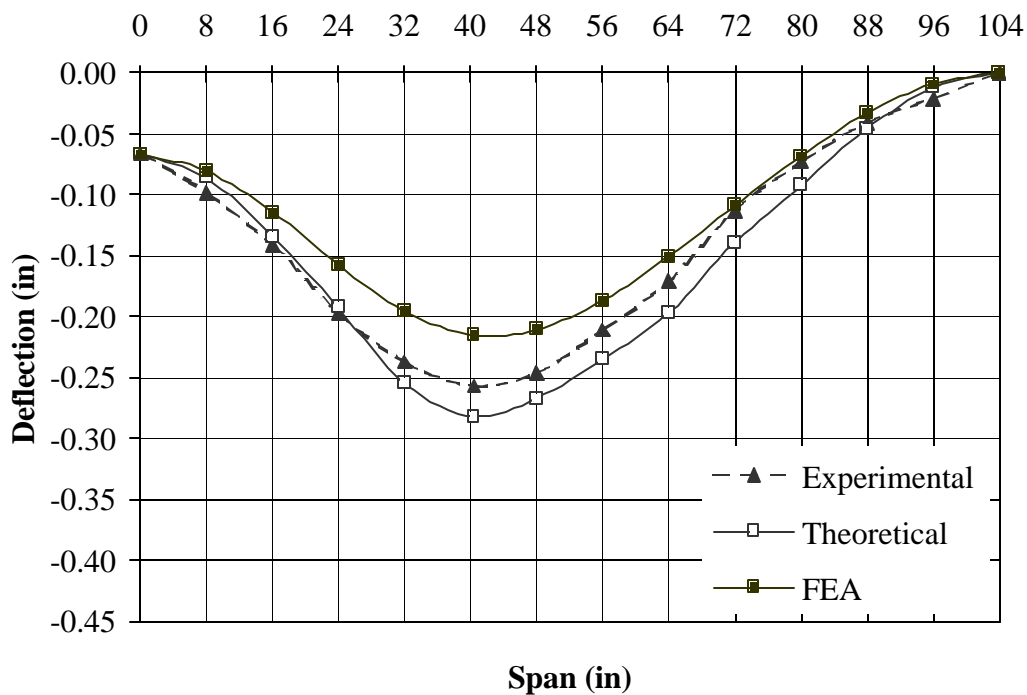


Figure B8: Deflection curves - JS4

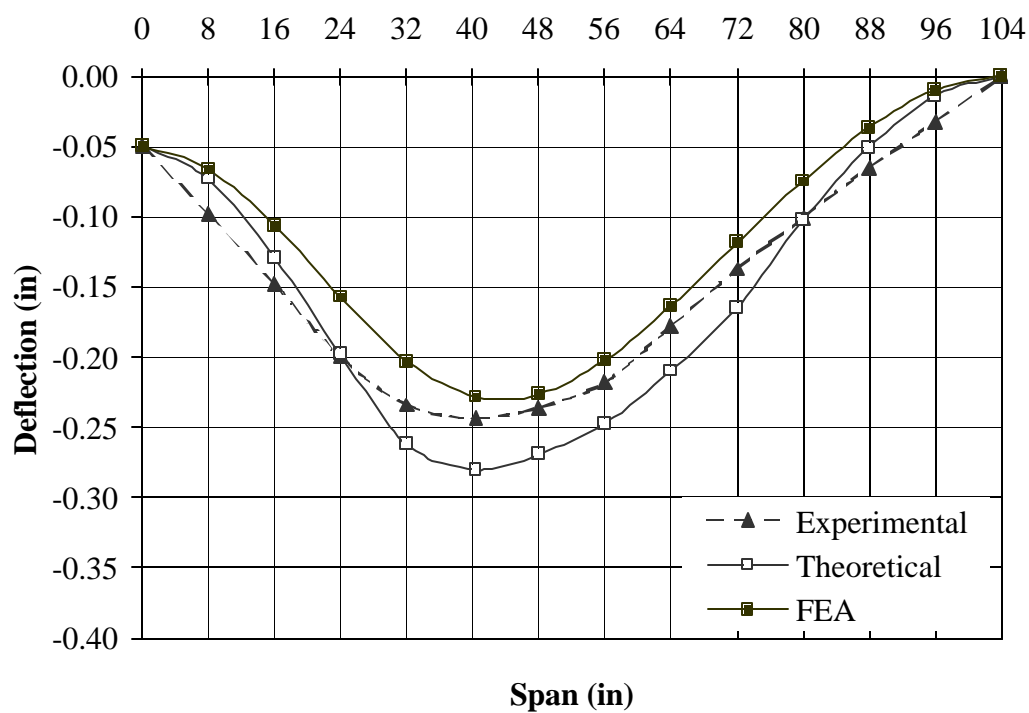


Figure B9: Deflection curves - JS5

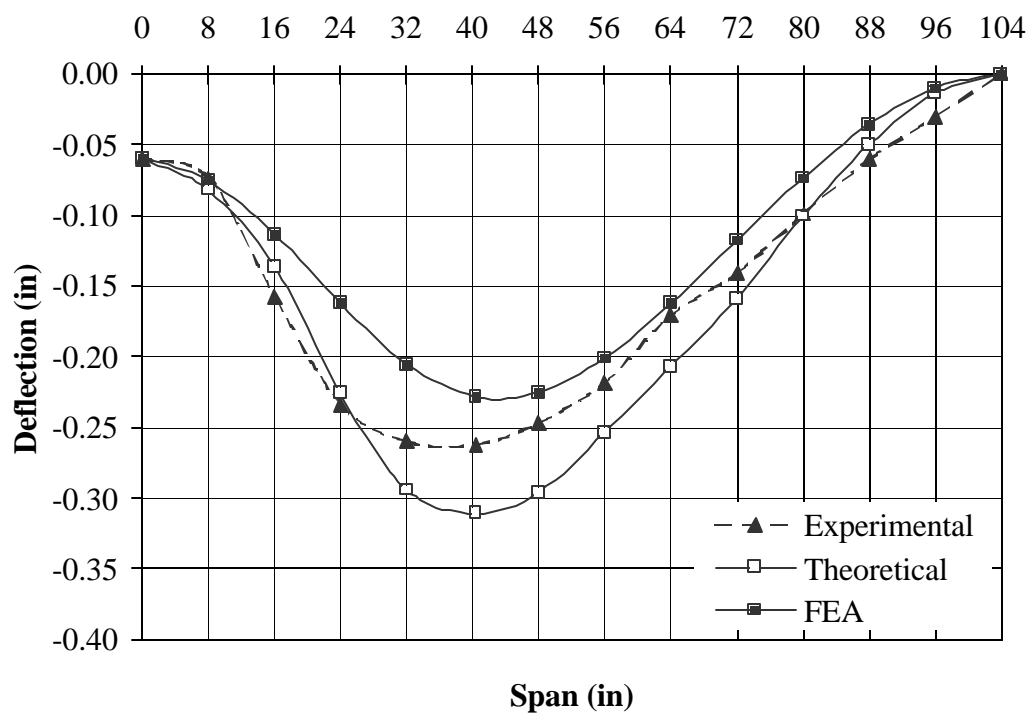


Figure B10: Deflection curves - JS6

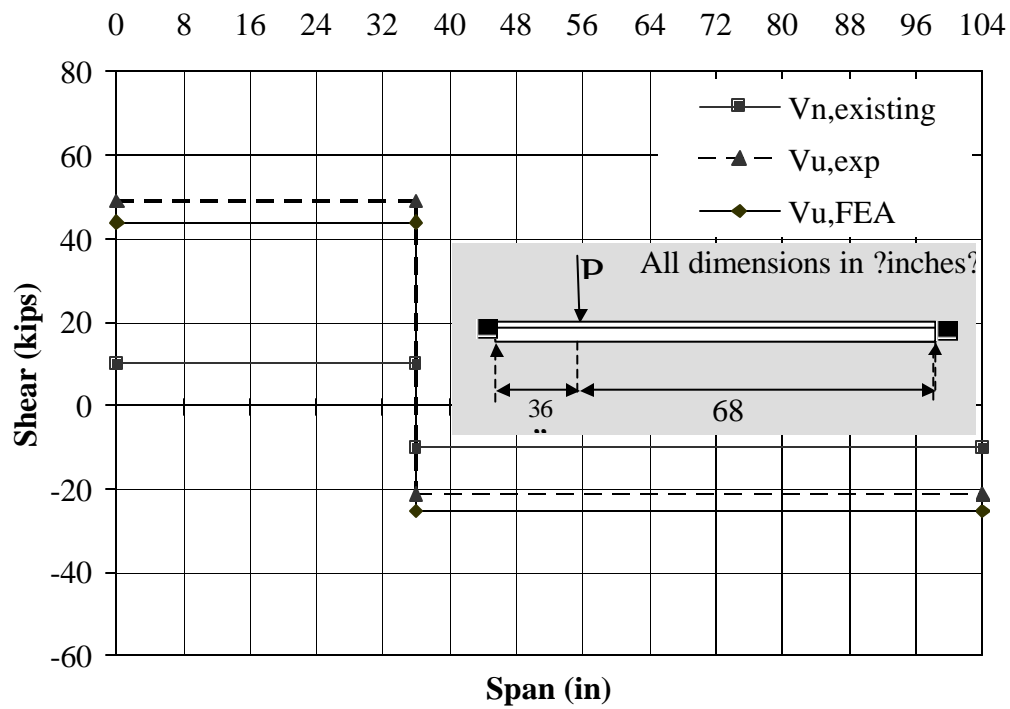


Figure B11: Shear force curves - JS1

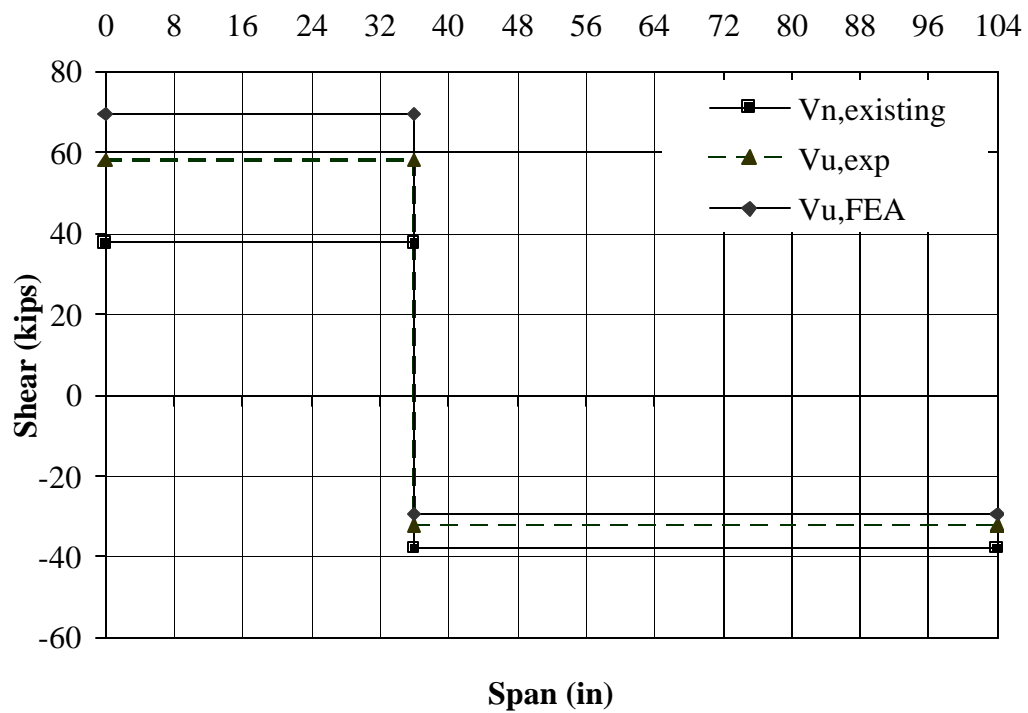


Figure B12: Shear force curves - JS3

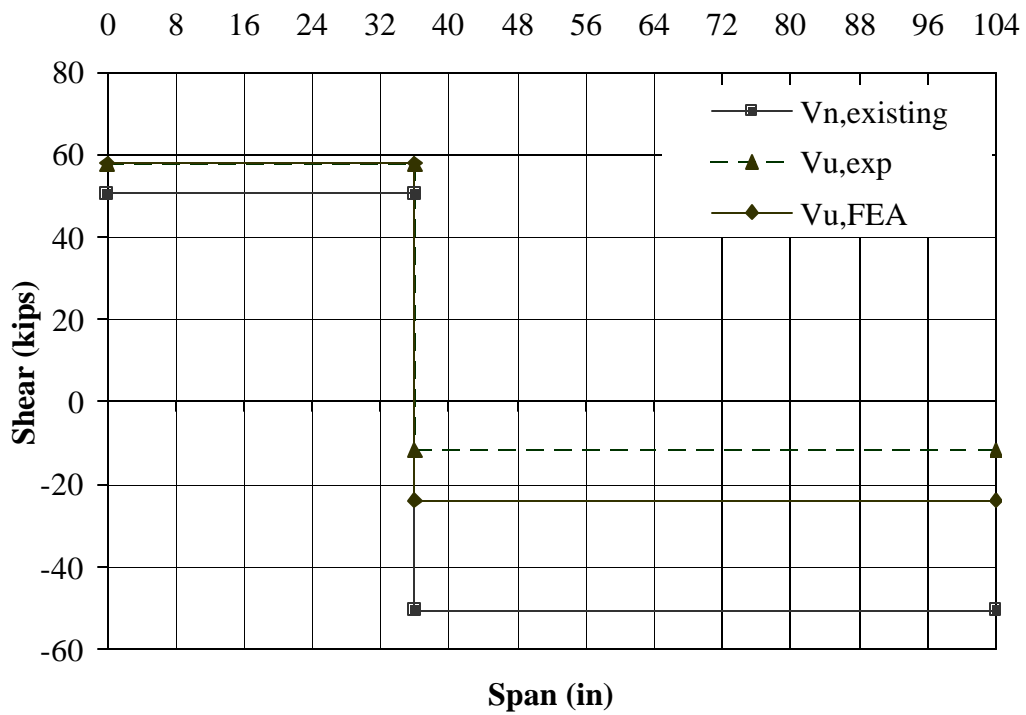


Figure B13: Shear force curves - JS4

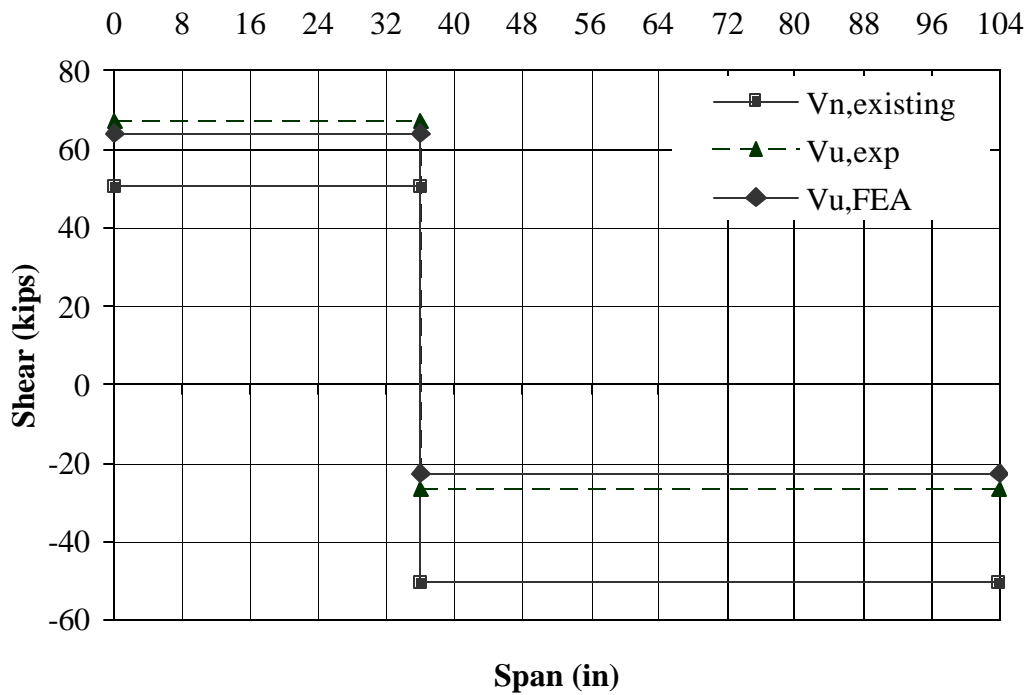


Figure B14: Shear force curves - JS5

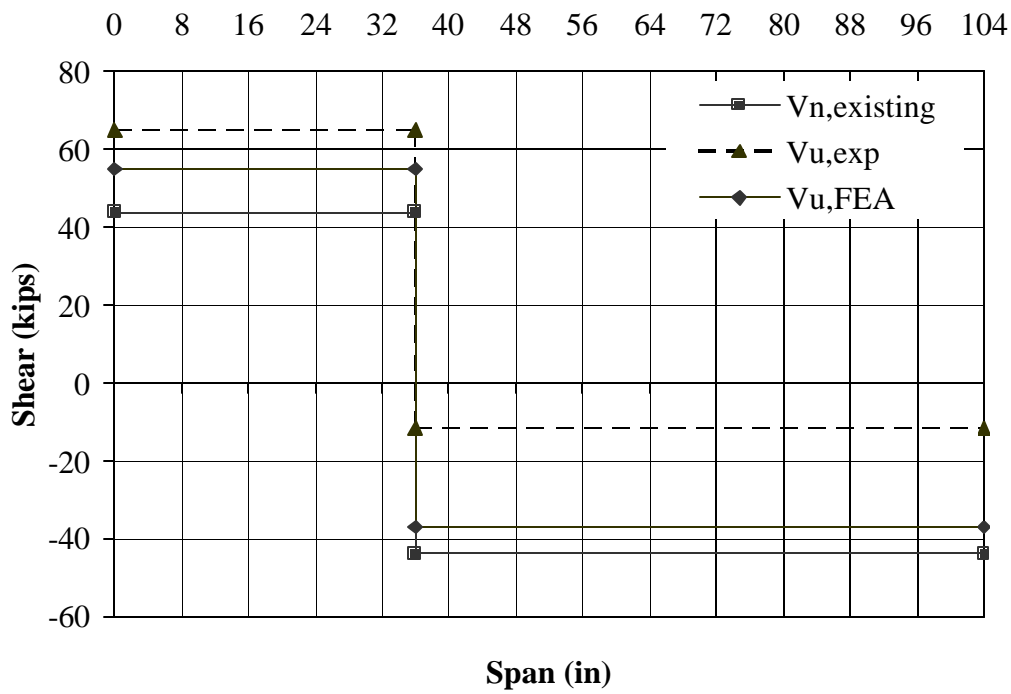


Figure B15: Shear force curves - JS6

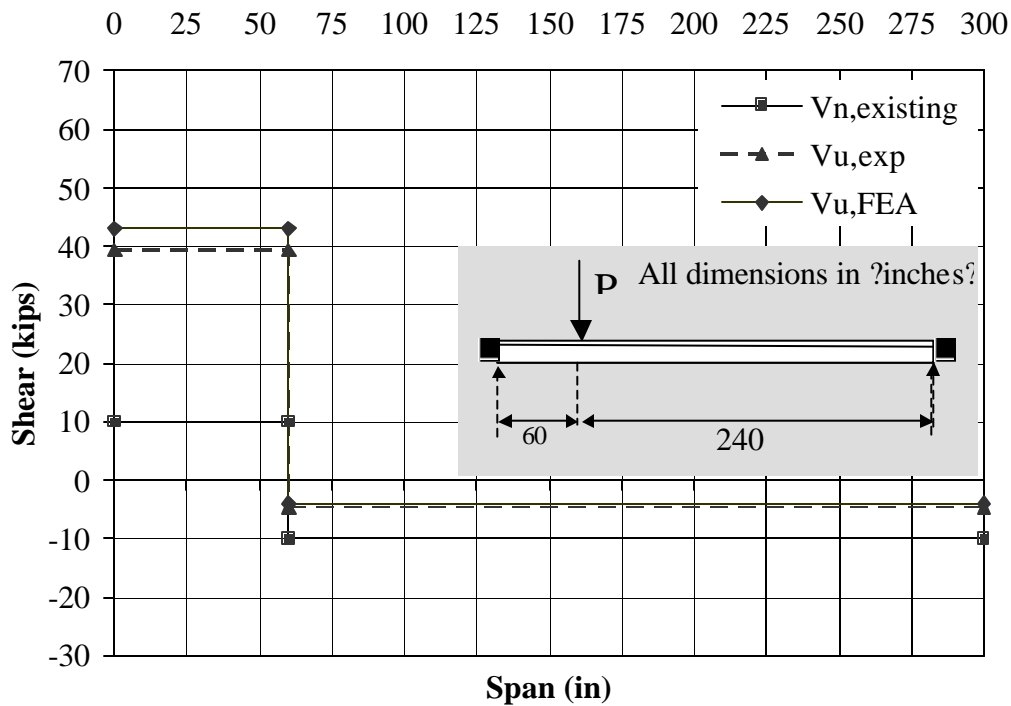


Figure B16: Shear force curves - JL1

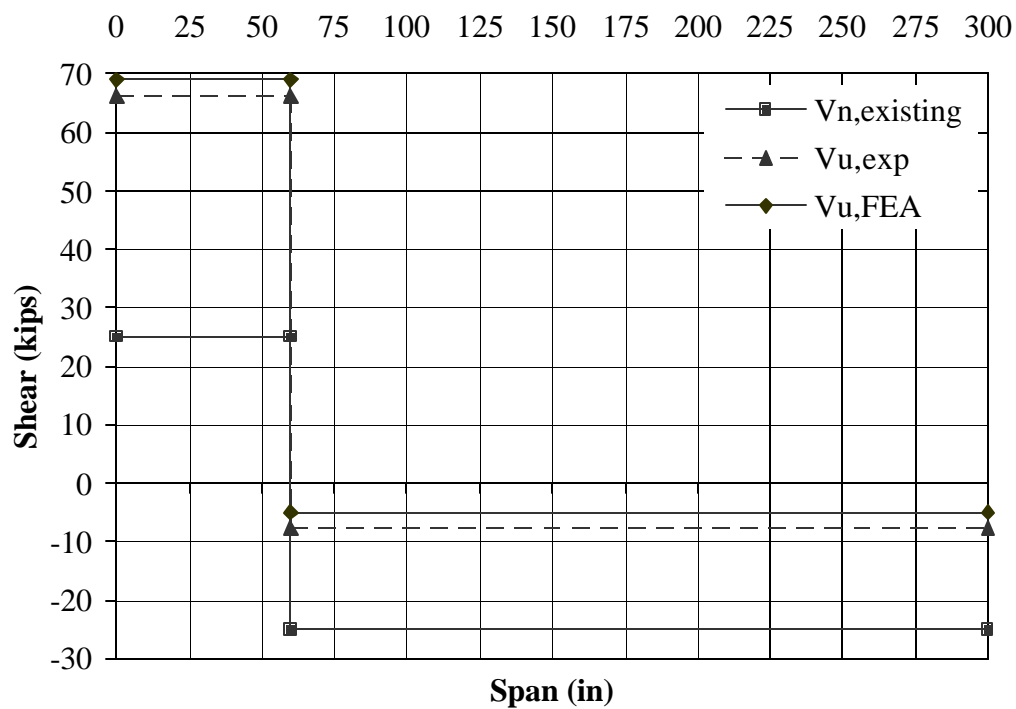


Figure B17: Shear force curves - JL2

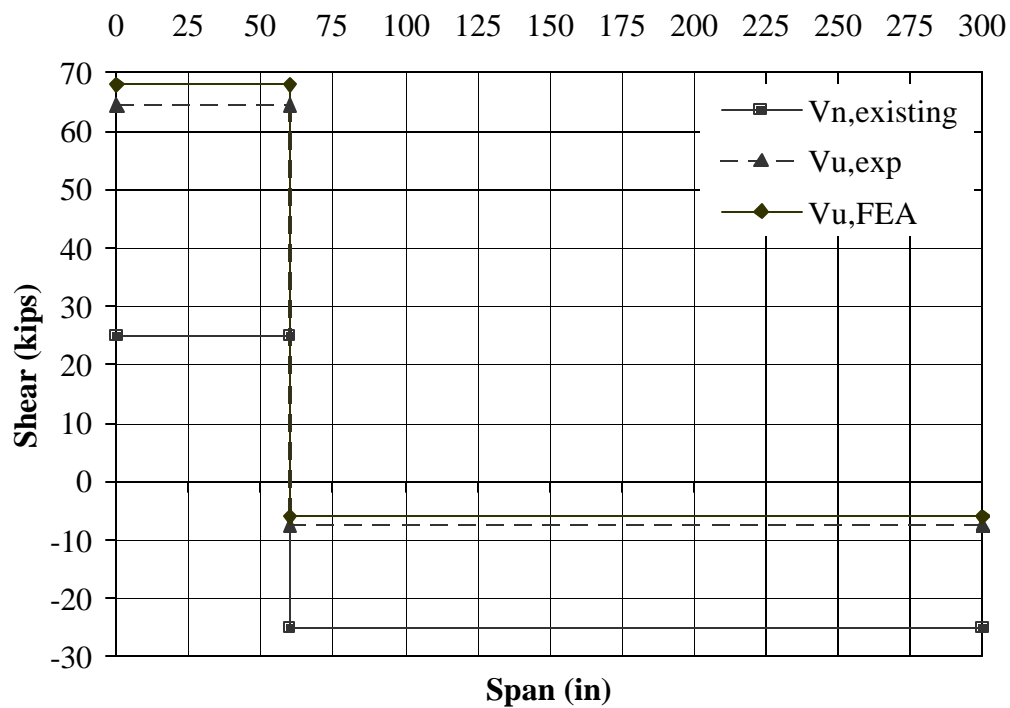


Figure B18: Shear force curves - JL3

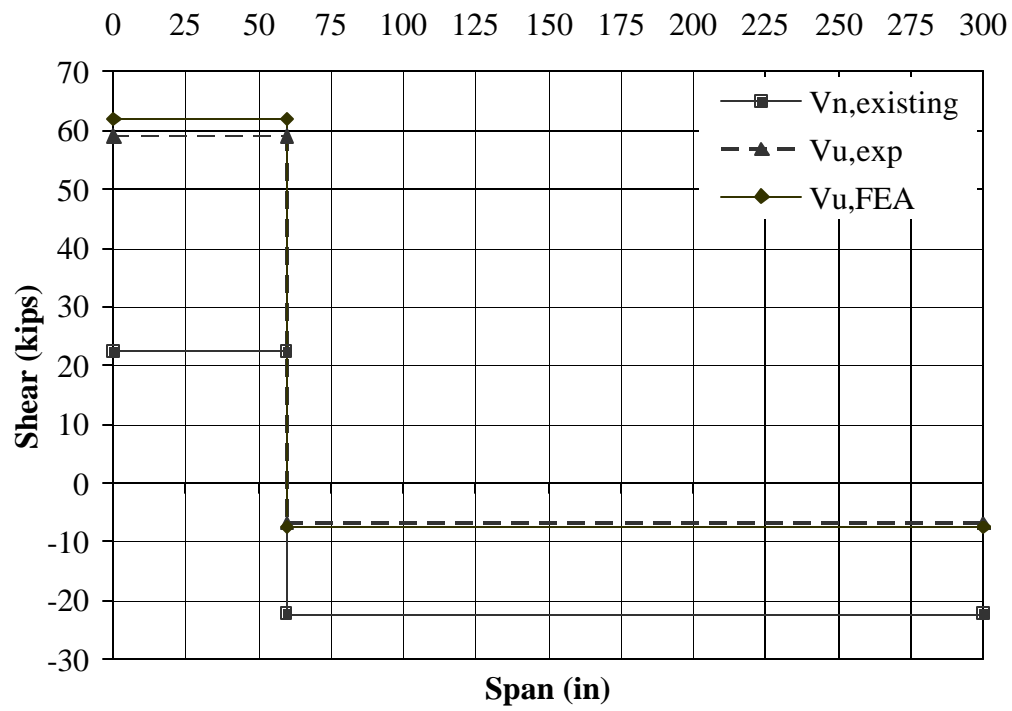


Figure B19: Shear force curves - JL4

APPENDIX C

DESIGN EXAMPLE

Design Example

Figure (D-1) shows the cross section of a simply supported T beam having a clear span of 60-in (1524-mm). The beam supports a uniformly distributed service (unfactored) dead load of 1 kip/ft (14.6-kN/m), including its own weight, and a uniformly distributed service live load of 1.6-kip/ft (23.4-kN/m). The beam was originally designed without any shear stirrups. With the change in the occupancy of the existing structure, it is estimated that an additional live load of 0.4-kip/ft (5.8-kN/m) is to be taken by the existing structure. It is desired to correct the structural deficiency by using externally bonded CFRP. The concrete strength is 3.5-ksi (25-MPa), the sheet thickness of CFRP is 0.0065-in (0.165-mm), the modulus of elasticity of CFRP is 33,000-ksi (228-GPa), and the tensile strength of CFRP is 550-ksi (3790-MPa).

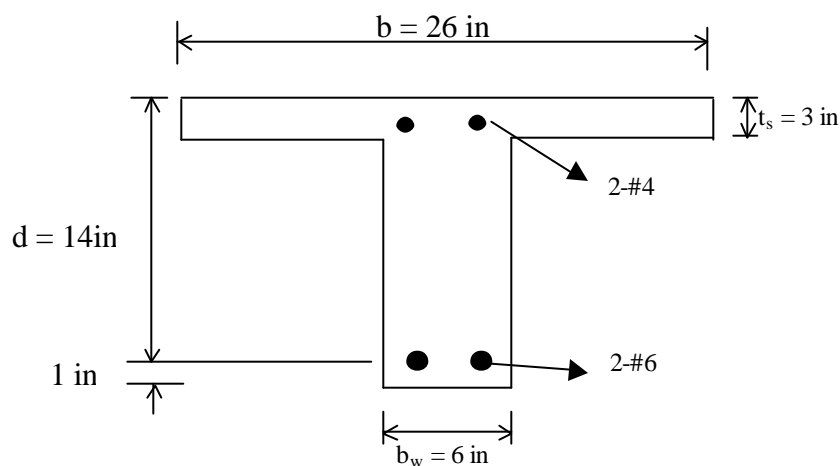


Figure C-1. T-beam cross-section

Compute the design factored shear force

New factored load:

$$w_u = 1.4 \times 1 + 1.7 \times 2 = 4.8 \text{ kip/ft}$$

$$V_u = \frac{w_u l}{2} = 12 \text{ -kip}$$

$$M_u = w_u l^2 / 8 = 15 \text{ -kip-ft}$$

Compute the nominal shear and moment capacity of the beam before strengthening

Compute the shear contribution of the concrete and steel in the traditional (ACI) manner.

$$V_c = (2\sqrt{f'_c} b_w d) = 2\sqrt{3500} \cdot 6 \cdot 14 = 10 \text{ - kips}$$

$$V_s = 0 \text{ kN (No stirrups)}$$

As per ACI 11.5.5, minimum shear reinforcement shall be provided in all RC flexural members where factored V_u exceeds one-half the shear strength provided by concrete ϕV_c .

Thus the design shear capacity of the beam is given by:

$$\phi V_{n, \text{existing}} = \phi V_c / 2 = 0.85 \cdot 10 / 2 = 4.25 \text{ - kips}$$

Moment capacity of the unstrengthened is calculated as:

$$a = A_s f_y / (0.85 f'_c b) = 0.226 \text{ in}$$

$$\phi Mn = \phi (A_s f_y (d - a/2)) = 0.85 (0.88 \cdot 50 \cdot (14 - 0.226/2)) = 43.83 \text{ kip-ft}$$

The member is safe in moment, as $M_u < Mn$

Since $V_u = 12$ -kips exceeds $\phi V_{n, \text{existing}}$ shear strengthening is required.

Find the required shear contribution that must be provided by CFRP, $V_{f, \text{req}}$.

$$V_u \leq \phi V_n$$

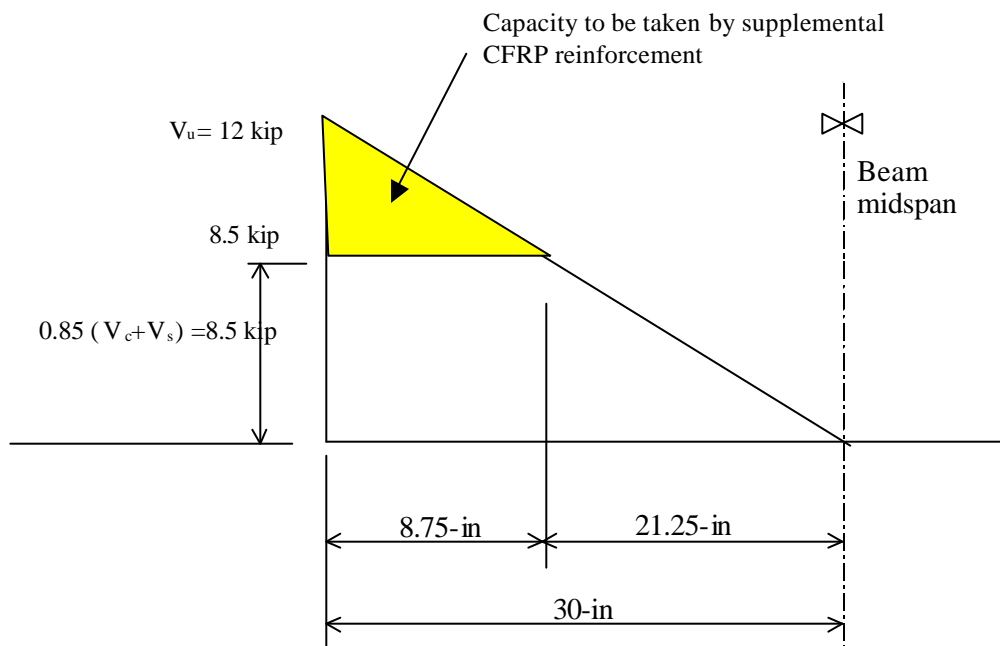


Figure C -2: Shear diagram-showing demand versus existing capacity

Use Equation (5-26) to calculate $V_{f, req}$.

$$V_u = \phi (V_c + V_s + ? V_f)$$

? is the additional reduction factor based on the known characteristics of the application but should not exceed 0.85 for three and two sided wrapping.

$$12 = 10 + 0.7 V_f$$

$$\therefore V_{f, req} = 4.84 \text{-kip}$$

The actual shear that has to be provided by CFRP is 4.84-kips.

Determine the reduction Coefficient for failure controlled by CFRP fracture

Assume one ply continuous U-wrap, without end anchor, will be used.

Compute ρ_f :

$$\rho_f = \frac{2 t_f}{b_w} \left(\frac{w_f}{s_f} \right)$$

For continuous vertical oriented ($\beta = 90^\circ$) CFRP, $w_f / s_f = 1$

$$\rho_f = \frac{2 (0.0065)}{6} = 0.00217$$

$$\rho_f E_f = 0.00217 \times 33000 = 0.0712 \text{ Msi} < 0.101 \text{ Msi.}$$

$$(1 \text{-Msi} = 1000 \text{-ksi})$$

\therefore Equation (4.11) is applicable

$$R = 26.62 (\rho_f E_f)^2 - 8.41 (\rho_f E_f) + 0.78$$

$$\therefore R_1 = 26.62 (0.0712)^2 - 8.44(0.0712) + (0.78) = 0.314$$

Determine the reduction Coefficient for failure controlled by CFRP debonding

$$d_f = d - t_s = 14 - 3 = 11 \text{ in}$$

Consider the effective bond length $L_e = 2$

The effective width of CFRP reinforcement can then be found from

$$w_{fe} = d_f - L_e = 11 - 2 = 9 \text{ in}$$

$$t_f E_f = 0.0065 * 33000 = 214 \text{ in-ksi}$$

$0.514 \geq t_f E_f \geq 0.114 \text{ in-Msi}$ Equation (4.12) is applicable.

$$R = \frac{(f'_c)^{2/3} w_{fe}}{e_{fu} d_f} [199.5 - 6.156 (t_f E_f)] \times 10^{-6}$$

$$\therefore R2 = \frac{(3.5)^{2/3} (9)}{(0.0167)(11)} [199.5 - 6.156(0.214)] \times 10^{-6} = 0.224$$

Determine the reduction Coefficient to control the shear crack width and loss of aggregate interlock

Using Equation (4.13):

$$R = \frac{0.006}{e_{fu}}$$

$$\therefore R3 = \frac{0.006}{0.0167} = 0.36$$

Determine the controlling reduction coefficient for the governing failure mode

$$R: = \min. (R1 \ R2 \ R3) \therefore R = 0.224$$

Compute the average effective stress of CFRP at ultimate

$$f_{fe} = R f_{fu}$$

$$f_{fe} = 0.224 \times 550 = 123.1\text{-ksi}$$

Find the shear contribution of the CFRP and compare to the required value

Using Equation (4.14):

$$V_f = \frac{A_f f_{fe} (\sin\beta + \cos\beta) d_f}{s_f} \leq [8\sqrt{f'_c} b_w d - V_s]$$

$$= \frac{2(0.0065)(1)(123.1)(1+0)(11)}{(1)} \leq (8\sqrt{3500}(6)(14) - 0)$$

$$= 17.6 \text{ kip} < 39.7 \text{ kip}$$

$V_f = 17.6 \text{ kip} > V_{f,req} = 4.84 \text{ kip} \therefore$ one ply continuous U-wrap without end anchor is sufficient.

The nominal shear capacity of the strengthened member is calculated by equation 4.17.

$$FV_n = F(V_c + ? V_f) = 0.85(10 + 0.85(17.6)) = 21.2 \text{ kip}$$

Final design

The final design is summarized in Figure (C-3). Note that, In this case, CFRP sheet assumed to extend beyond the critical point with distance equal to the stirrups spacing (1-in).

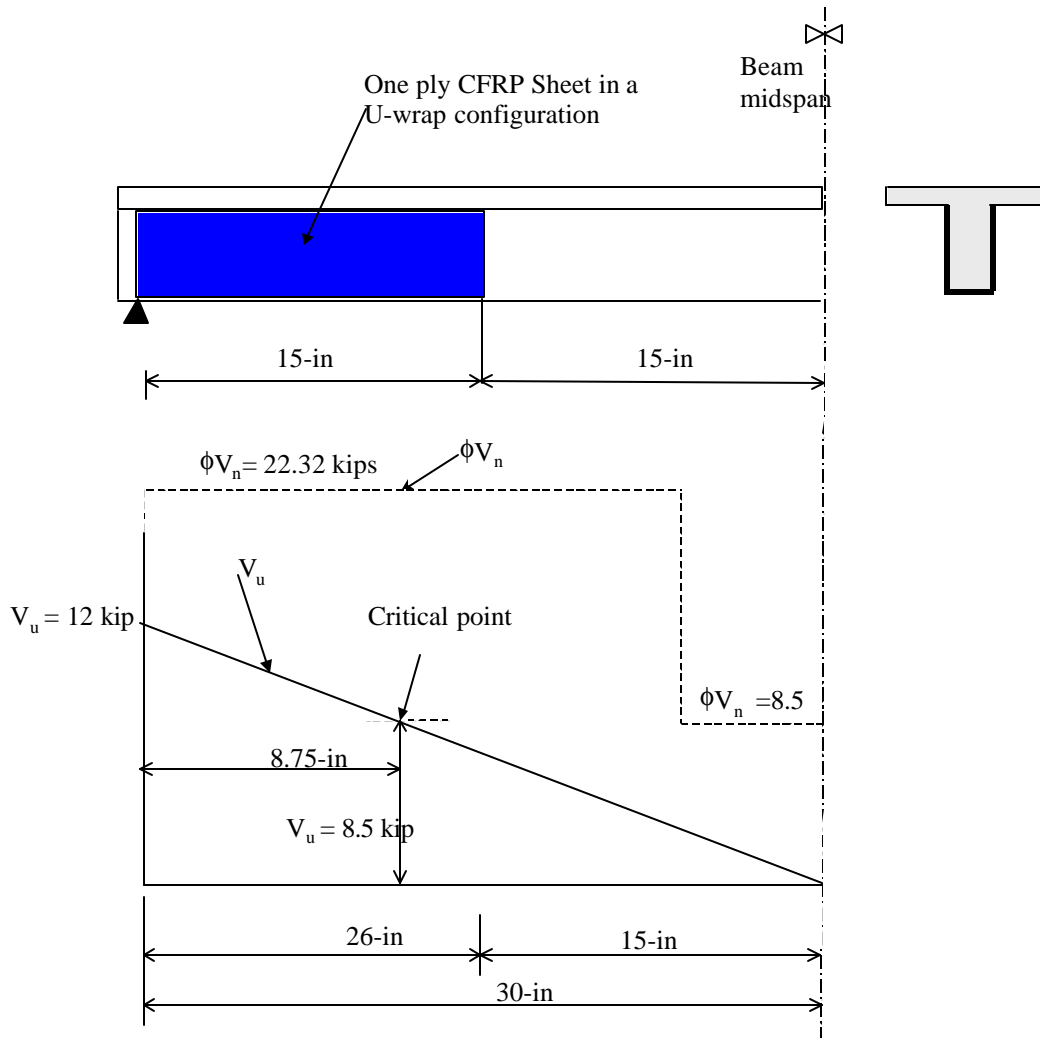


Figure C-3: Final Shear Force Diagram

BIBLIOGRAPHY

- ACI-318-95, (1995), "Building Code Requirements for Structural Concrete and Commentary", American Concrete Institute, Farmington Hills, Michigan, USA.
- Araki, N., Matsuzaki, Y., Nakano, K., Kataoka, T., and Fukuyama, H., (Oct. 1997), "Shear Capacity of Retrofitted RC Members with Continuous Fiber Sheets", *Non-Metallic (FRP) Reinforcement for Concrete Structures, Proceedings of the Third Symposium*, Vol. I, Japan, pp.515-521.
- Arduini, M., Nanni, A., Di Tommaso, A., and Focacci, F., (Oct. 1997), "Shear Response of Continuous Beams Strengthened with Carbon FRP Sheets", *Non-Metallic (FRP) Reinforcement for Concrete Structures, Proceedings of the Third Symposium*, Vol. I, Japan, pp.459-466.
- Chaallal, O., Nollet, M.J., Jr., and Tarantino, B., (1998), "Use of CFRP Strips for Flexure and Shear Strengthening of RC Members", Second International Conference on Composites in Infrastructures, Tucson, Arizona, USA, pp. 249-260.
- Chajes, M.J., Thompson, T.A., Jr., and Tarantino, B. (Sep. 1995), "Reinforcement of Concrete Structures using Externally Bonded Composite Materials", *Non-Metallic (FRP) Reinforcement for Concrete Structures, Proceedings of the Third Symposium*, Vol. I, Japan, pp. 501-508.
- Chung, H.W., (1998), "On Testing of Very Short Concrete Specimens", *Cement, Concrete & Aggregates*, ASTM, Vol. II, No.1, pp. 35-42.
- Cobb, A., (1997), "Procedure for the Design of Reinforced Concrete Bending Members Externally Bonded with FRP laminates", Thesis in Department of Architectural Engineering, The Pennsylvania State University, Pennsylvania, USA.
- El-Mihilmy, M.T., and Tedesco, J.W., (Sept. 2000), "Deflection of Reinforced Concrete Beams Strengthened with FRP Plates", *ACI Structural Journal*, Vol. 97, No. 5, pp. 679-688.
- Funakawa, I., Shimono, K., Watanabe, T., Asada, S., and Ushijima, S., (Oct 1997), "Experimental Study of Shear Strengthening with Continuous Fiber Reinforcement Sheet and Methyl MetaAcrylate Resin", *Non-Metallic (FRP) Reinforcement for Concrete Structures, Proceedings of the Third Symposium*, Vol. I, Japan, pp.465-482.
- Khalifa, A., (1999), "Shear performance of RC Beams Strengthened with Advanced Composites", Ph.D. Dissertation, Department of Civil Engineering, University of Alexandria, Egypt.

- Khalifa, A., Gold, W., Nanni, A., and Abdel -Aziz M. I., (Nov. 1998), “Contribution of Externally Bonded FRP to the Shear Capacity of RC Flexural Members”, *Journal of Composites for Construction*, ASCE, Vol. 2, No. 4, pp.195-202.
- Khalifa, A., Alkhrdaji, T., Nanni, A., and Lansburg, A., (Oct.1999), “Anchorage of Surface Mounted FRP Reinforcement”, *Concrete International*, ACI, Vol. 97, No. 5, pp.161-168.
- Khalifa, A., Tumialan, G., Nanni, A., and Belarbi, A., (Oct. 1999), “Shear Strengthening of Continuous RC Beams Using Externally Bonded CFRP Sheets”, *Non-Metallic (FRP) Reinforcement for Concrete Structures, Proceedings of the Fourth Symposium*, Vol. I, Maryland, USA, pp. 689-696.
- Khalifa, A., and Nanni, A., (2000), “ Rehabilitation of Rectangular Simply Supported RC Beams with Shear Deficiencies Using CFRP Composites”, *Journal of Construction and Building Materials*, Vol. 94, pp. 65-72.
- Kamiharako, A., Maruyama, K., Takada, K., and Shimomura, T., (Oct 1997), “ Evaluation of Shear Contribution of FRP Sheets Attached to Concrete Beams”, *Non-Metallic (FRP) Reinforcement for Concrete Structures, Proceedings of the Third Symposium*, Vol. I, Japan, pp. 467-475.
- MacGregor, J., (1997), “Reinforced Concrete Mechanics and Design”, Prentice-Hall Inc., upper Saddle River, New Jersey, USA, pp.186-225.
- Master Builders Technologies, (1998), “MBrace Composite Strengthening System-Engineering Design Guidelines”, Second Ed., Cleveland, OH, pp.140.
- Mettemeyer, M., (1999), “In Situ Rapid Load Testing of Concrete Structures”, MSc Thesis, Department of Civil Engineering, The University of Missouri, Rolla, MO.
- Miller, Brian D., (1999), “Bond Between Carbon Fiber Reinforced Polymer Sheets and Concrete”, MS Thesis, Department of Civil Engineering, University of Missouri, Rolla, MO.
- Meier, U., (1987), “Bridge Repair with High Performance Composite Materials”, *Material und Technik*, Vol. 4, pp. 125-128.
- Ramamruthum, S., (1994), “Theory of Structures”, Dhanpat Rai & sons, Nai sarak, Delhi, India, pp.86-165.
- Malek, A., and Saadathmanesh, H., (July-Aug. 1998), “ Ultimate Shear Capacity of Reinforced Concrete Beams Strengthened with Web-Bonded Fiber-Reinforced Plastic”, *ACI Structural Journal*, Vol. II, pp. 391-399.

- Sato, Y., Katsumata, H., and Kobatake, Y., (Oct 1997), "Shear Strengthening of Existing Reinforced Concrete Beams By CFRP Sheets", *Non-Metallic (FRP) Reinforcement for Concrete Structures, Proceedings of the Third Symposium*, Vol. I, Japan, pp.507-514.
- Supernant, B.A., (1994), " Understanding Concrete Core Testing", NRMCA Publications No. 185, National Ready Mixed Concrete Association, Maryland, USA.
- Taerwe, L., Khalil, H., and Matthys, S., (Oct 1997), "Behavior of RC beams Strengthened in Shear by External CFRP Sheets", *Non-Metallic (FRP) Reinforcement for Concrete Structures, Proceedings of the Third Symposium*, Vol. I, Japan, pp.483-490.
- Tumialan, J.G., (1998), "Concrete Cover Delamination in Reinforced Concrete Beams Strengthened with CFRP Sheets", MSc Thesis, Department of Civil Engineering, The University of Missouri, Rolla, MO.
- Tumialan, J.G, Belarbi, A., Nanni, A., (1999), "Reinforced Concrete Beams Strengthened with CFRP Composites: Failure due to Concrete Cover Delamination", Report No: CIES 99/01, Department of Civil Engineering, University of Missouri, Rolla, MO.
- Umezu, K., Fujita, M., Nakai, H., and Tamaki, K., (Oct 1997), " Shear Behavior of RC Beams with Aramid Fiber Sheets", *Non-Metallic (FRP) Reinforcement for Concrete Structures, Proceedings of the Third Symposium*, Vol. I, Japan, pp. 491-498.